Supplementary Information For:

A fluorescent zirconium organic framework displaying rapid and nanomolar level detection of Hg(II) and nitroantibiotics

Subhrajyoti Ghosh, [a] *Felix Steinke,* [b] *Abhijeet Rana* [a] *and Shyam Biswas* [a]*

[a]*Department of Chemistry, Indian Institute of Technology Guwahati, Guwahati, 781039 Assam, India.*

[b]*Institut für Anorganische Chemie, Christian-Albrechts-Universität, Max-Eyth-Strasse 2, 24118 Kiel, Germany*

* Corresponding author. Tel: 91-3612583309, Fax: 91-3612582349.

E-mail address: sbiswas@iitg.ac.in.

Materials and characterization methods:

The synthesis and characterisation procedures for benzo[1,2-b:4,5-b']dithiophene-2,6-dicarboxylic acid linker are described below. All the chemicals were purchased from commercial sources and used without further purification. A Bruker Avance III 400 spectrometer was utilized for recording ^{1}H NMR and ^{13}C NMR spectra at 400 MHz and 100 MHz respectively. The mass spectrum (in ESI mode) was measured with an Agilent 6520 Q-TOF high-resolution mass spectrometer. Fourier transform infrared (FT-IR) spectroscopy data were recorded in the region 400-4000 cm^{-1} at room temperature with the Perkin Elmer Spectrum Two FT-IR spectrometer. The following indications were used to indicate the corresponding absorption bands: very strong (vs), strong (s), medium (m), weak (w), shoulder (sh) and broad (br). Thermogravimetric (TG) experiments were carried out with a heating rate of 5 °C min^{-1} under air atmosphere using a Netzsch STA-409CD thermogravimetric analyser. Powder X-ray diffraction (PXRD) instrument Stoe Stadi MP diffractometer equipped with a MYTHEN 1K detector ($CuK_{\alpha 1}$-radiation, λ = 1.5406 Å) was used for the PXRD measurements for the Rietveld refinement. All the other PXRD data were collected by using Rigaku Smartlab X-ray diffractometer (model TTRAX III) with Cu-Kα radiation (λ = 1.54056 Å), 50 kV of operating voltage and 100 mA of operating current. Specific surface area for N_2 sorption was calculated on a Quantachrome Autosorb iQMP gas sorption analyser at -196 °C. FE-SEM images were collected with a Zeiss (Sigma 300) scanning electron microscope. The compound was activated at 100 °C for 24 h under dynamic vacuum. Fluorescence emission studies were performed at room temperature using a HORIBA JOBIN YVON Fluoromax-4 spectrofluorometer. Fluorescence lifetime measurements were performed by time correlated single-photon counting (TCSPC) method by an Edinburgh Instrument Life-Spec II instrument. The fluorescence decays were analyzed by reconvolution method using the FAST software provided by Edinburgh Instruments. The UV-Vis spectra were measured with a PerkinElmer Lambda 25 UV-Vis spectrometer.

Preparation of MOF (IITG-5a) suspension for the fluorescence sensing experiments:

The probe **IITG-5a** (2 mg) was taken in a 5 mL glass vial and 3 mL Milli-Q water/ MeOH was added to it to make a homogeneous suspension. Then, the suspension was sonicated for 30 min and kept it for overnight to make the suspension stable. During the fluorescence titration time, we used 100 µL of above mentioned suspension of **IITG-5a** and 3000 µL of Milli-Q water/MeOH was added to it in a quartz cuvette. All the fluorescence spectra were collected by exciting the suspension at 310 nm (for aqueous suspension) and 370 nm (for methanolic suspension), within the range of 350-550 nm for Hg^{2+} sensing and 390-550 nm for antibiotics (NFZ and NFT) sensing. The solutions of the different competitive analytes of Hg^{2+} and nitro-antibiotics (NFZ and NFT) (concentration = 10 mM) were added in an incremental manner to **IITG-5a** suspension.

Synthesis procedure of benzo[1,2-b:4,5-b']dithiophene-2,6-dicarboxylic acid linker:

The ligand was synthesized using a two-step synthesis procedure (Scheme 1). The diethyl benzo[1,2-b:4,5-b']dithiophene-2,6-dicarboxylate was synthesized according to previously reported literature procedure.[1] Then, 850 mg (2.77 mmol) of the obtained ester product was dissolved in a mixture of 10 mL of THF, 10 of mL of EtOH and 10 mL of 1(M) LiOH. After that, the mixture was refluxed for 3 h at 80 °C. After 3 h, these solvents were evaporated

under vacuum. Thereafter, the remaining liquid part was acidified with 3 (M) HCl solution. At last, the obtained solid precipitate was filtered, washed with 10 mL of water and then dried in an oven at 80 °C for 12 h. Yield: 565 mg (2.03 mmol, 73%). ^{1}H NMR (400 MHz, DMSO-d_6): δ = 8.68 (s, 2H), 8.17 (s, 2H) ppm ^{13}C NMR (100 MHz, DMSO-d_6): δ = 163.50, 138.51, 138.38, 136.75, 129.68, 120.05 ppm. ESI-MS (m/z): 276.0665 for $(M-H)^-$ ion (M = mass of benzo[1,2-b:4,5-b']dithiophene-2,6-dicarboxylic acid linker). In Figures S1-S3, the NMR and mass spectra of the synthesized benzo[1,2-b:4,5-b']dithiophene-2,6-dicarboxylic acid linker are shown.

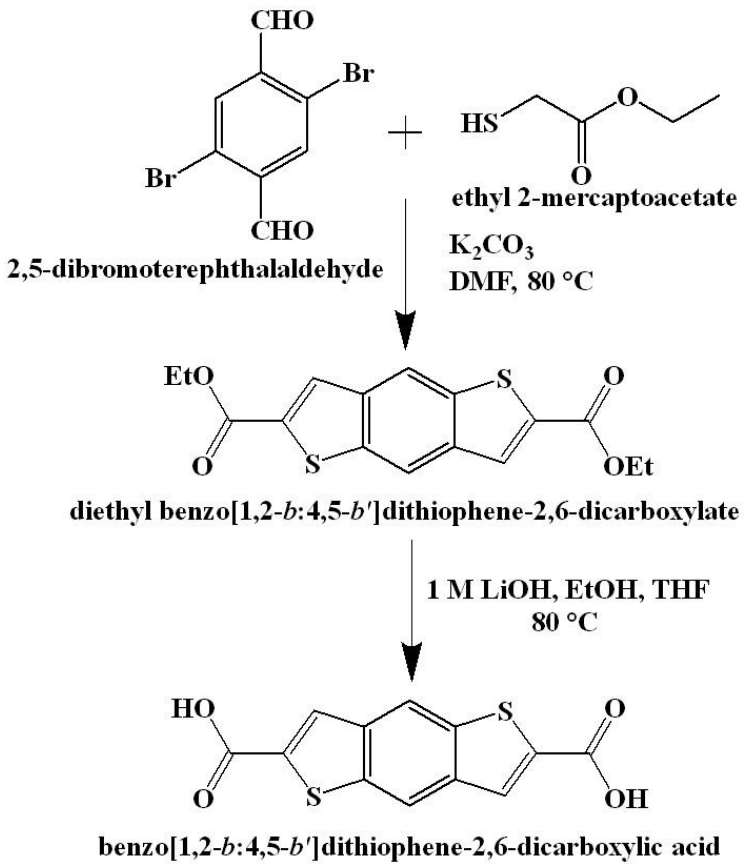

Scheme S1. Reaction scheme for the preparation of benzo[1,2-b:4,5-b']dithiophene-2,6-dicarboxylic acid linker.

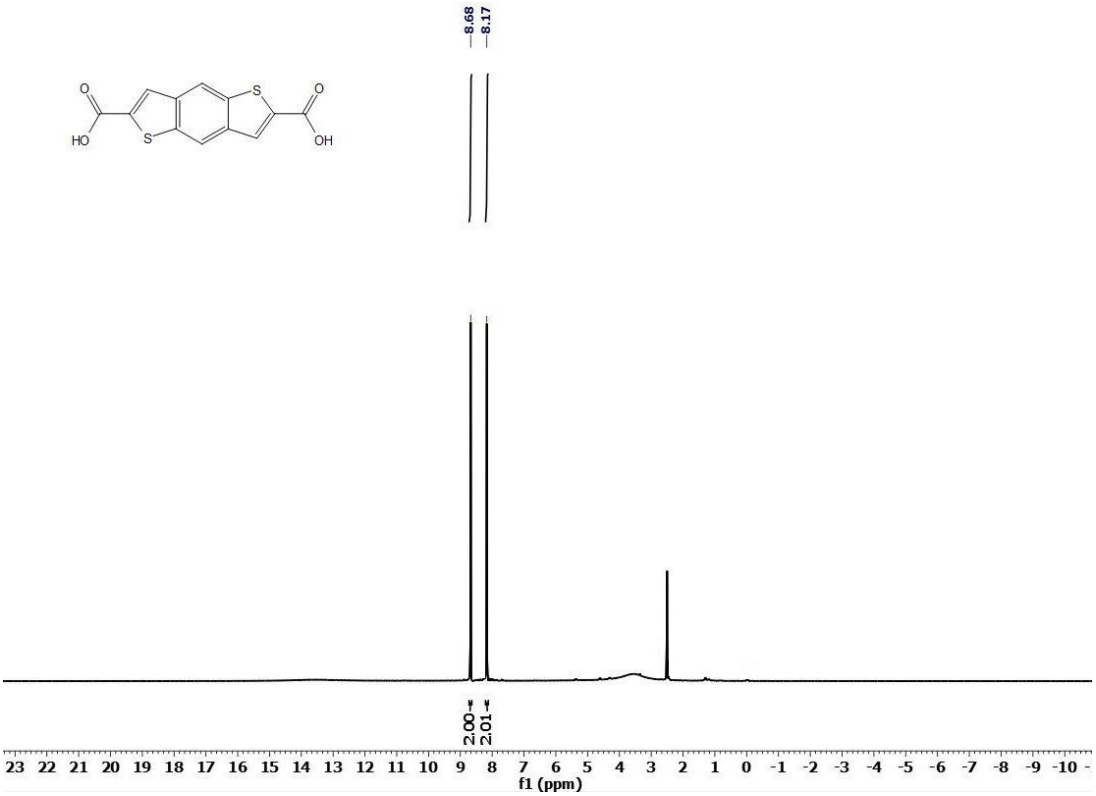

Fig. S1. ^{1}H NMR spectrum of benzo[1,2-b:4,5-b']dithiophene-2,6-dicarboxylic acid linker in DMSO-d_6.

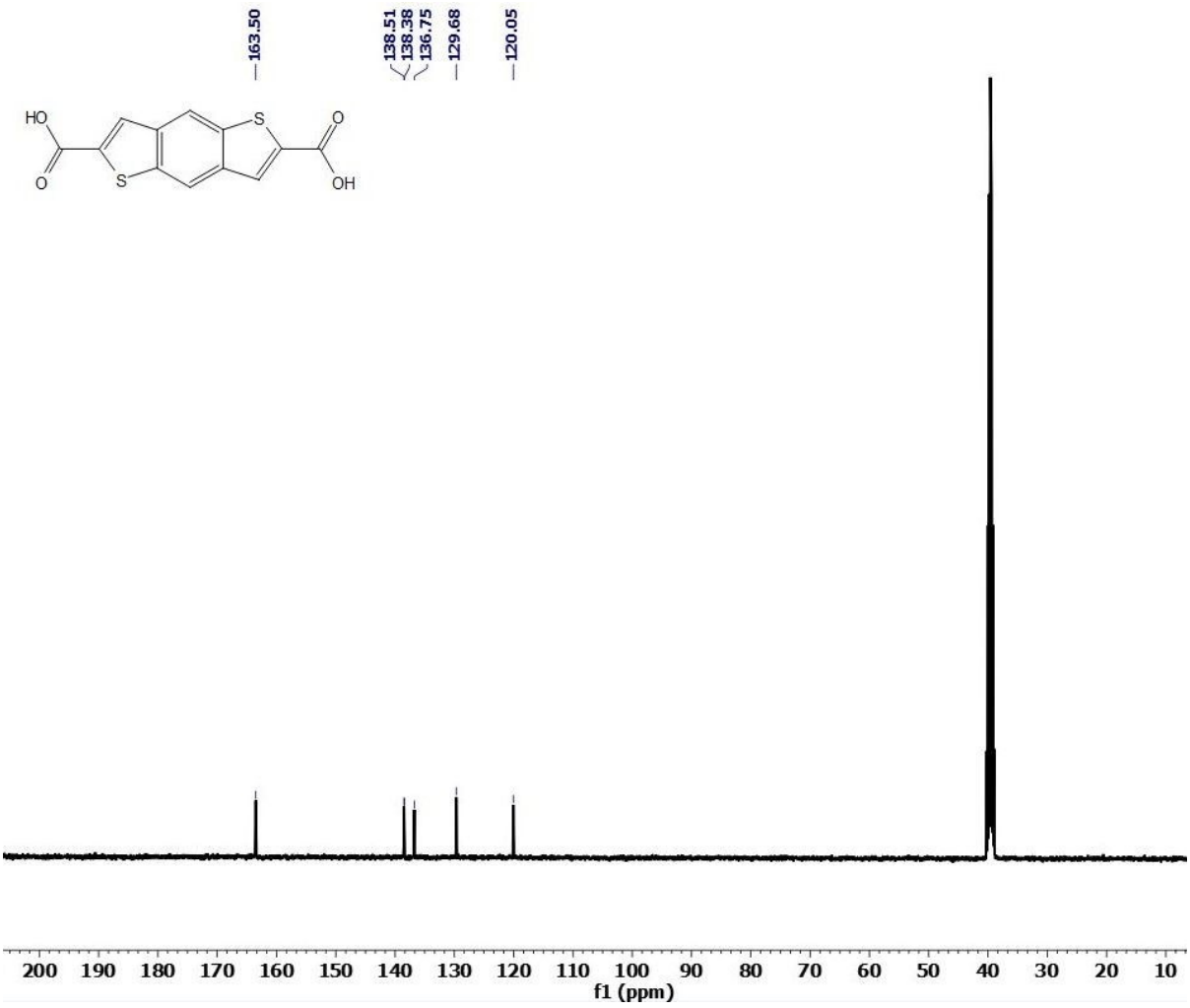

Fig. S2. ^{13}C NMR spectrum of benzo[1,2-b:4,5-b']dithiophene-2,6-dicarboxylic acid linker in DMSO-d_6.

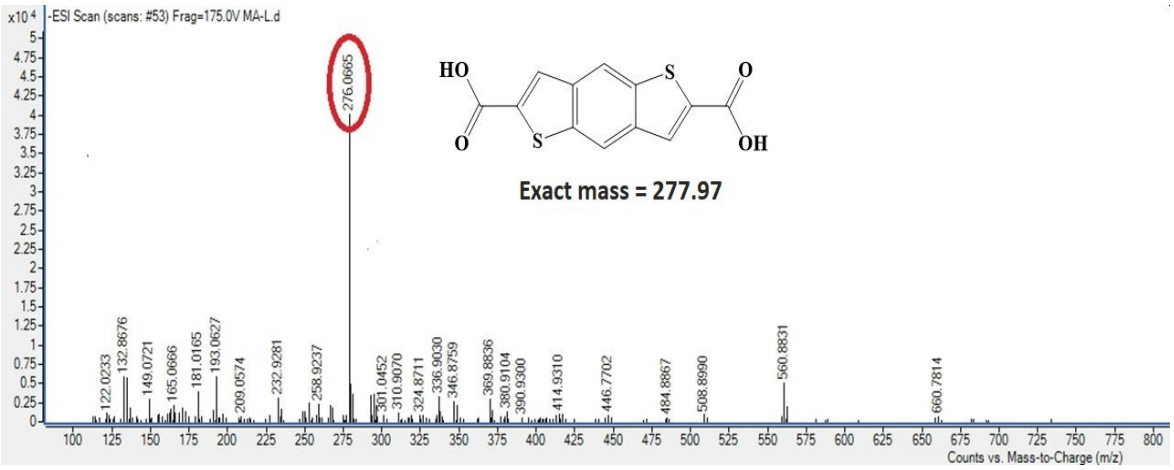

Fig. S3. ESI-MS spectrum of benzo[1,2-b:4,5-b']dithiophene-2,6-dicarboxylic acid linker measured in methanol. The spectrum shows m/z peak at 276.0665, which corresponds to $(M-H)^-$ ion (M = mass of benzo[1,2-b:4,5-b']dithiophene-2,6-dicarboxylic acid linker).

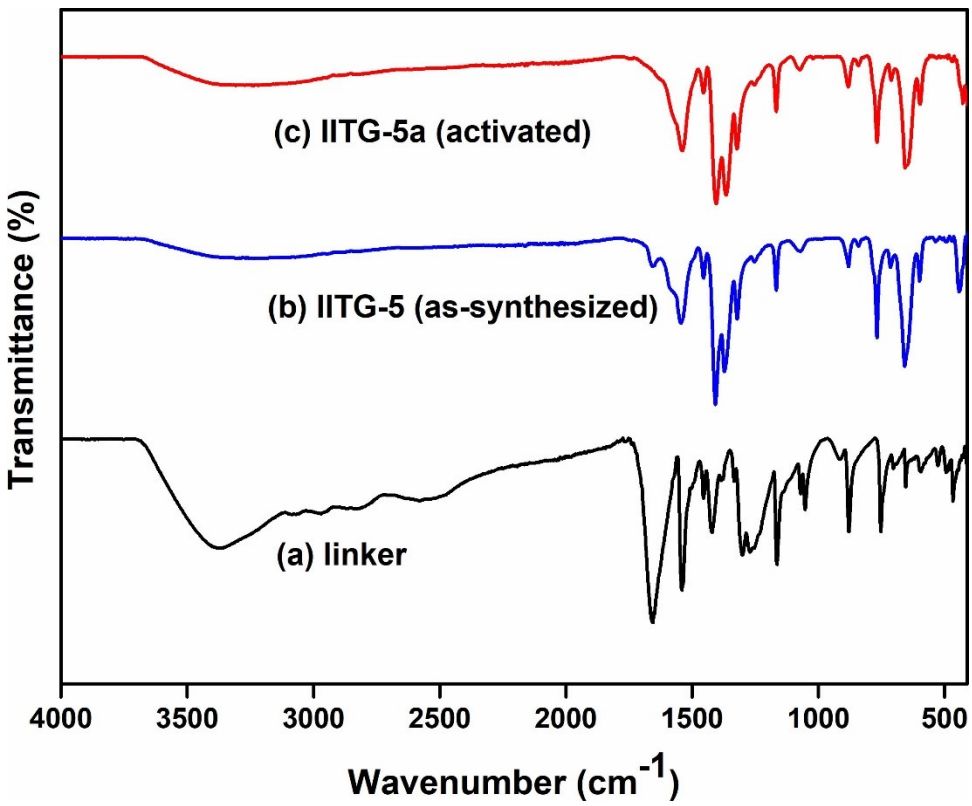

Fig. S4. FT-IR spectra of (a) linker, (b) as-synthesized **IITG-5** and (c) activated **IITG-5a**.

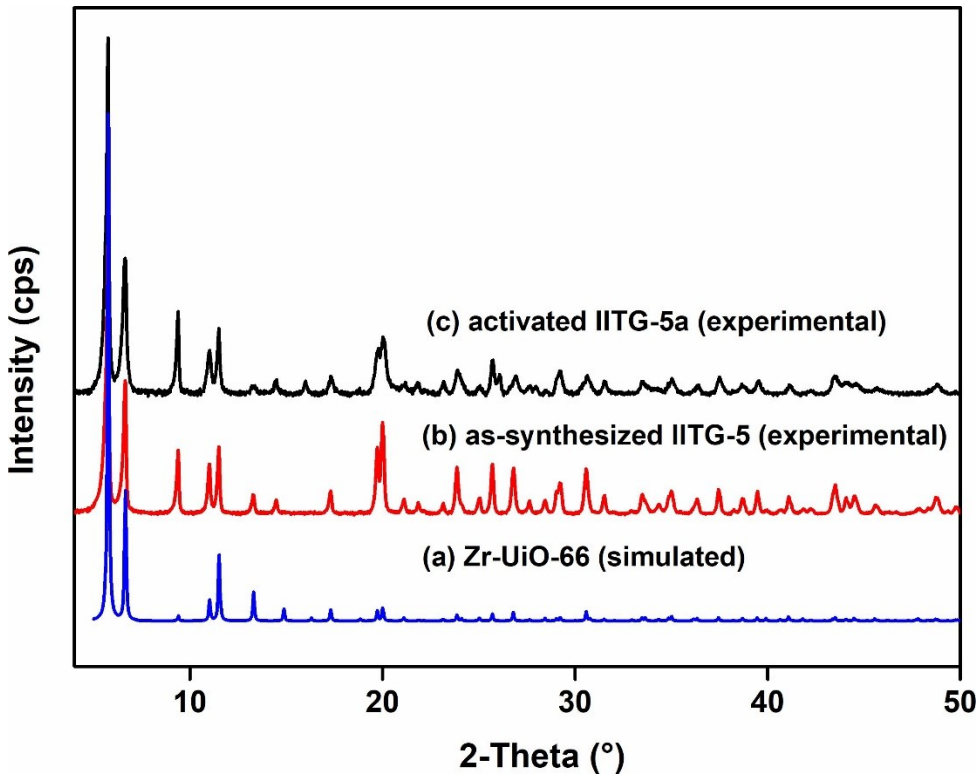

Fig. S5. PXRD patterns of (a) Zr-UiO-66 (blue), (b) as-synthesized **IITG-5** (red) and (c) activated **IITG-5a** (black).

Table S1. Selected bond lengths in the structure of **IITG-5a**.

Atom 1	Atom 2	Bond length	Atom 1	Atom 2	Bond length
Zr1	O1	2.25(2)	C2	S1	1.75(4)
Zr1	O2	2.178(16)	C3	C4	1.38(13)
C1	C2	1.38(4)	S1	C4	1.73(4)
C2	C2	1.37(6)	C4	C5	1.46(8)
C2	C3	1.39(10)	C5	O1	1.28(4)

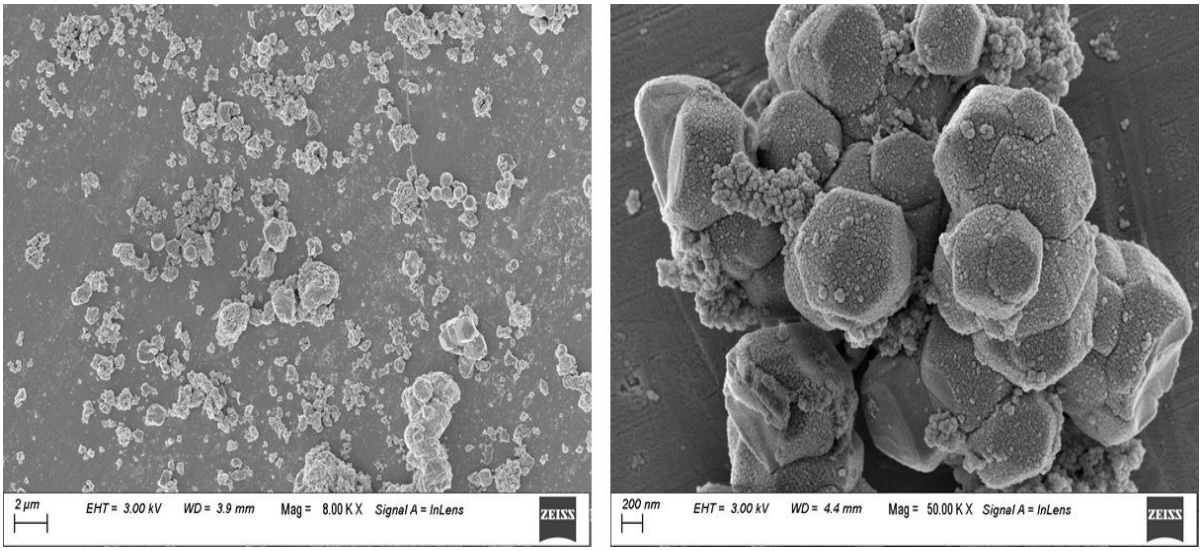

Fig. S6. FE-SEM images of as-synthesized **IITG-5a**.

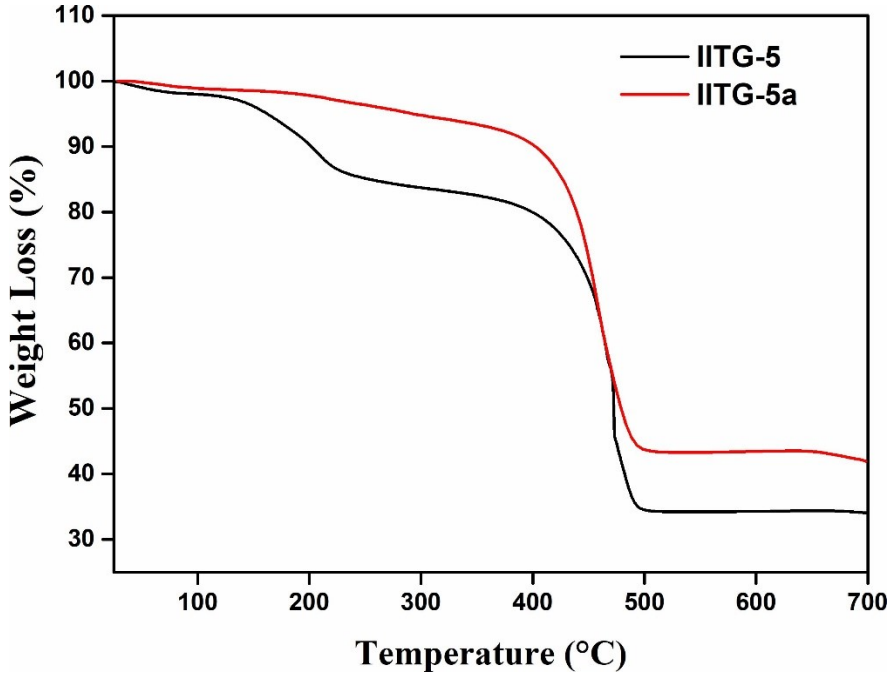

Fig. S7. Thermogravimetric analysis curves of as-synthesized **IITG-5** (black) and thermally activated **IITG-5a** (red) recorded under air atmosphere in the temperature range of 25-700 °C with a heating rate of 5 °C min^{-1}.

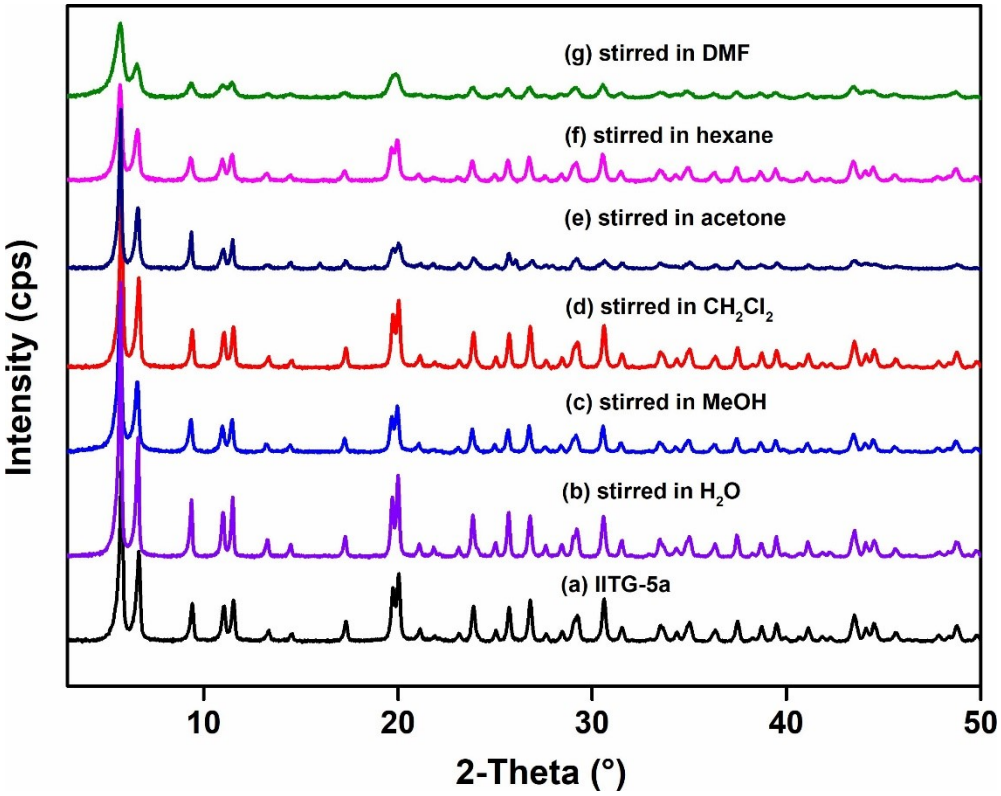

Fig. S8. PXRD patterns of **IITG-5a** in different forms: (a) activated (**IITG-5a**), after stirred with (b) H_2O (c) MeOH (d) CH_2Cl_2 (e) acetone (f) hexane and (g) DMF for 6 h.

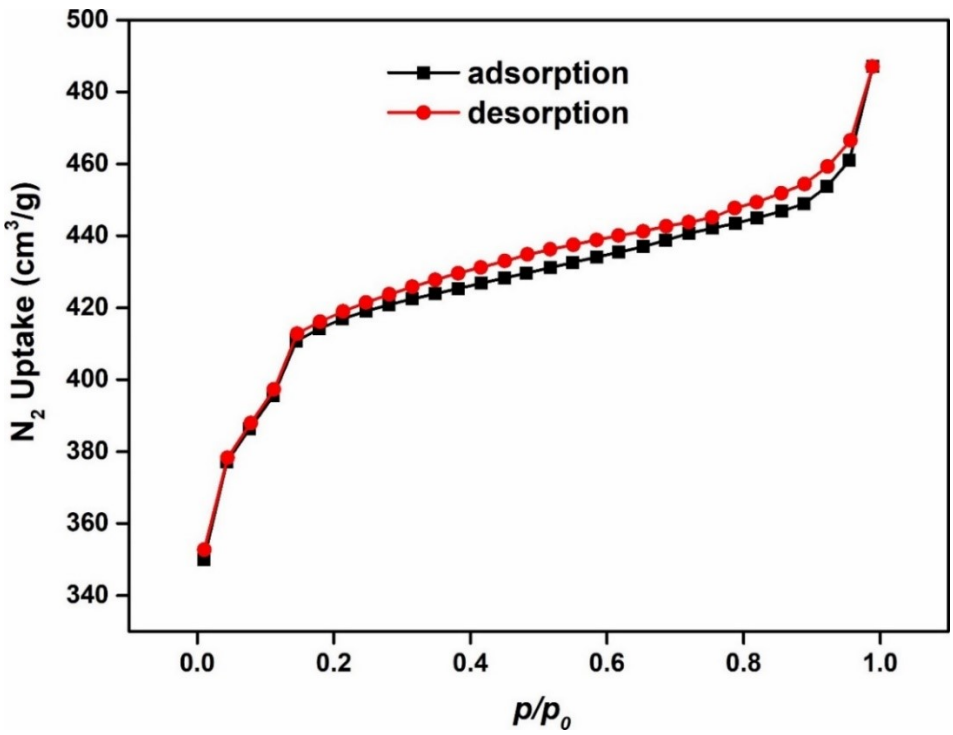

Fig. S9. N_2 adsorption (black squares) and desorption (red circles) isotherms of thermally activated **IITG-5a** recorded at –196 °C.

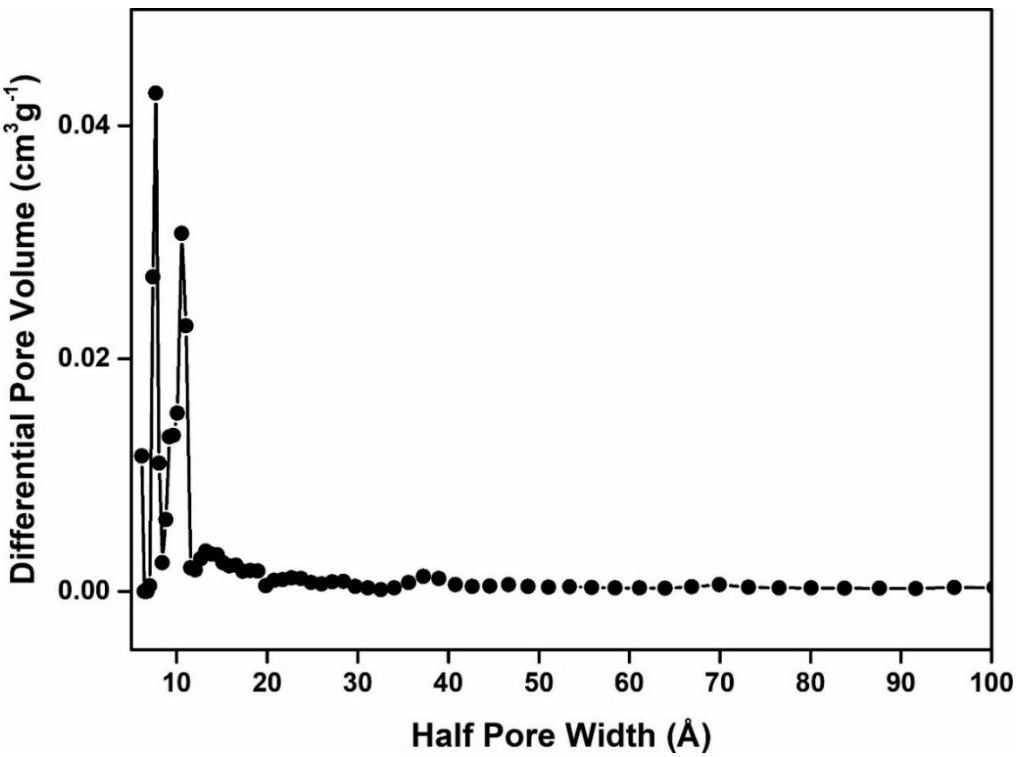

Fig. S10. Density functional theory pore-size distribution of compound **IITG-5a** as determined from its N_2 adsorption isotherms at -196 °C.

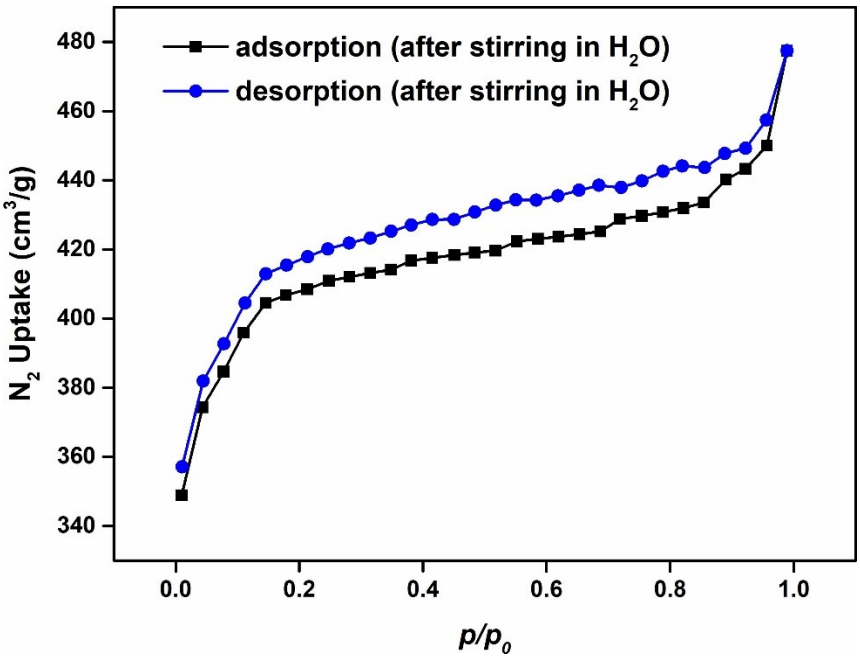

Fig. S11. N_2 adsorption (black squares) and desorption (blue circles) isotherms of **IITG-5a** after stirring in H_2O for 6 h recorded at –196 °C.

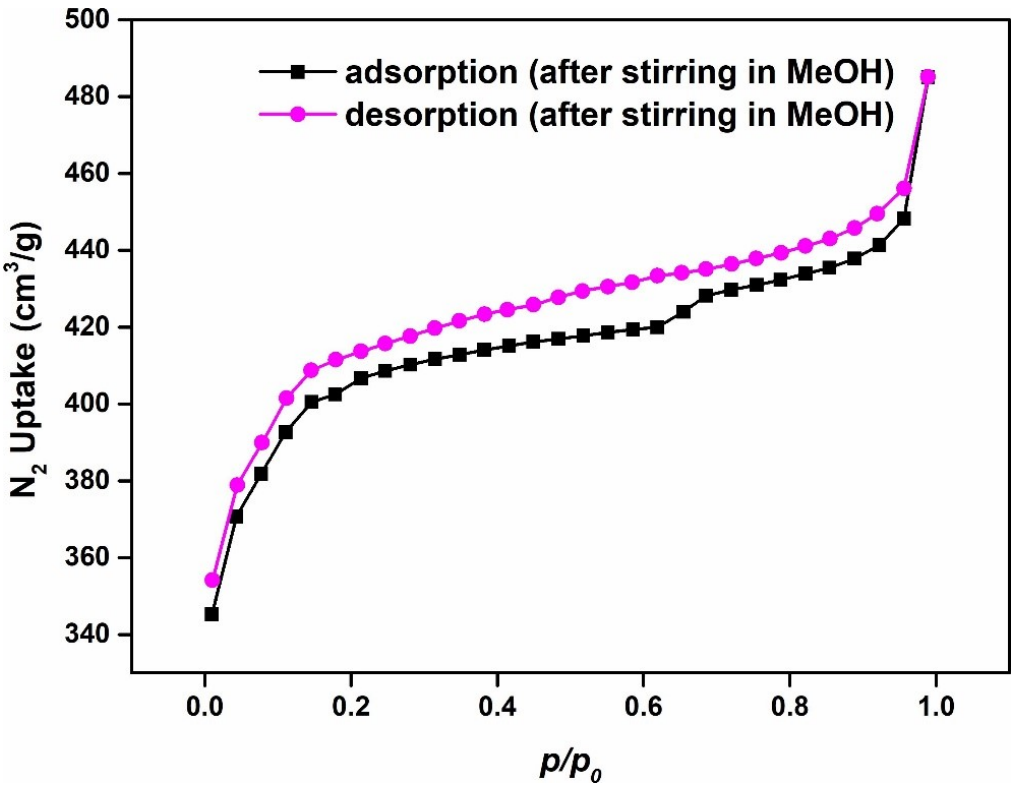

Fig. S12. N_2 adsorption (black squares) and desorption (pink circles) isotherms of **IITG-5a** after stirring in MeOH for 6 h recorded at –196 °C.

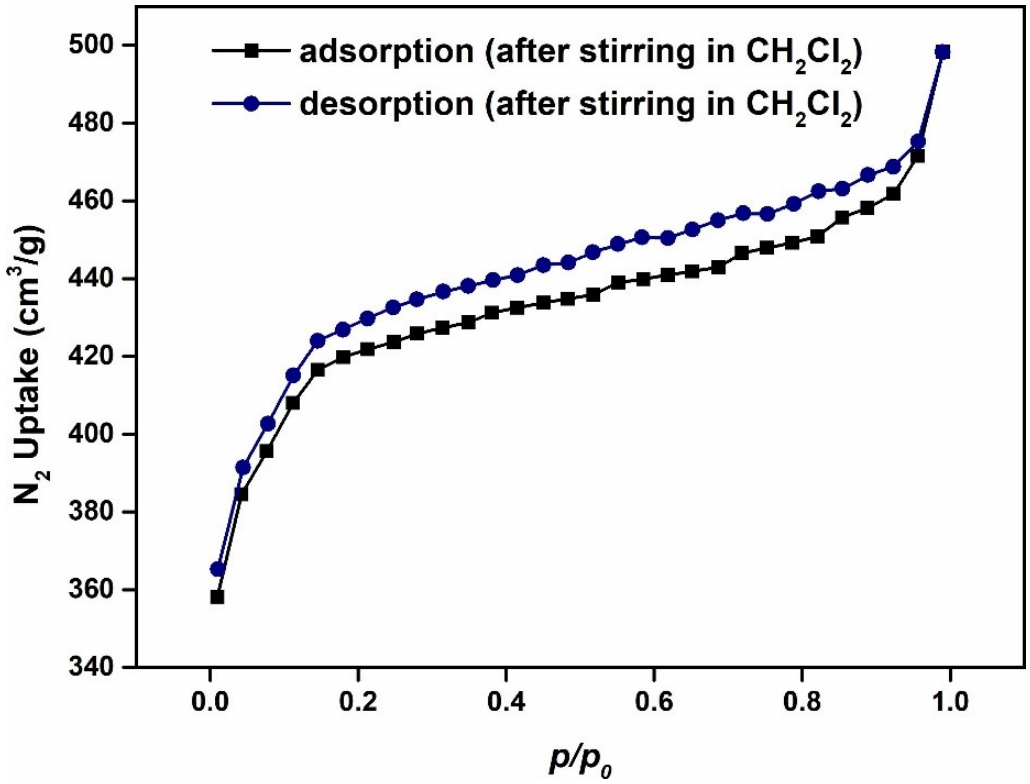

Fig. S13. N_2 adsorption (black squares) and desorption (navy-blue circles) isotherms of **IITG-5a** after stirring in CH_2Cl_2 for 6 h recorded at –196 °C.

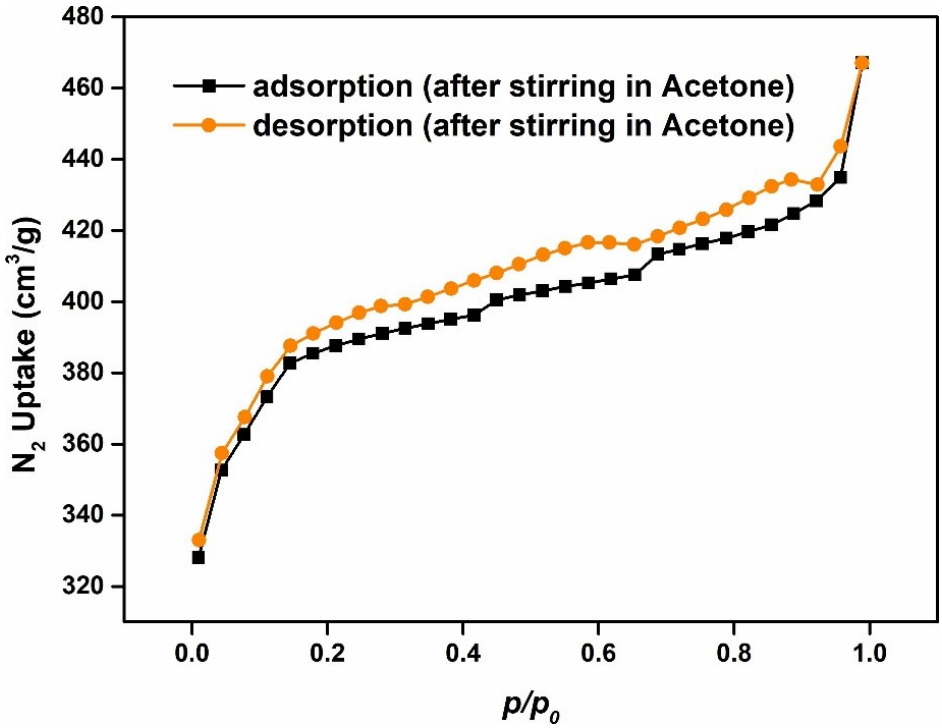

Fig. S14. N_2 adsorption (black squares) and desorption (orange circles) isotherms of **IITG-5a** after stirring in acetone for 6 h recorded at –196 °C.

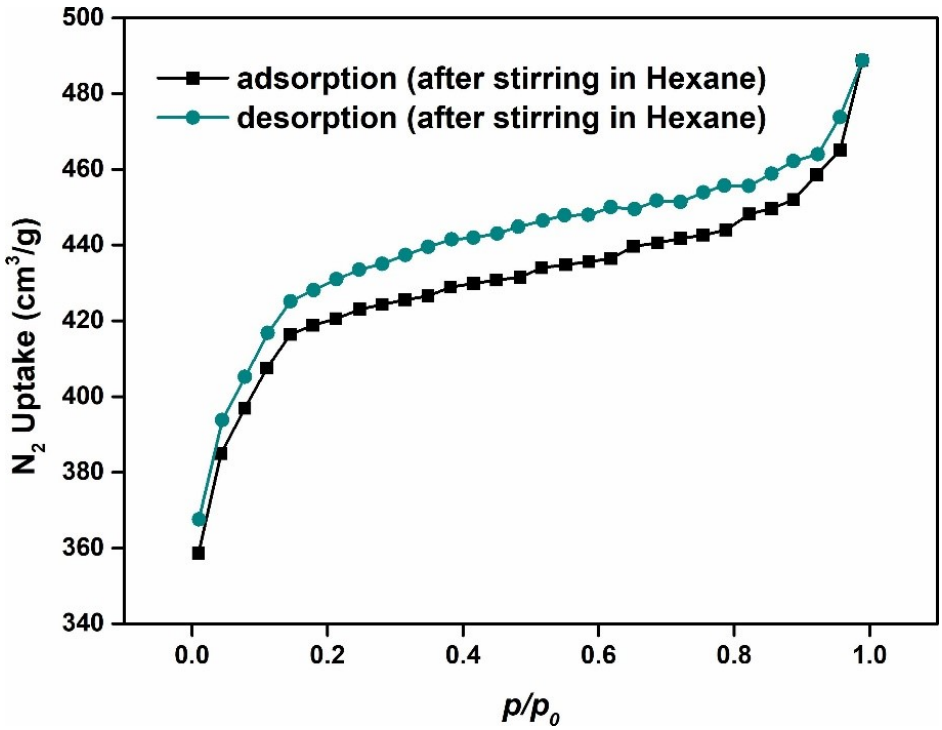

Fig. S15. N_2 adsorption (black squares) and desorption (dark cyan circles) isotherms of **IITG-5a** after stirring in hexane for 6 h recorded at –196 °C.

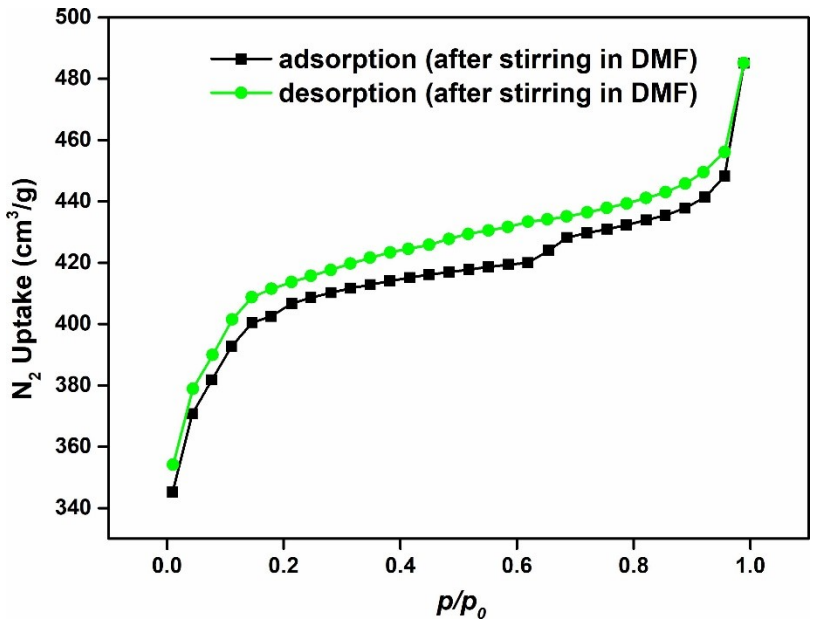

Fig. S16. N_2 adsorption (black squares) and desorption (green circles) isotherms of **IITG-5a** after stirring in DMF for 6 h recorded at –196 °C.

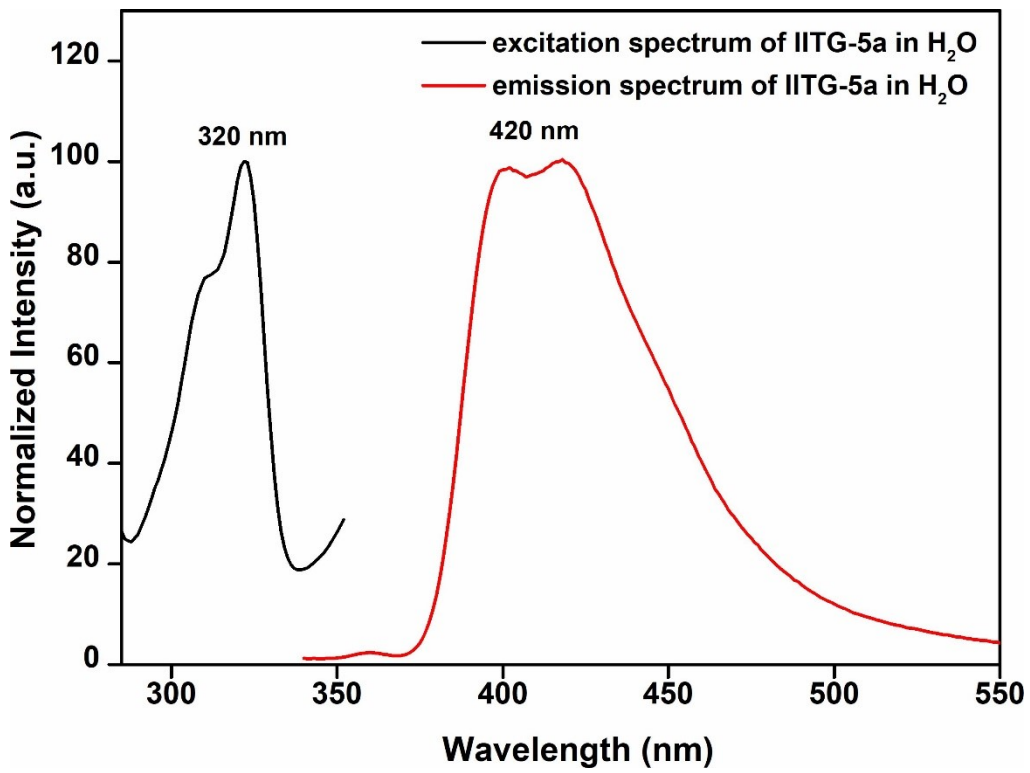

Fig. S17. Excitation (black) and emission (red) spectra of **IITG-5a** in water.

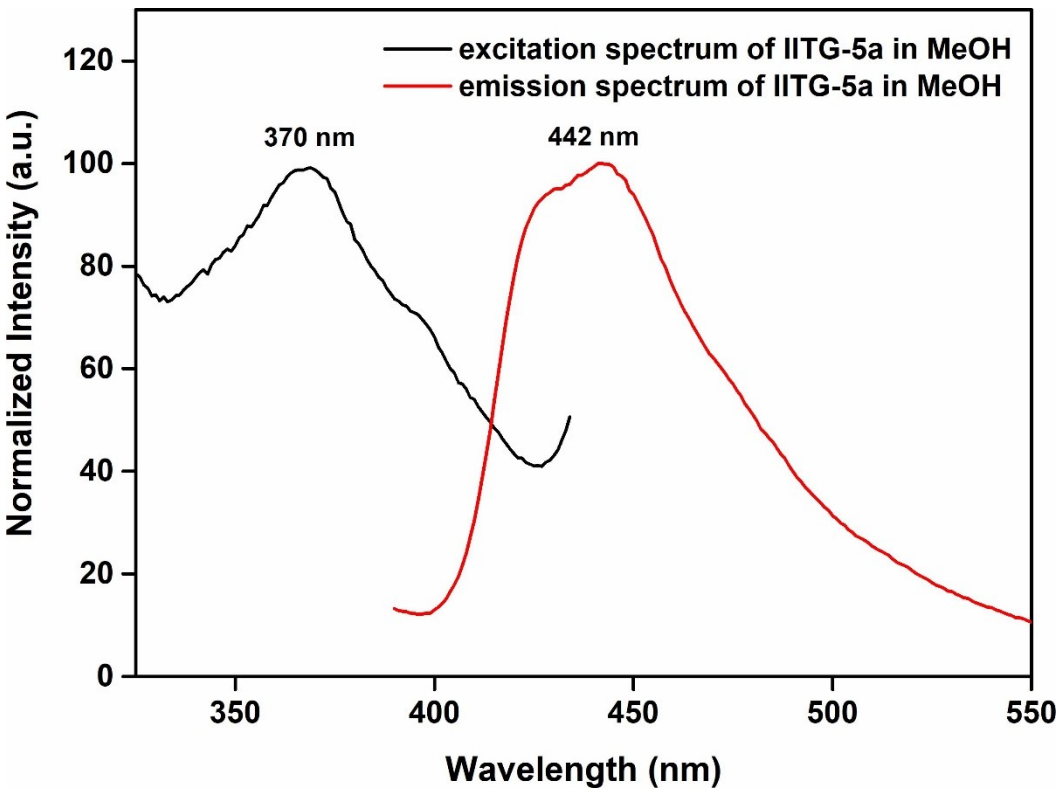

Fig. S18. Excitation (black) and emission (red) spectra of **IITG-5a** in MeOH.

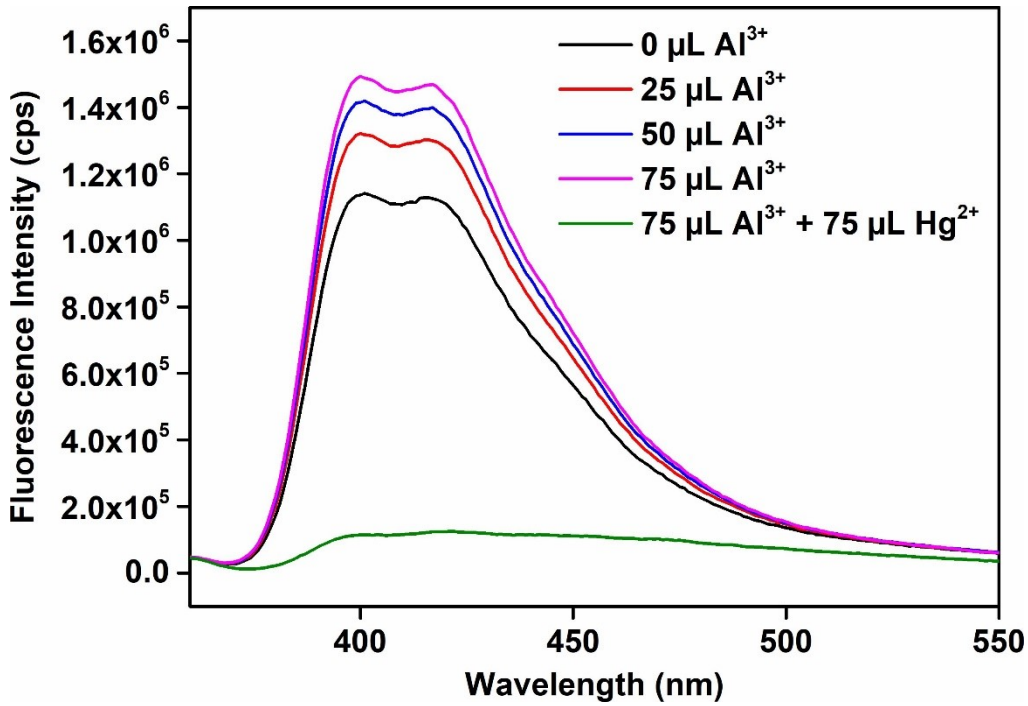

Fig. S19. Quenching in fluorescence emission intensity of the aqueous solution of **IITG-5a** after addition of 75 μL of 10 mM aqueous Hg^{2+} solution in presence of 75 μL of 10 mM aqueous solution of Al^{3+}.

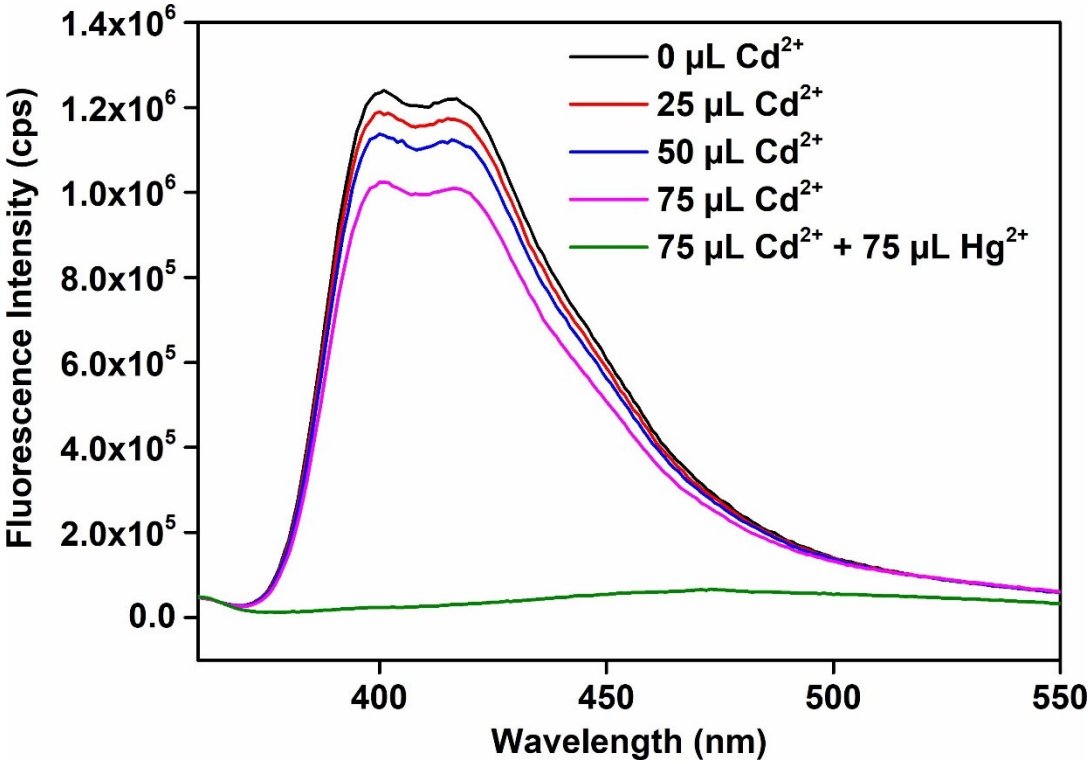

Fig. S20. Quenching in fluorescence emission intensity of the aqueous solution of **IITG-5a** after addition of 75 µL of 10 mM aqueous Hg^{2+} solution in presence of 75 µL of 10 mM aqueous solution of Cd^{2+}.

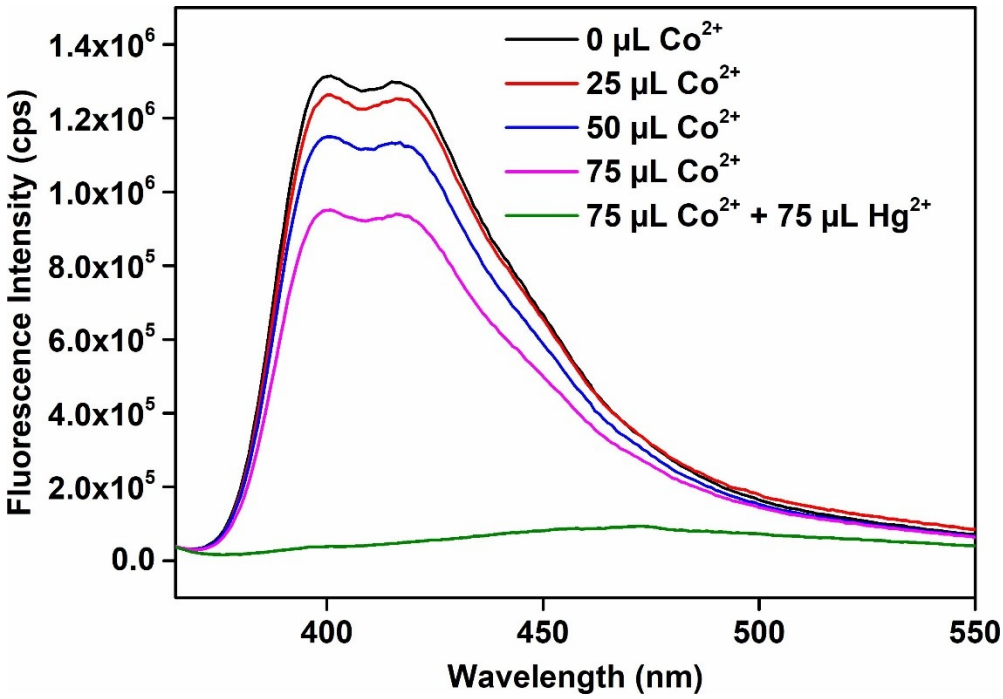

Fig. S21. Quenching in fluorescence emission intensity of the aqueous solution of **IITG-5a** after addition of 75 µL of 10 mM aqueous Hg^{2+} solution in presence of 75 µL of 10 mM aqueous solution of Co^{2+}.

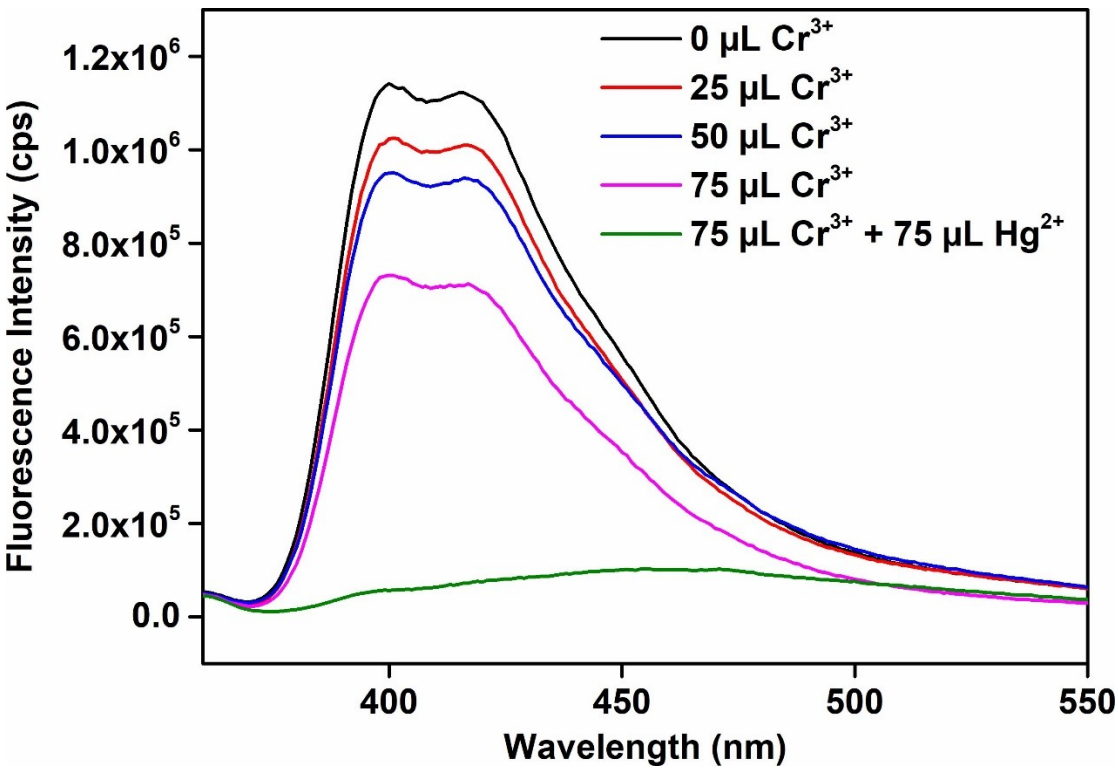

Fig. S22. Quenching in fluorescence emission intensity of the aqueous solution of **IITG-5a** after addition of 75 μL of 10 mM aqueous Hg^{2+} solution in presence of 75 μL of 10 mM aqueous solution of Cr^{3+}.

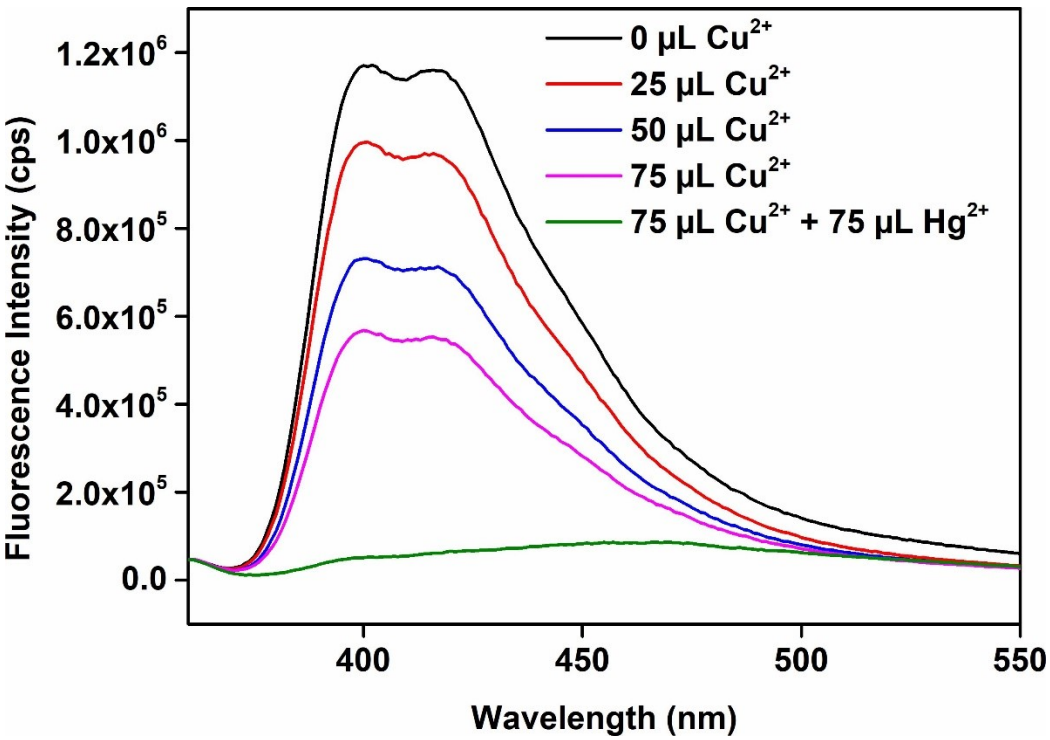

Fig. S23. Quenching in fluorescence emission intensity of the aqueous solution of **IITG-5a** after addition of 75 μL of 10 mM aqueous Hg^{2+} solution in presence of 75 μL of 10 mM aqueous solution of Cu^{2+}.

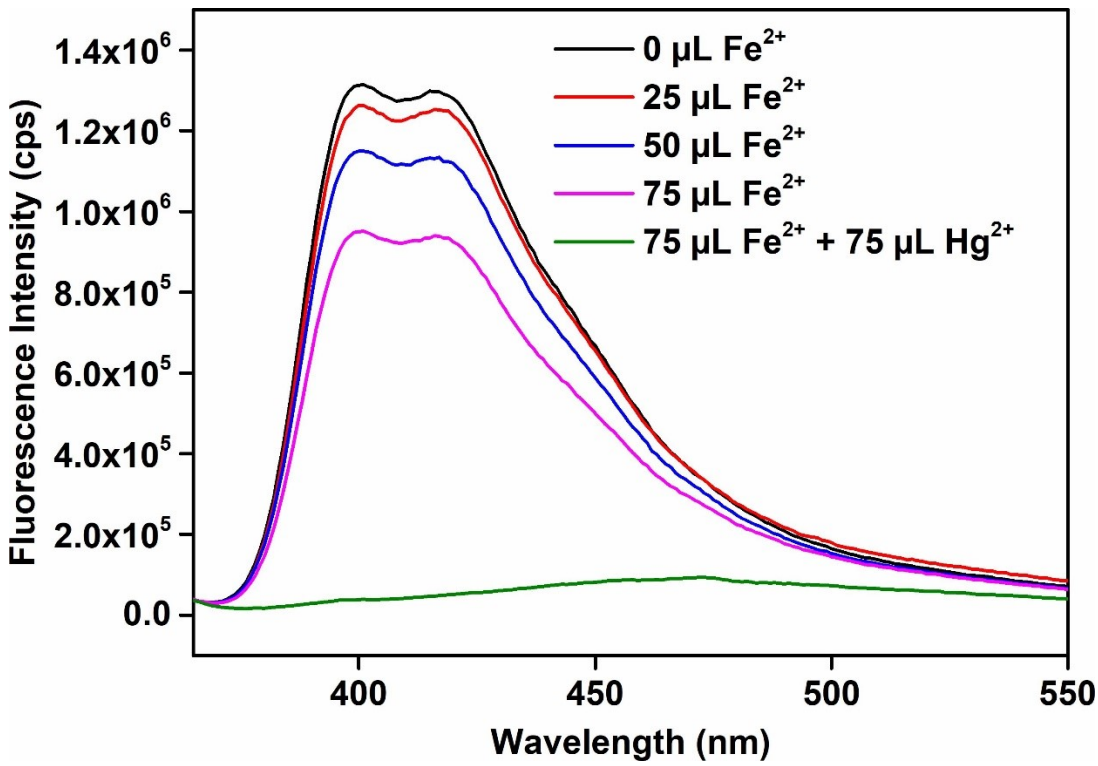

Fig. S24. Quenching in fluorescence emission intensity of the aqueous solution of **IITG-5a** after addition of 75 μL of 10 mM aqueous Hg^{2+} solution in presence of 75 μL of 10 mM aqueous solution of Fe^{2+}.

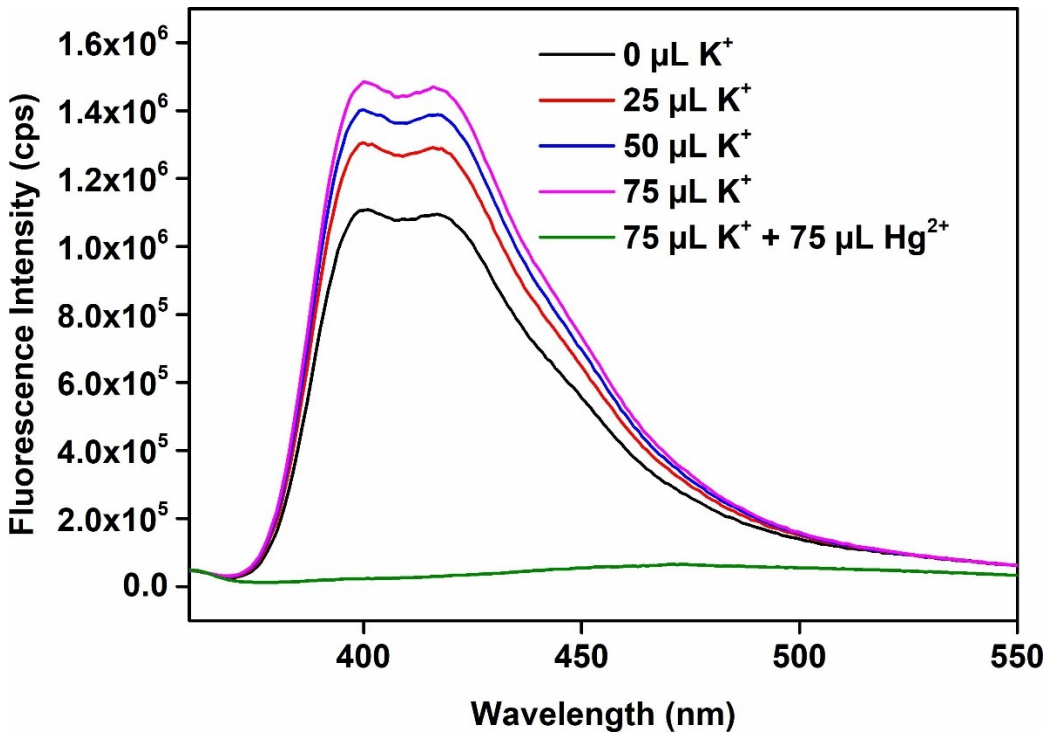

Fig. S25. Quenching in fluorescence emission intensity of the aqueous solution of **IITG-5a** after addition of 75 μL of 10 mM aqueous Hg^{2+} solution in presence of 75 μL of 10 mM aqueous solution of K^{+}.

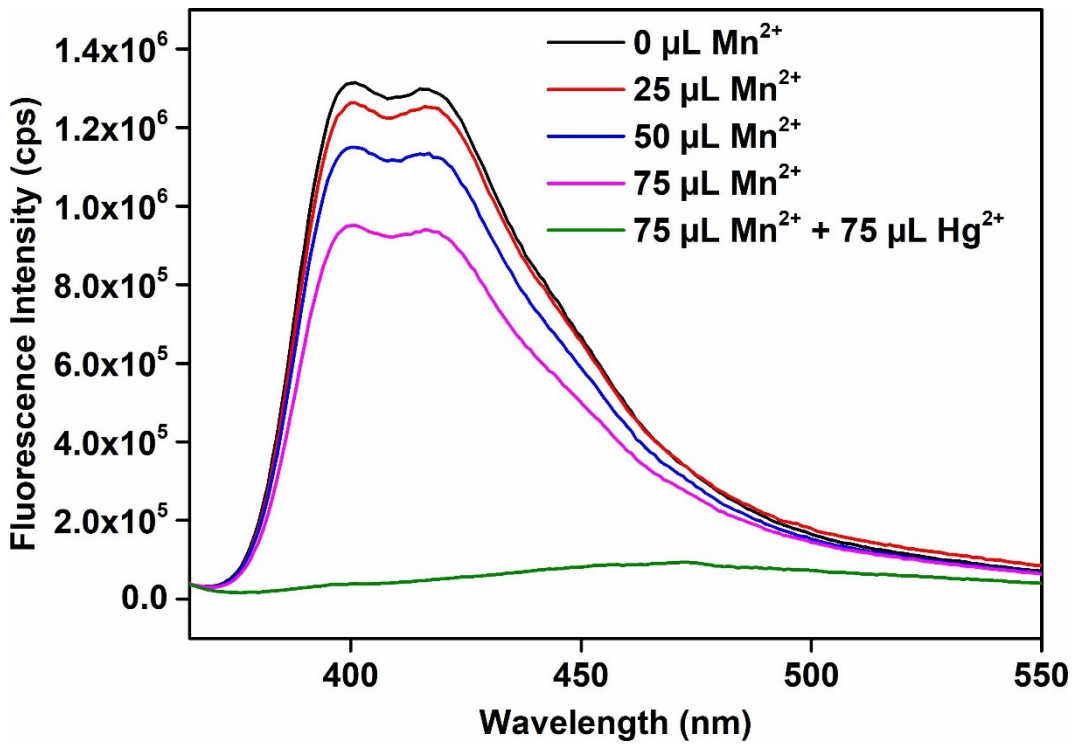

Fig. S26. Quenching in fluorescence emission intensity of the aqueous solution of **IITG-5a** after addition of 75 μL of 10 mM aqueous Hg^{2+} solution in presence of 75 μL of 10 mM aqueous solution of Mn^{2+}.

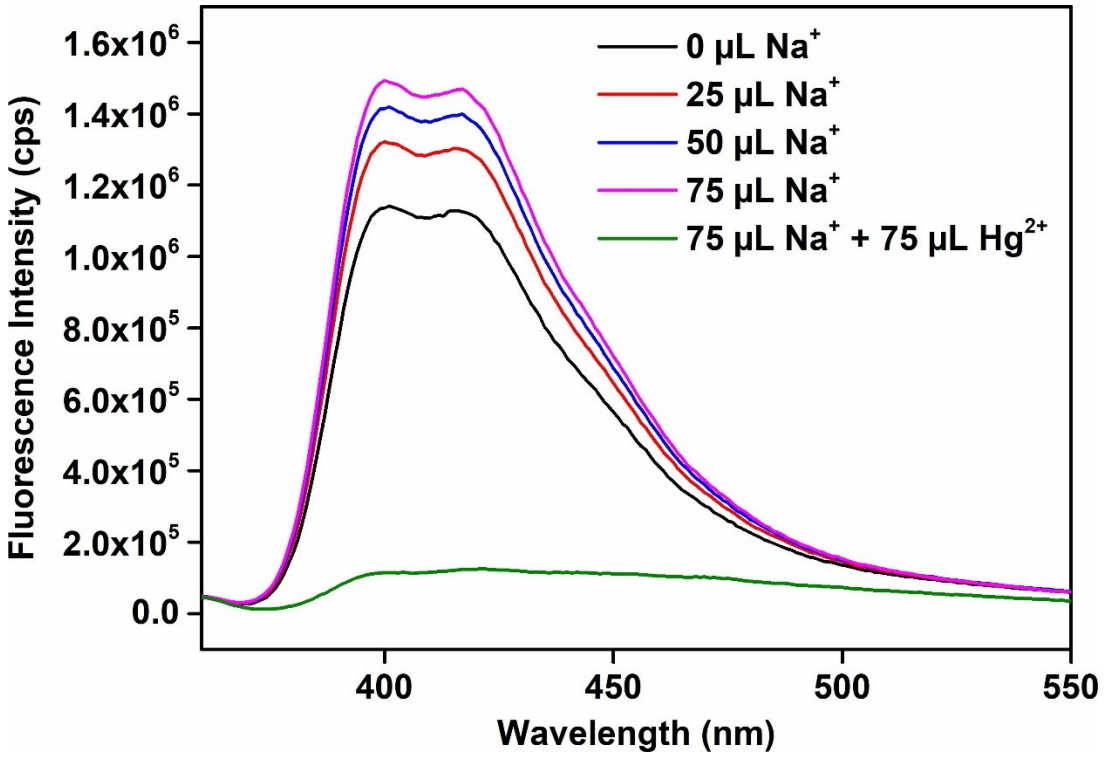

Fig. S27. Quenching in fluorescence emission intensity of the aqueous solution of **IITG-5a** after addition of 75 μL of 10 mM aqueous Hg^{2+} solution in presence of 75 μL of 10 mM aqueous solution of Na^{+}.

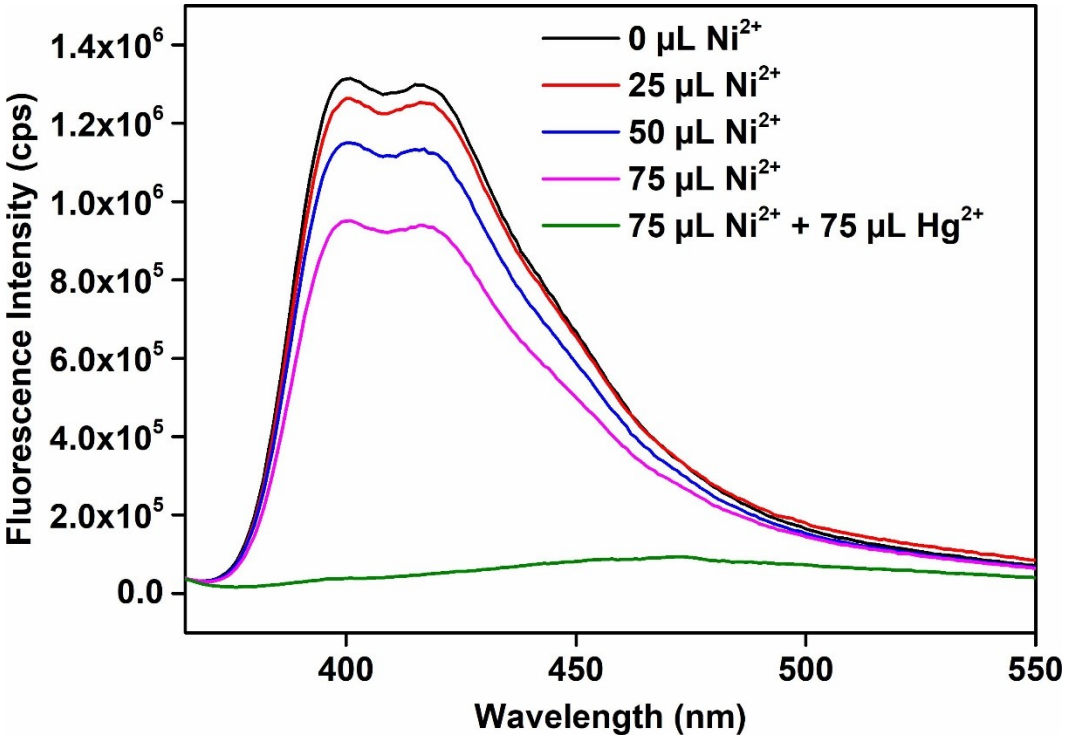

Fig. S28. Quenching in fluorescence emission intensity of the aqueous solution of **IITG-5a** after addition of 75 μL of 10 mM aqueous Hg^{2+} solution in presence of 75 μL of 10 mM aqueous solution of Ni^{2+}.

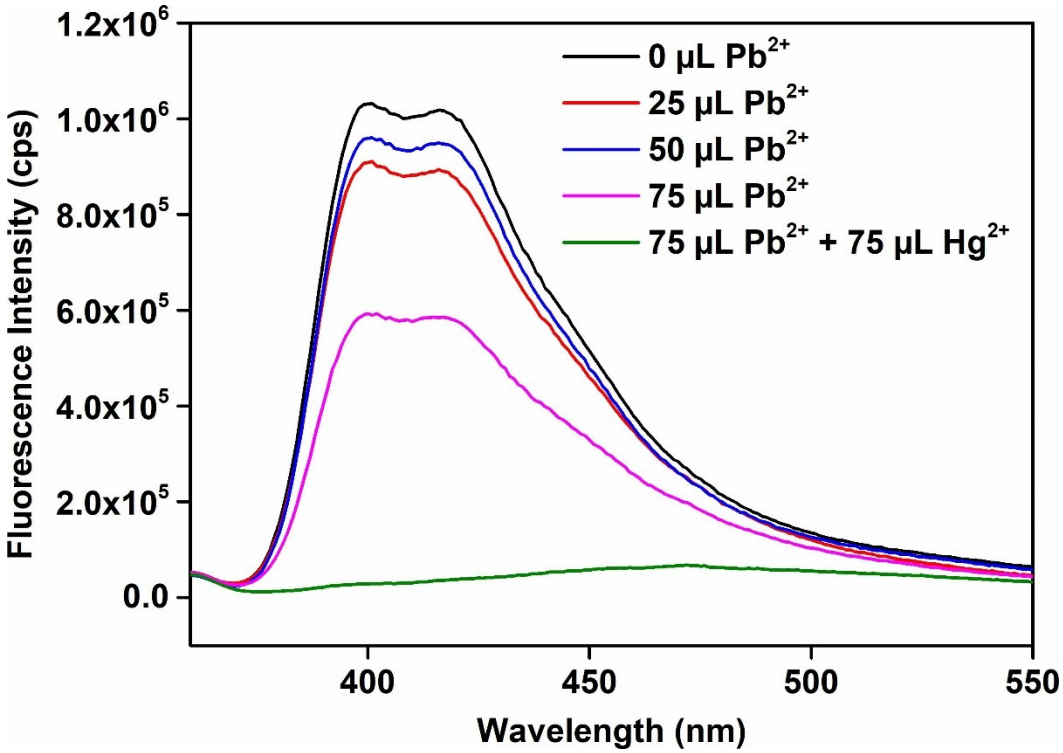

Fig. S29. Quenching in fluorescence emission intensity of the aqueous solution of **IITG-5a** after addition of 75 μL of 10 mM aqueous Hg^{2+} solution in presence of 75 μL of 10 mM aqueous solution of Pb^{2+}.

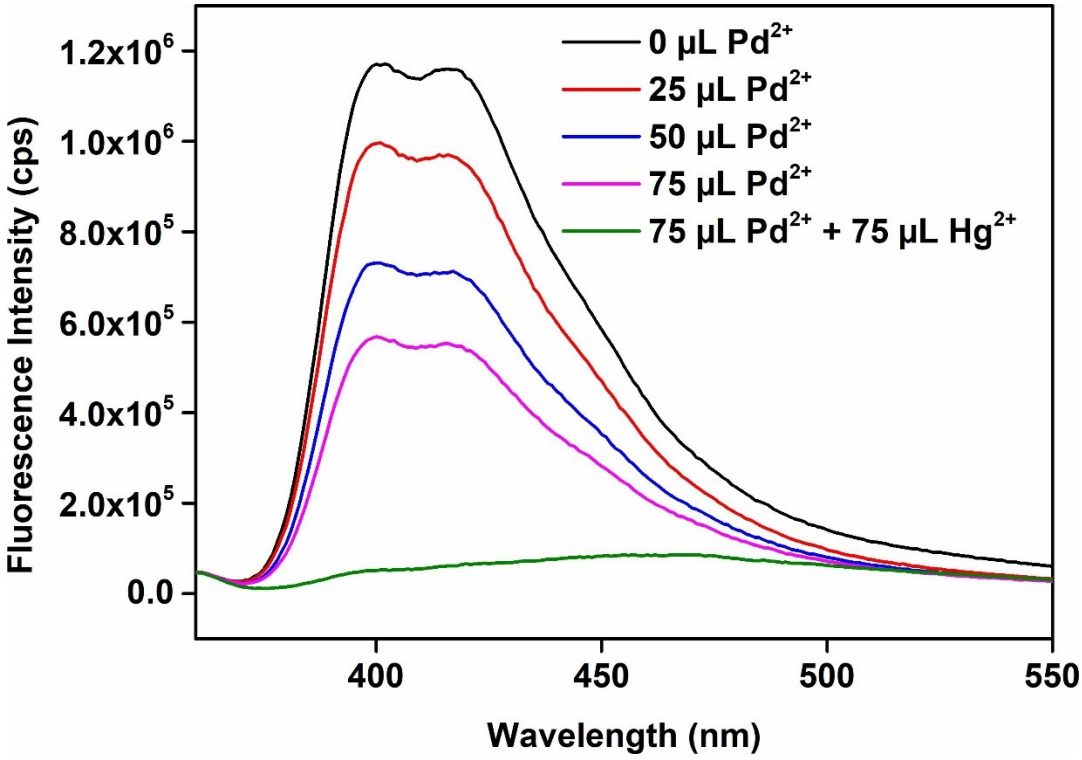

Fig. S30. Quenching in fluorescence emission intensity of the aqueous solution of **IITG-5a** after addition of 75 μL of 10 mM aqueous Hg^{2+} solution in presence of 75 μL of 10 mM aqueous solution of Pd^{2+}.

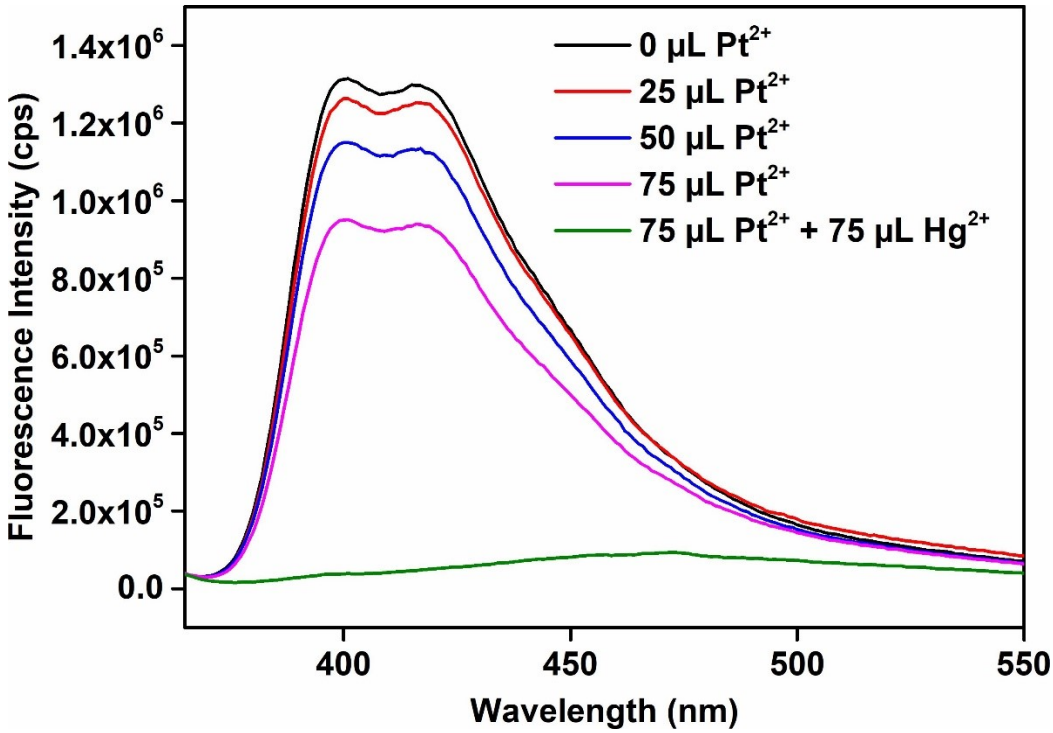

Fig. S31. Quenching in fluorescence emission intensity of the aqueous solution of **IITG-5a** after addition of 75 μL of 10 mM aqueous Hg^{2+} solution in presence of 75 μL of 10 mM aqueous solution of Pt^{2+}.

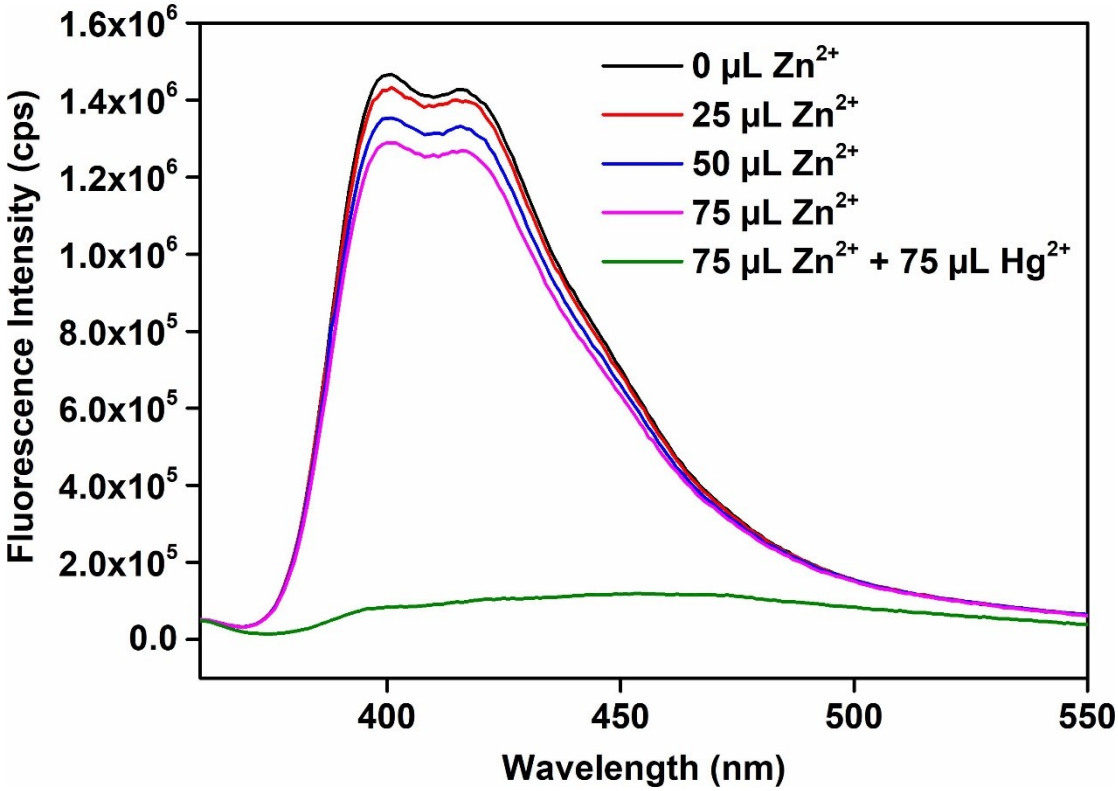

Fig. S32. Quenching in fluorescence emission intensity of the aqueous solution of **IITG-5a** after addition of 75 μL of 10 mM aqueous Hg^{2+} solution in presence of 75 μL of 10 mM aqueous solution of Zn^{2+}.

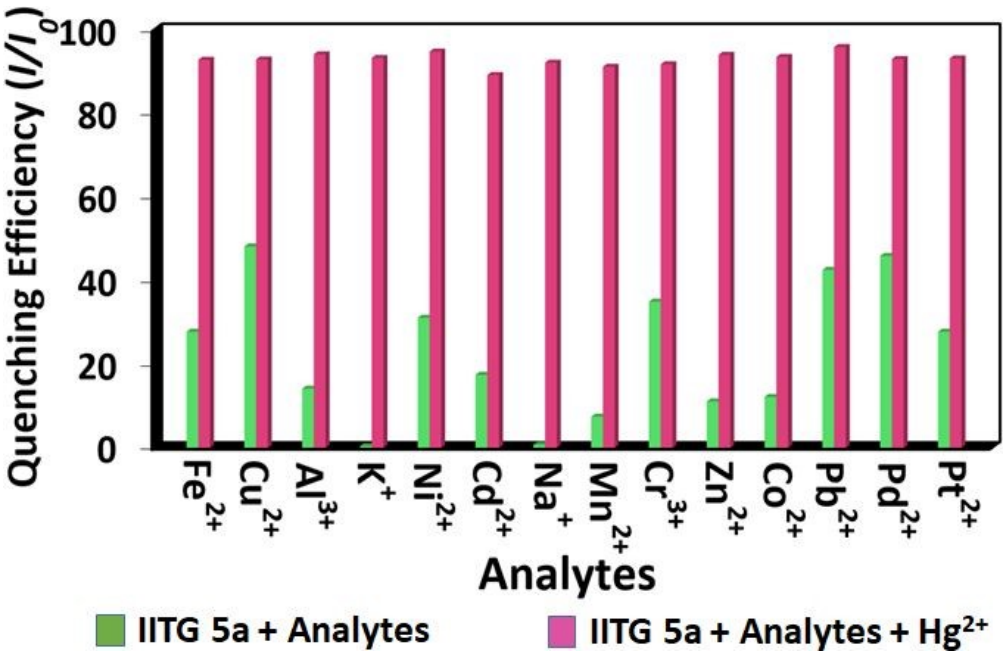

Fig. S33. Change in emission response of **IITG-5a** after the inclusion of 75 μL of 10 mM Hg^{2+} in the co-existence of 75 μL of 10 mM solutions (in H_2O) of various competitor metal ions of Hg^{2+} (λ_{ex} = 320 nm, λ_{em} = 420 nm).

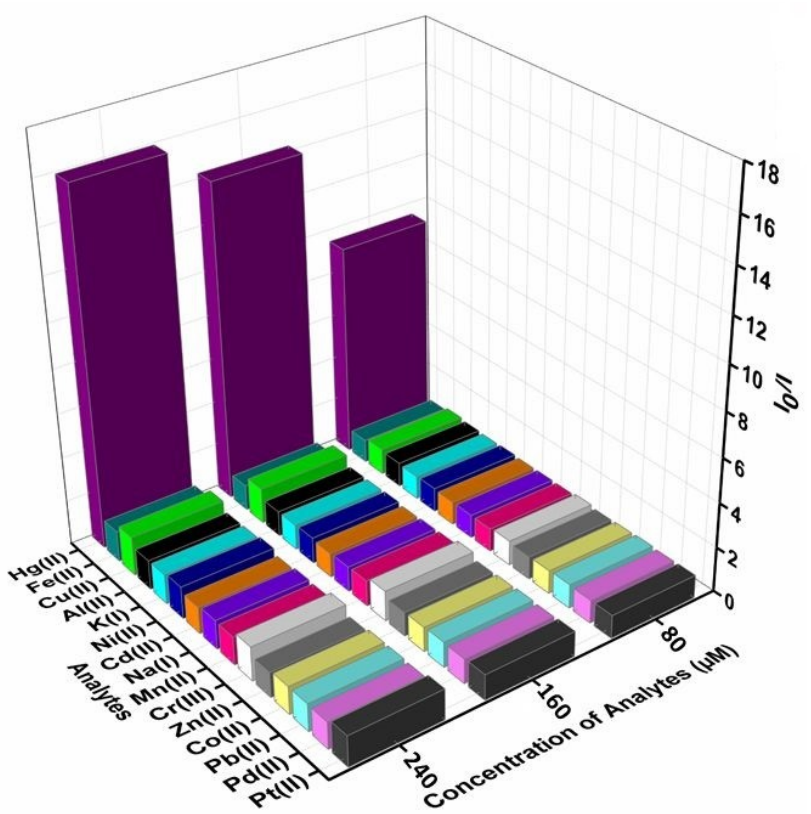

Fig. S34. S-V plots for the decrease in luminescence intensities of **IITG-5a** with gradual addition of various analytes in case of Hg^{2+} sensing.

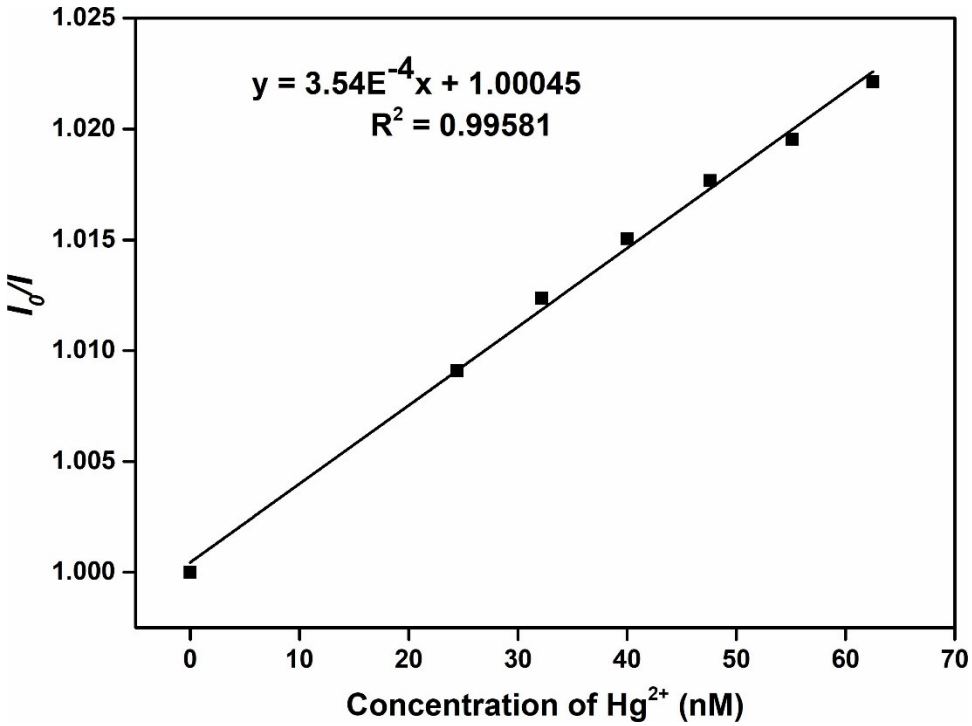

Fig. S35. Stern-Volmer plot for the fluorescence emission quenching of **IITG-5a** in presence of Hg^{2+} solution.

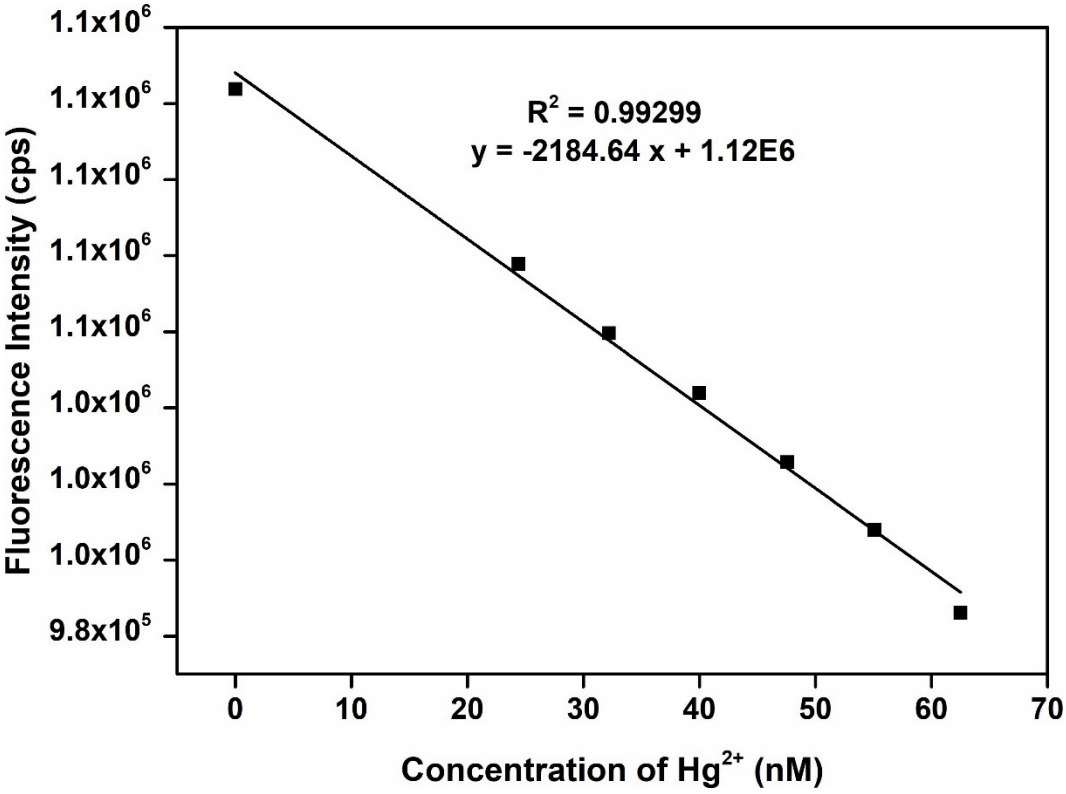

Fig. S36. Change in the fluorescence intensity of **IITG-5a** in water as a function of concentration of Hg^{2+}.

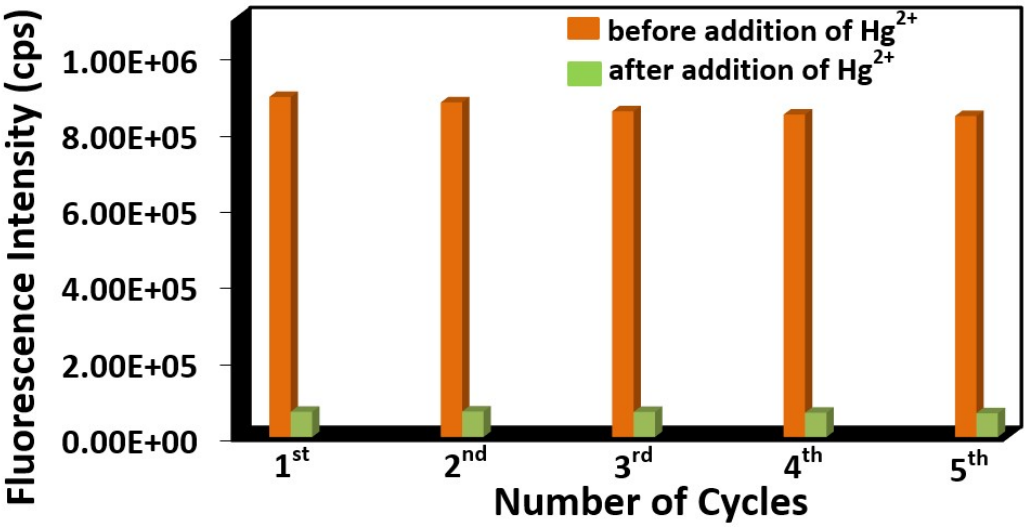

Fig. S37. Recyclability plot of **IITG-5a** towards the sensing of Hg^{2+} in water.

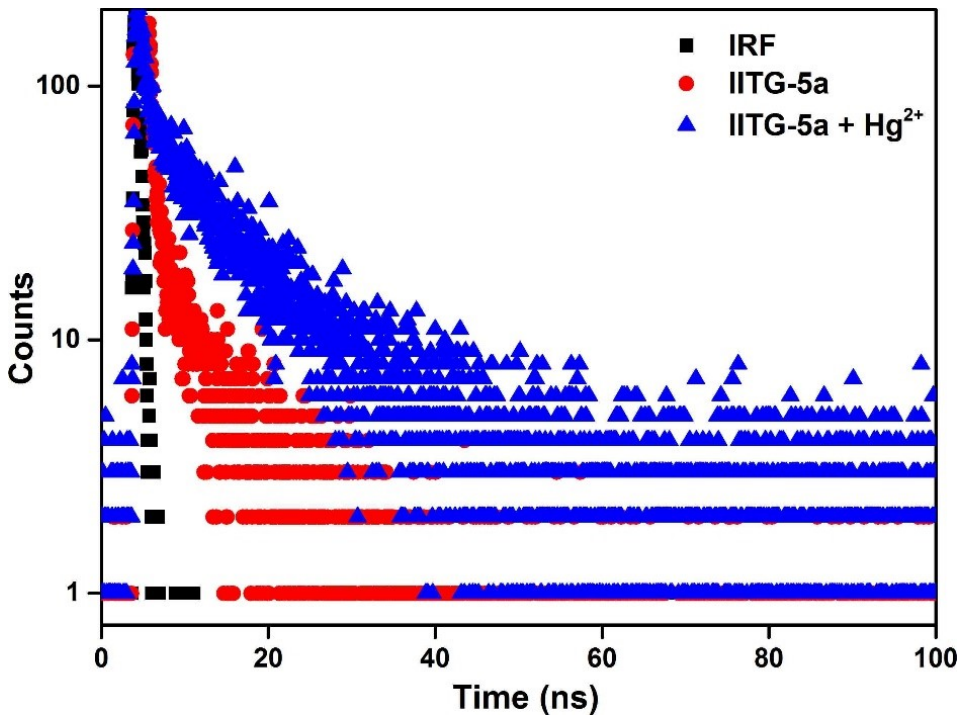

Fig. S38. Lifetime decay profile of **IITG-5a** in absence and presence of Hg^{2+} solution (λ_{ex} = 320 nm, monitored at 308 nm). Here, IRF = instrument response function.

Table S2. Fluorescence lifetimes of **IITG-5a** before and after the addition of Hg^{2+} solution (λ_{ex} = 320 nm, pulsed diode laser).

Volume of NFT solution added (μL)	a_1	a_2	τ_1 (ns)	τ_2 (ns)	$<\tau>$* (ns)
0	0.82	0.18	0.61	8.81	2.08
100	0.78	0.22	0.58	7.39	2.07

* $<\tau> = a_1\tau_1 + a_2\tau_2$

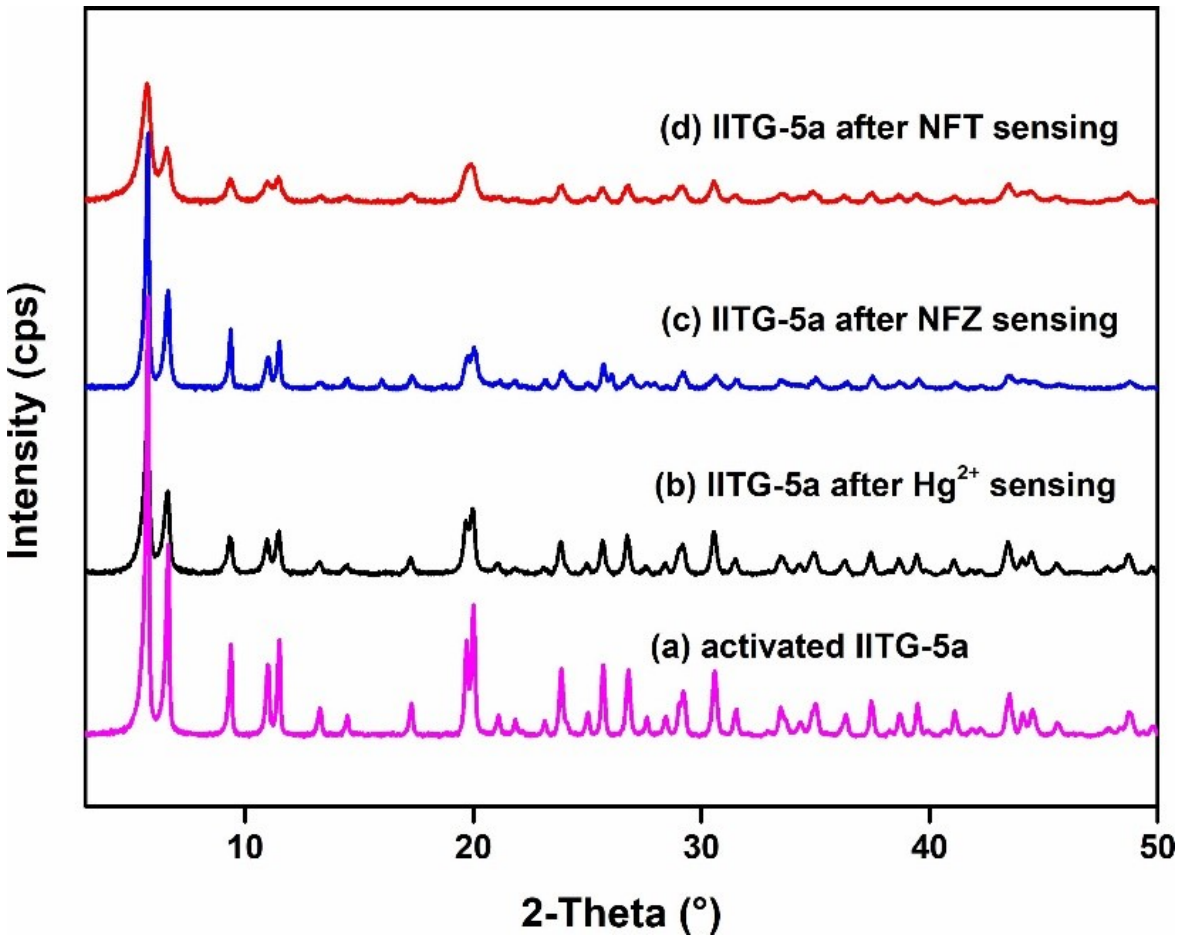

Fig. S39. PXRD patterns of compound **IITG-5a** before (a) and after (b) treatment with Hg^{2+} in aqueous medium, (c) after treatment with NFZ, and (d) after treatment with NFT in MeOH.

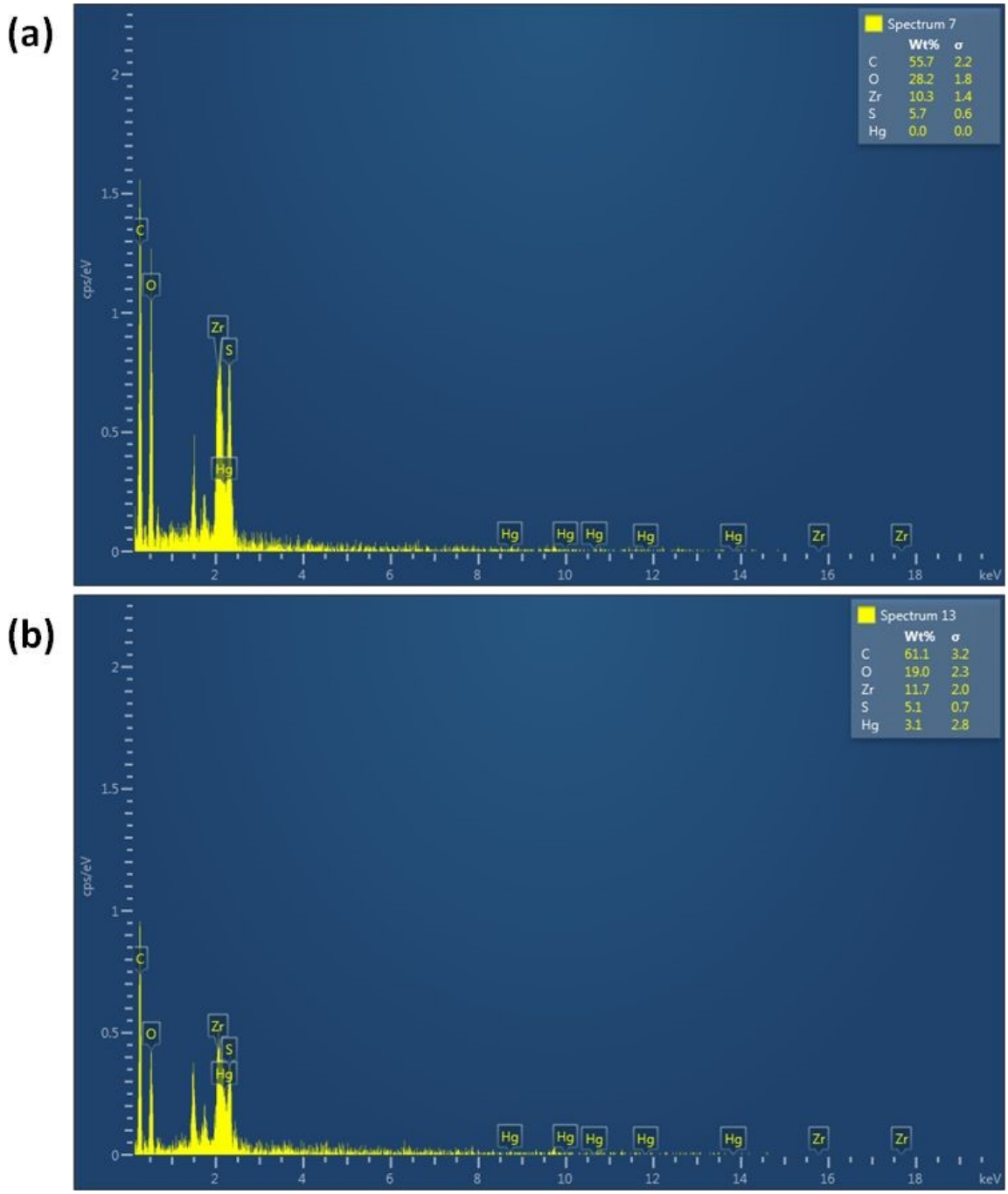

Fig. S40. EDX spectrum of **IITG-5a** (a) before and (b) after treatment with 10 mM Hg^{2+} solution under sensing conditions.

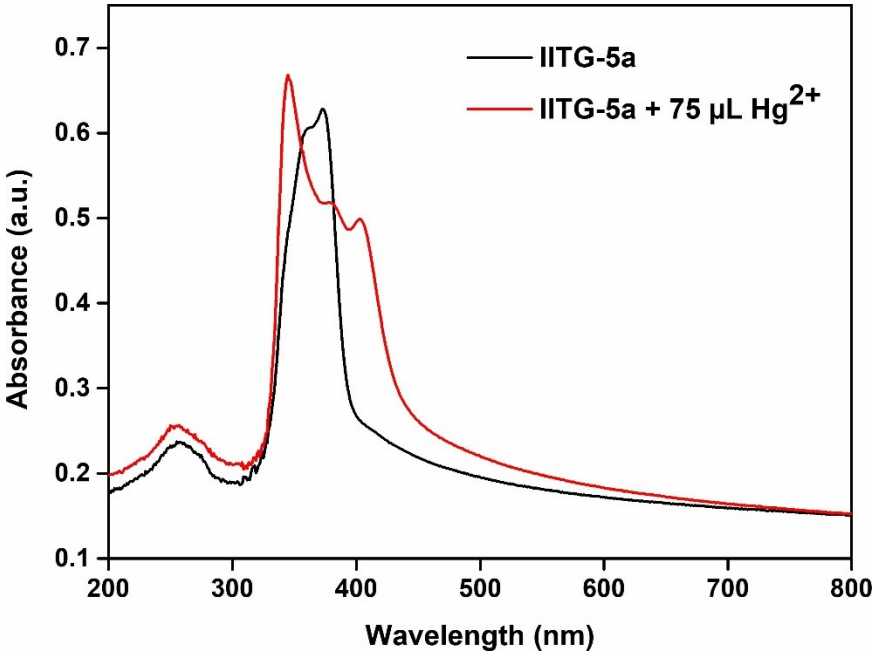

Fig. S41. UV-Vis spectra of compound **IITG-5a** in absence (black) and presence (red) of solution (75 μL, 10 mM).

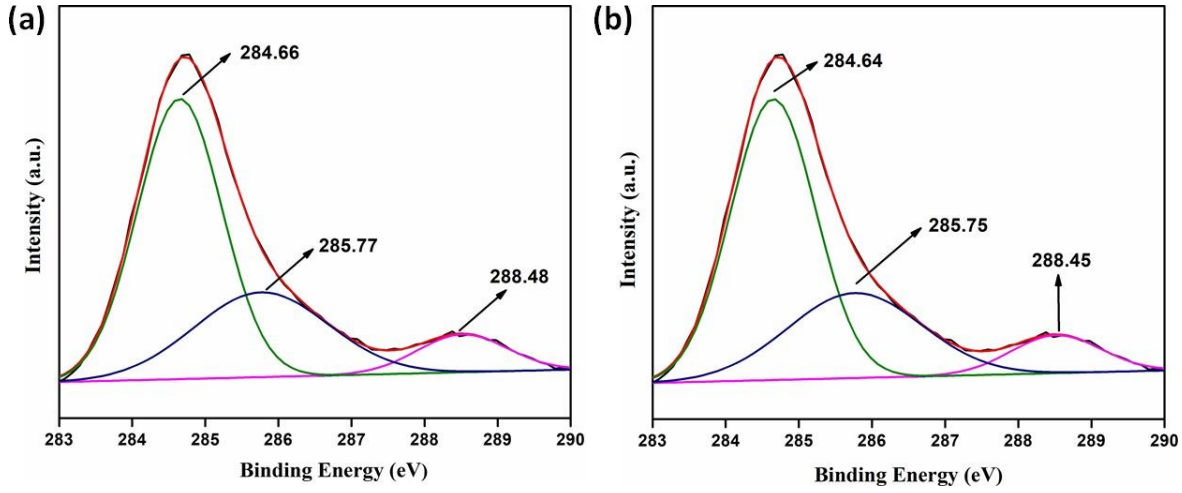

Fig. S42. Fitted XPS spectra of C (1s) before (a) and after (b) treatment of **IITG-5a** with Hg^{2+}.

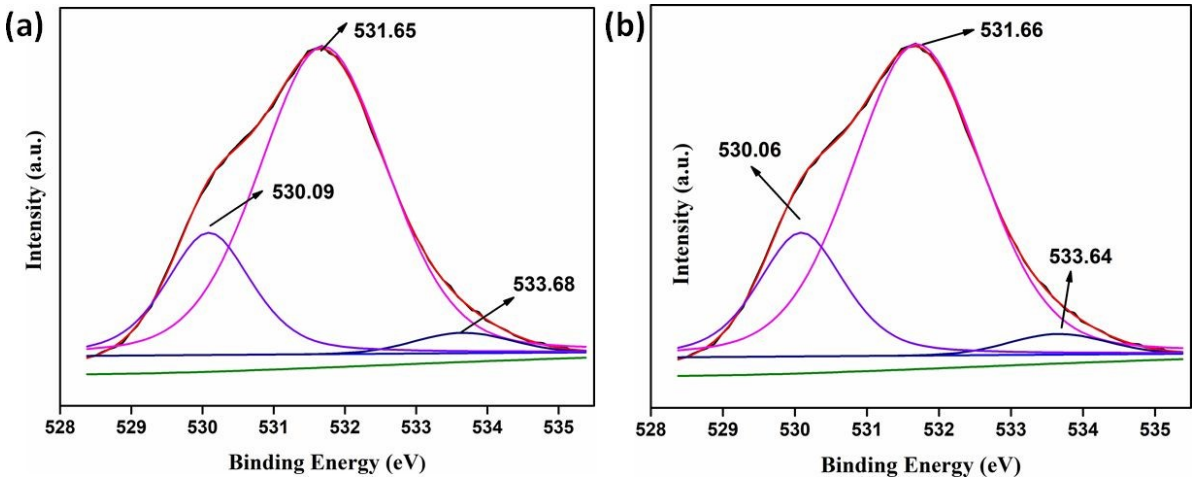

Fig. S43. Fitted XPS spectra of O (1s) before (a) and after (b) treatment of **IITG-5a** with Hg^{2+}.

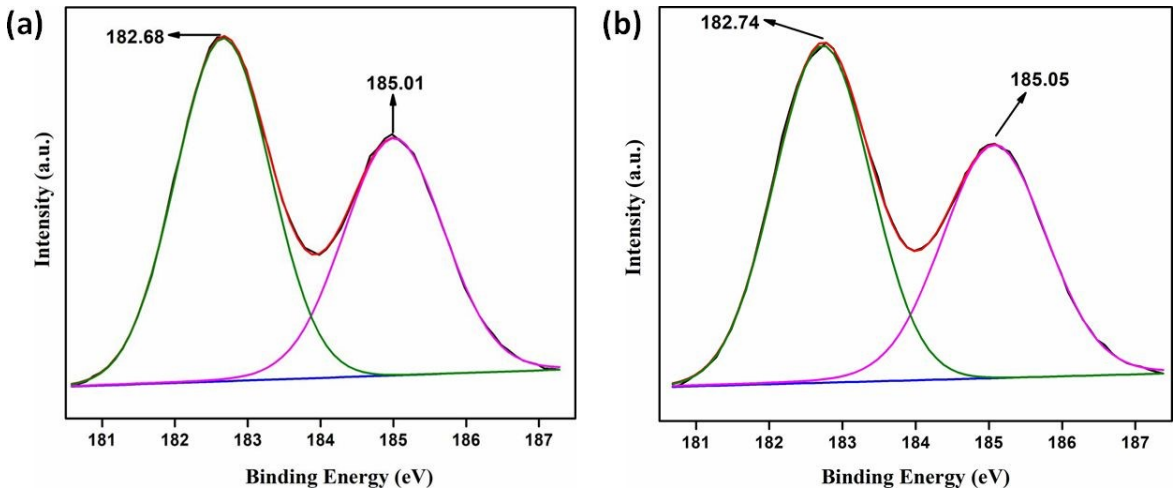

Fig. S44. Fitted XPS spectra of Zr (3d) before (a) and after (b) treatment of **IITG-5a** with Hg^{2+}

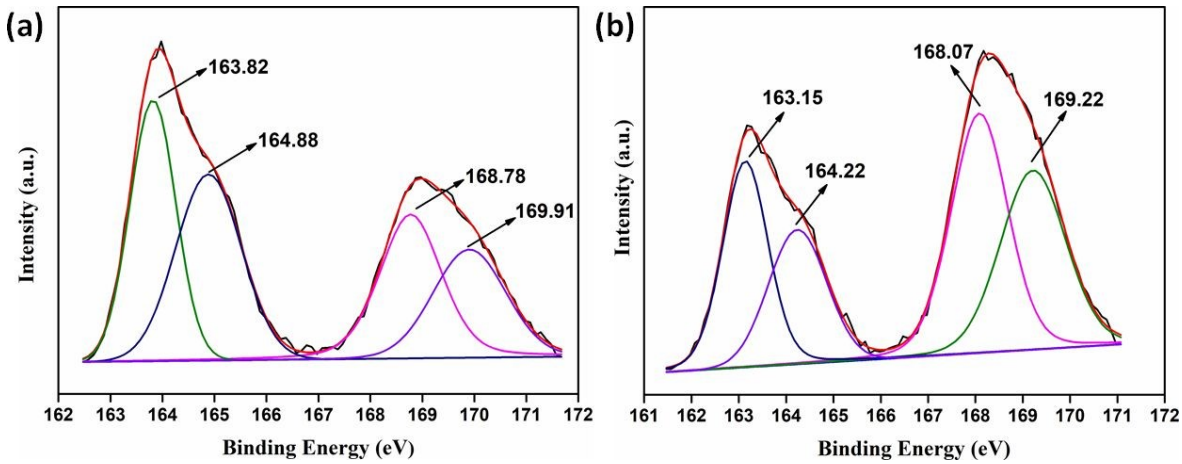

Fig. S45. Fitted XPS spectra of S (2p) before (a) and after (b) treatment of **IITG-5a** with Hg^{2+}.

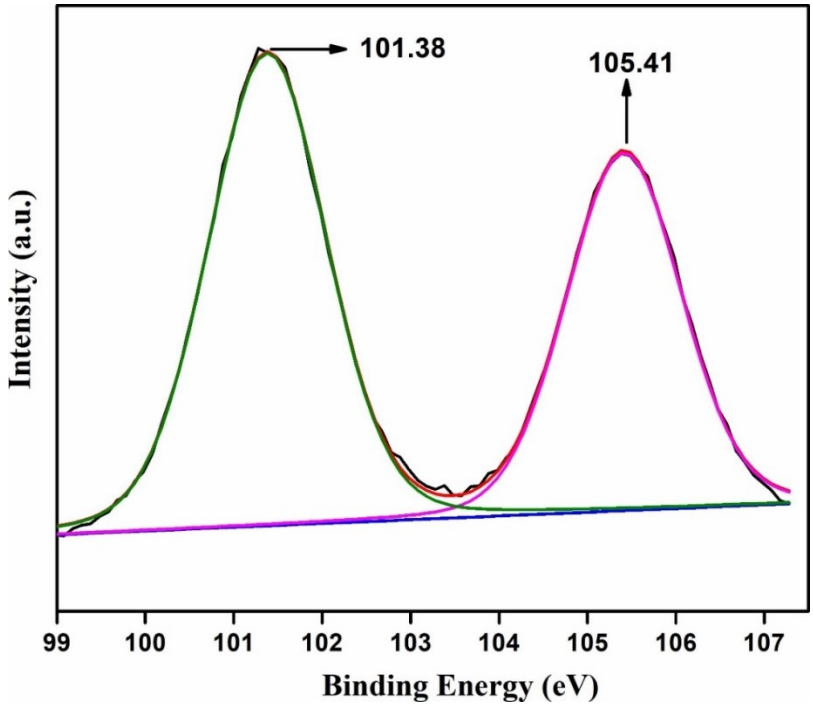

Fig. S46. Fitted XPS spectrum of Hg (4f) after treatment of **IITG-5a** with Hg^{2+}.

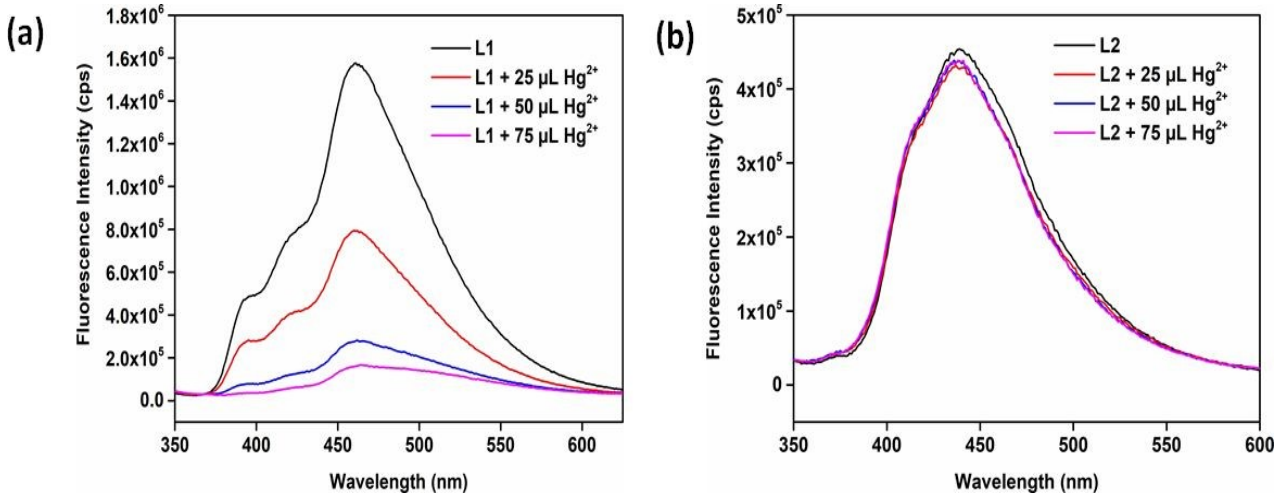

Fig. S47. Change in fluorescence emission intensity of the aqueous solution of **L1** (a) and **L2** (b) linkers after addition of 75 μL of 10 mM aqueous Hg^{2+} solution.

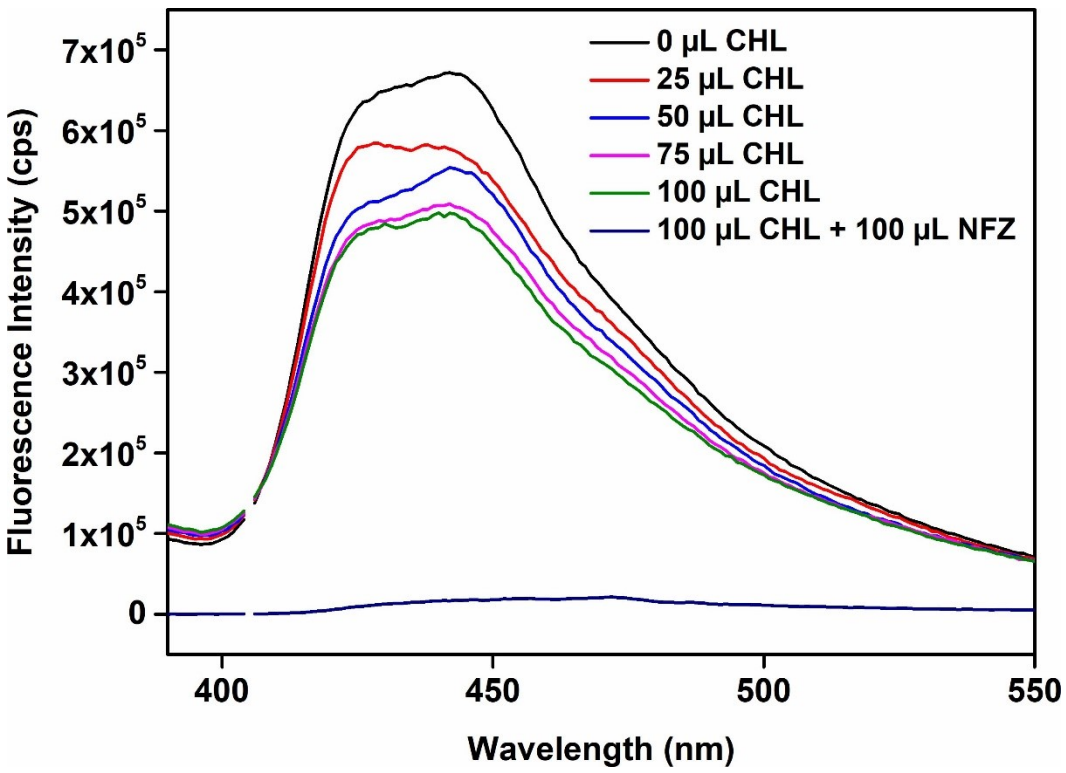

Fig. S48. Quenching in fluorescence emission intensity of the methanolic solution of **IITG-5a** after addition of 100 µL of 10 mM methanolic NFZ solution in presence of 100 µL of 10 mM methanolic solution of CHL.

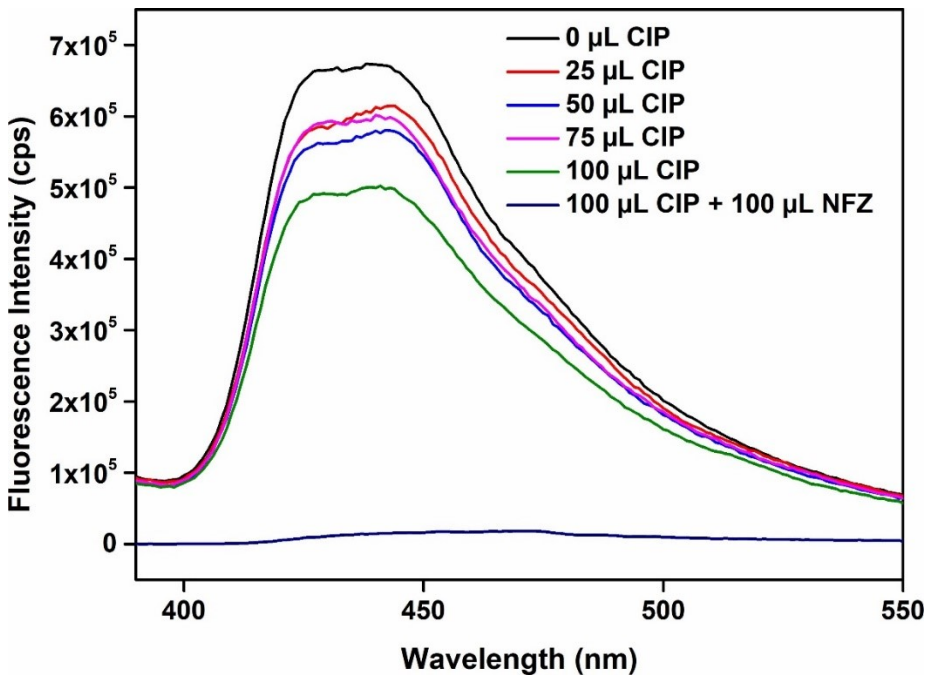

Fig. S49. Quenching in fluorescence emission intensity of the methanolic solution of **IITG-5a** after addition of 100 µL of 10 mM methanolic NFZ solution in presence of 100 µL of 10 mM methanolic solution of CIP.

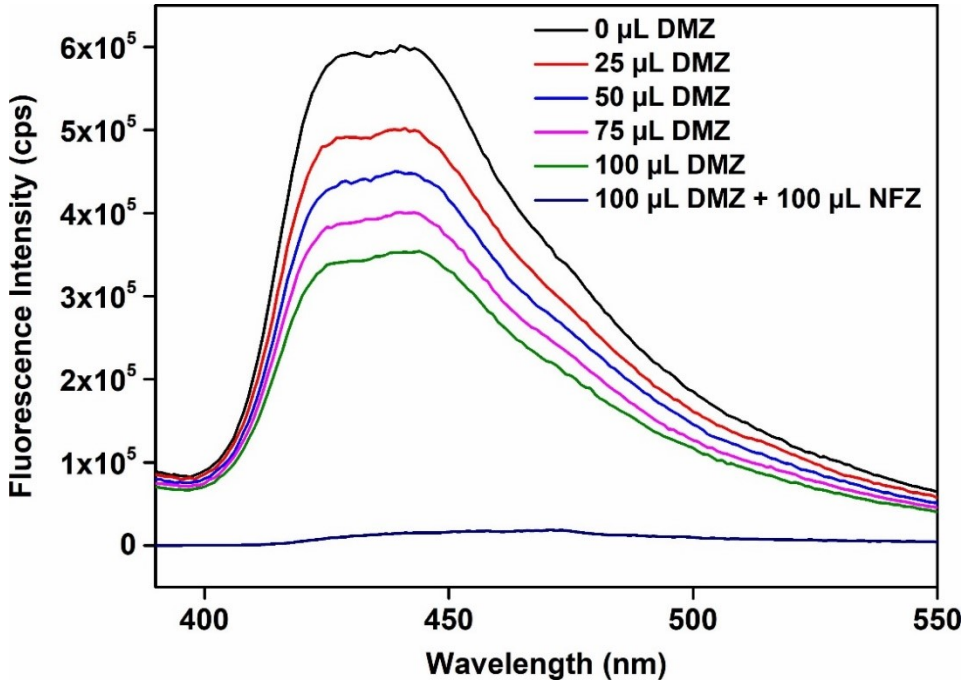

Fig. S50. Quenching in fluorescence emission intensity of the methanolic solution of **IITG-5a** after addition of 100 μL of 10 mM methanolic NFZ solution in presence of 100 μL of 10 mM methanolic solution of DMZ.

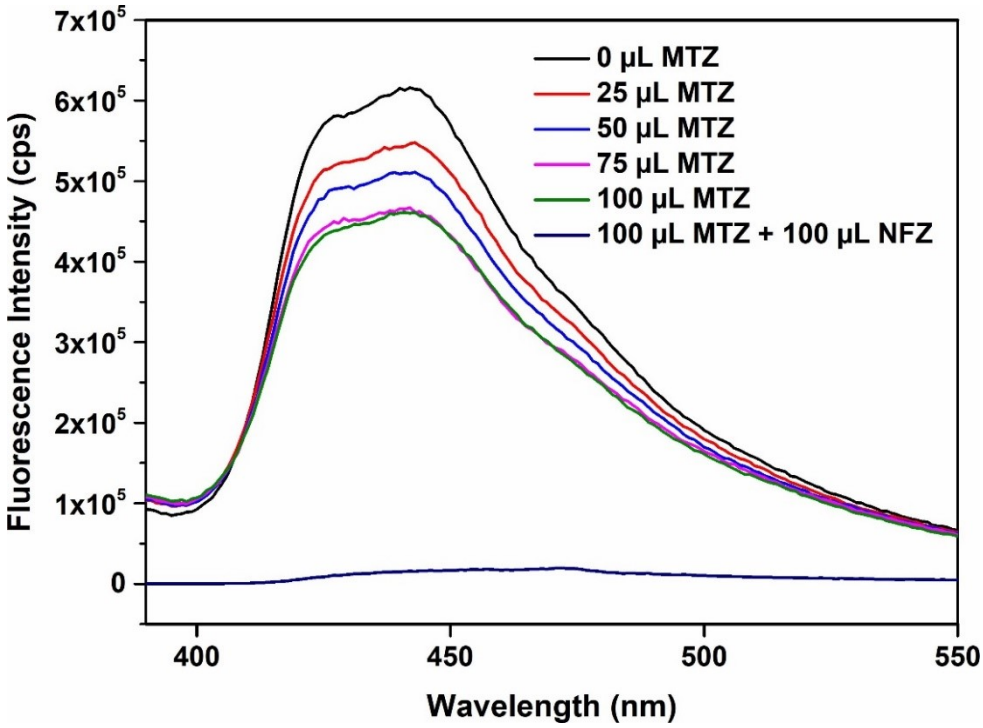

Fig. S51. Quenching in fluorescence emission intensity of the methanolic solution of **IITG-5a** after addition of 100 μL of 10 mM methanolic NFZ solution in presence of 100 μL of 10 mM methanolic solution of MTZ.

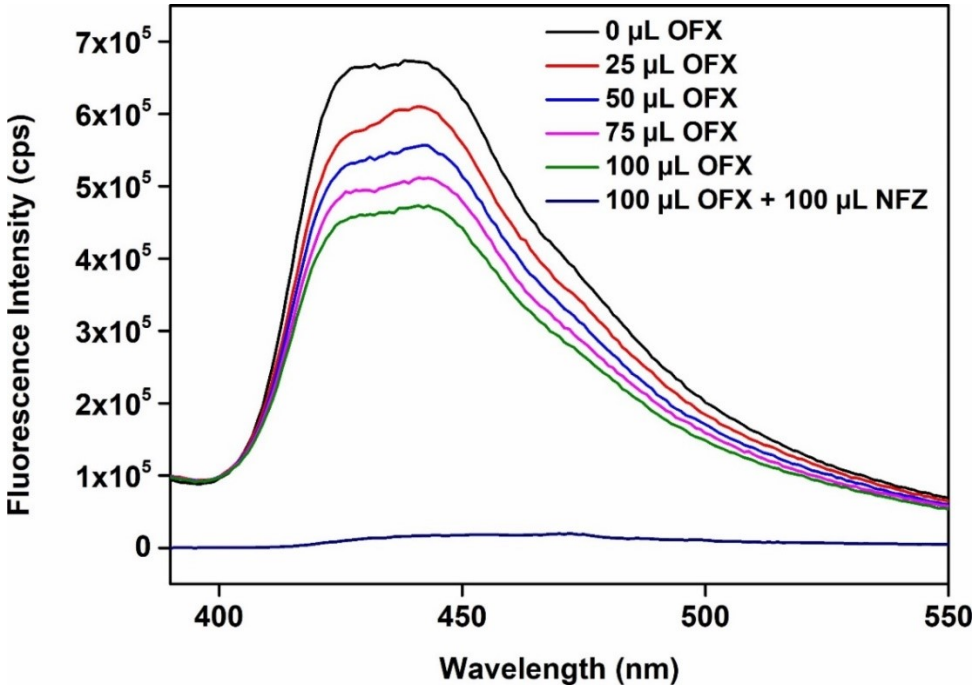

Fig. S52. Quenching in fluorescence emission intensity of the methanolic solution of **IITG-5a** after addition of 100 µL of 10 mM methanolic NFZ solution in presence of 100 µL of 10 mM methanolic solution of OFX.

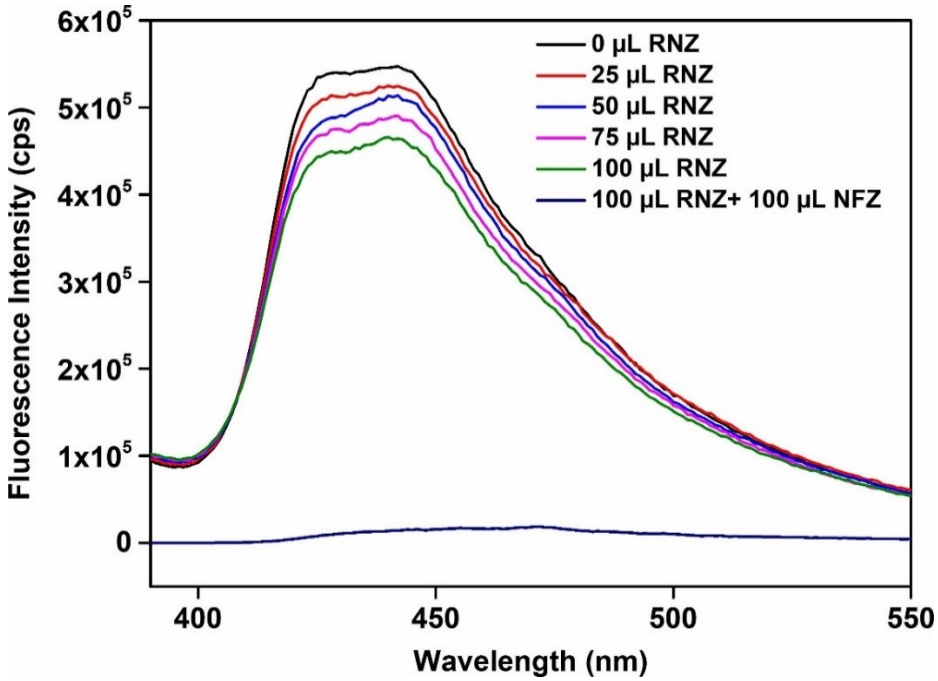

Fig. S53. Quenching in fluorescence emission intensity of the methanolic solution of **IITG-5a** after addition of 100 µL of 10 mM methanolic NFZ solution in presence of 100 µL of 10 mM methanolic solution of RNZ.

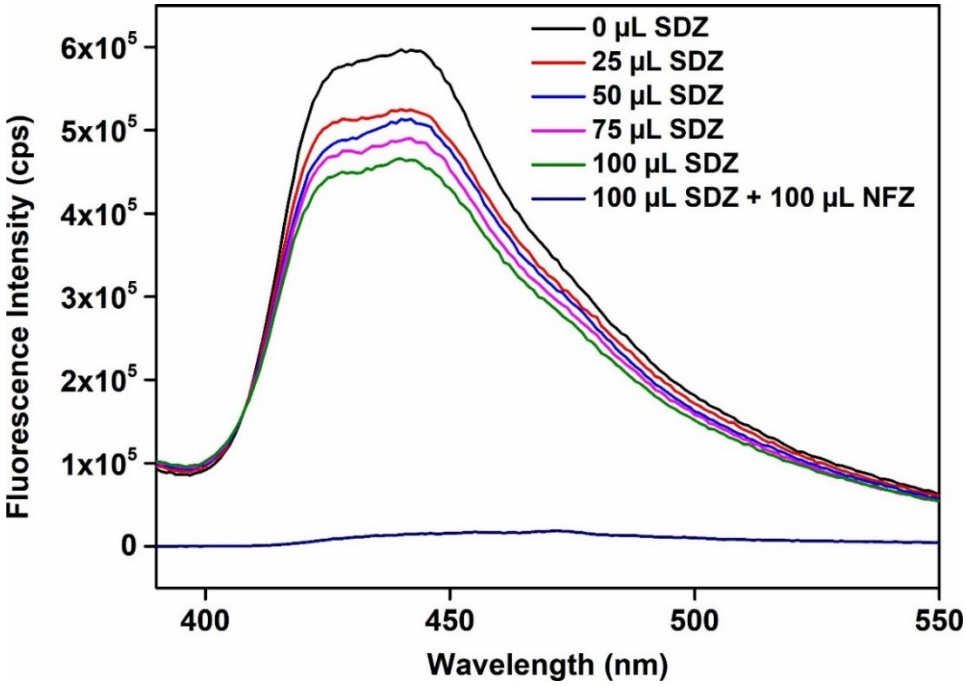

Fig. S54. Quenching in fluorescence emission intensity of the methanolic solution of **IITG-5a** after addition of 100 µL of 10 mM methanolic NFZ solution in presence of 100 µL of 10 mM methanolic solution of SDZ.

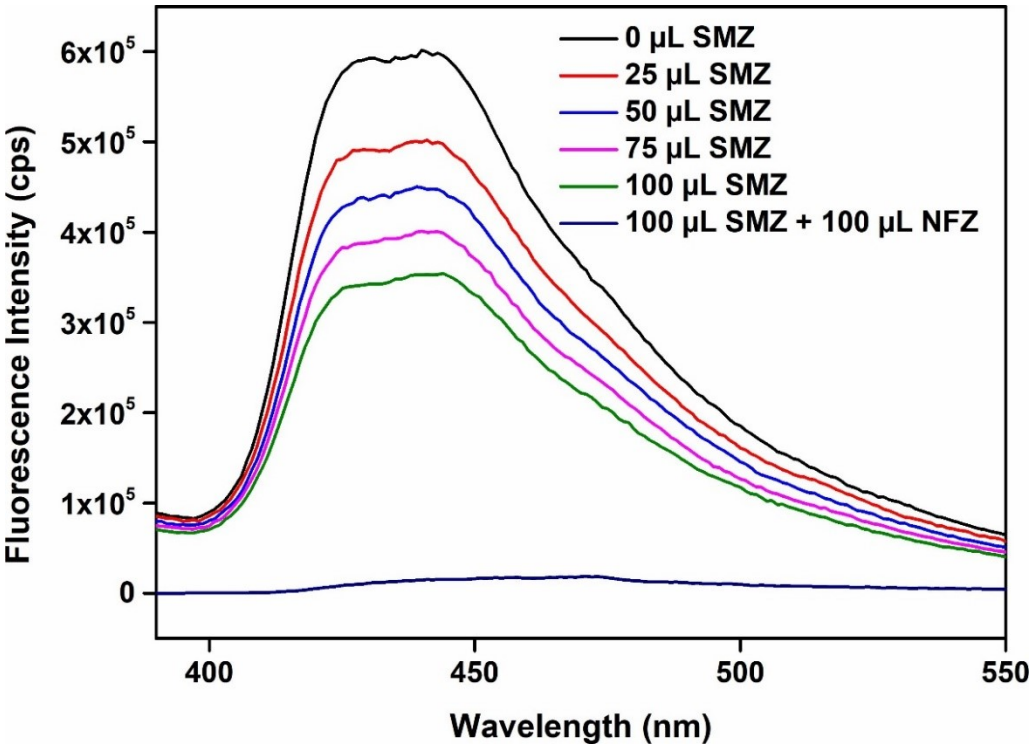

Fig. S55. Quenching in fluorescence emission intensity of the methanolic solution of **IITG-5a** after addition of 100 µL of 10 mM methanolic NFZ solution in presence of 100 µL of 10 mM methanolic solution of SMZ.

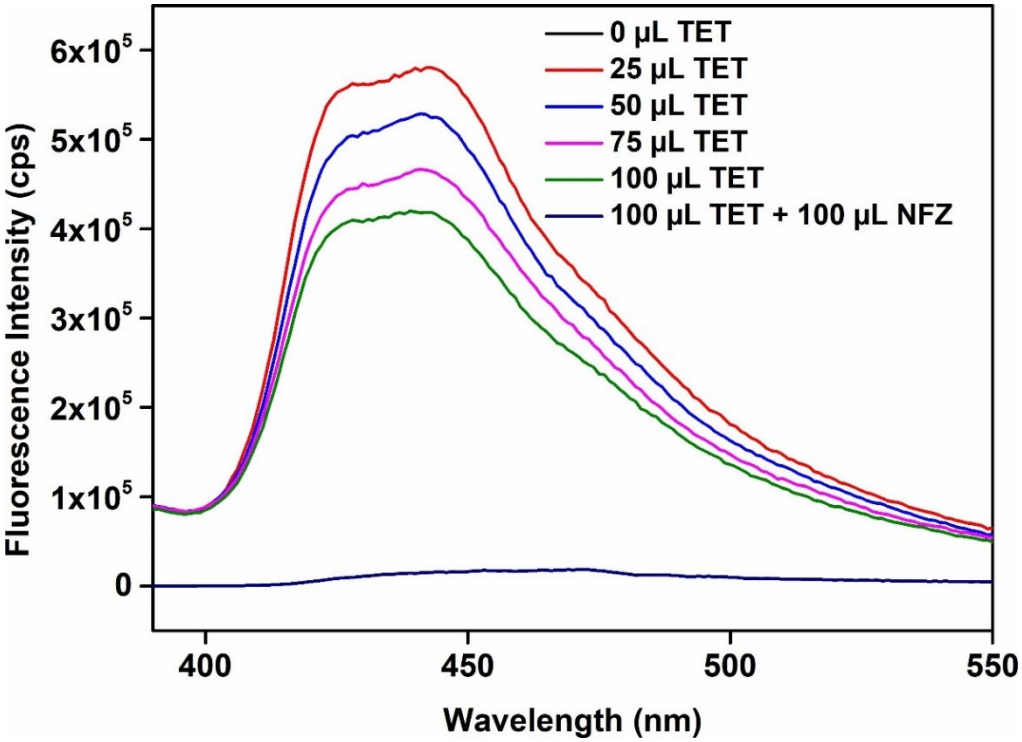

Fig. S56. Quenching in fluorescence emission intensity of the methanolic solution of **IITG-5a** after addition of 100 μL of 10 mM methanolic NFZ solution in presence of 100 μL of 10 mM methanolic solution of TET.

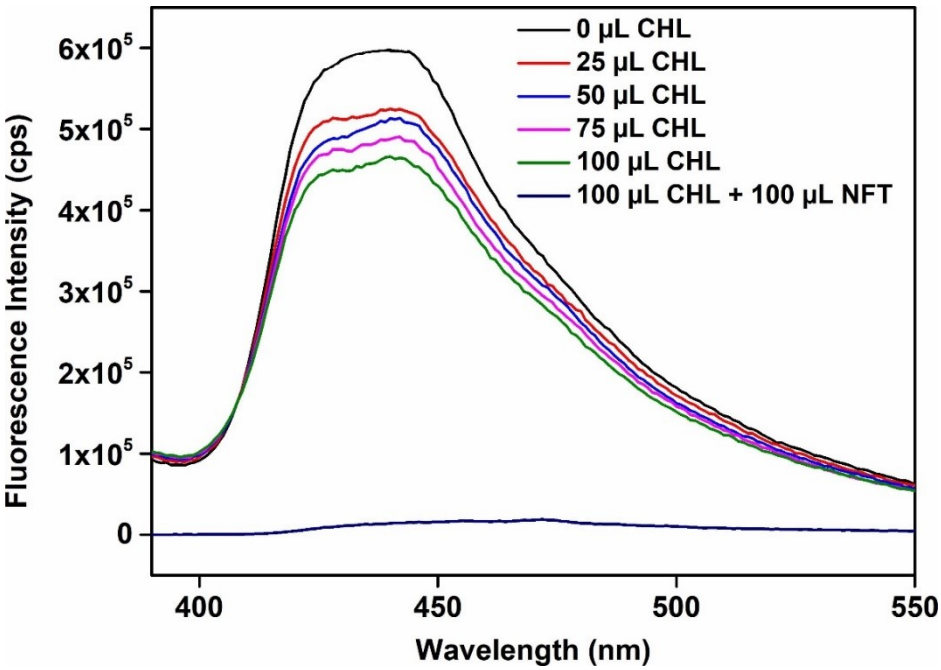

Fig. S57. Quenching in fluorescence emission intensity of the methanolic solution of **IITG-5a** after addition of 100 μL of 10 mM methanolic NFT solution in presence of 100 μL of 10 mM methanolic solution of CHL.

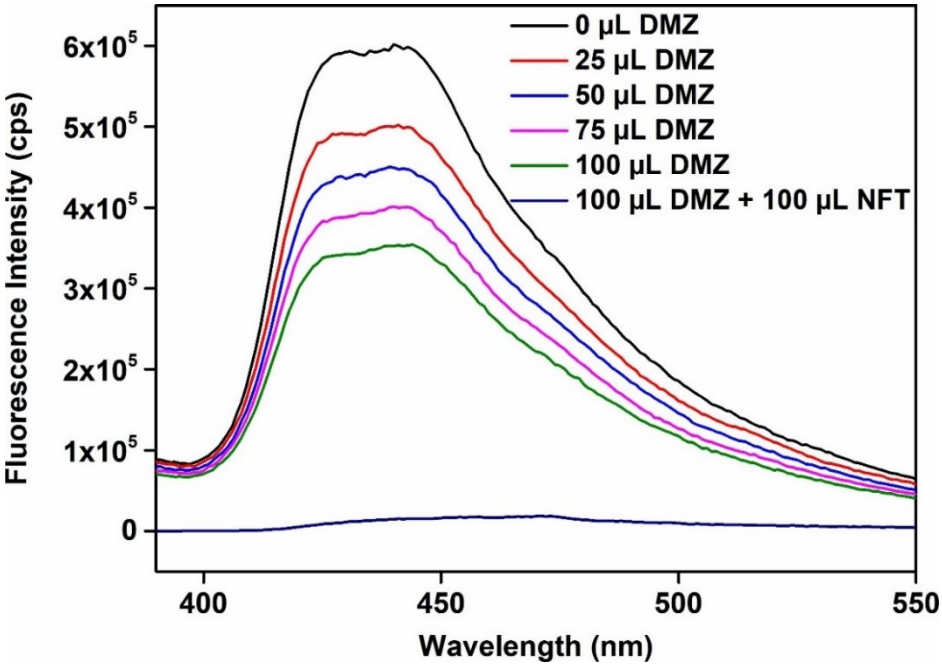

Fig. S58. Quenching in fluorescence emission intensity of the methanolic aqueous solution of **IITG-5a** after addition of 100 µL of 10 mM methanolic NFT solution in presence of 100 µL of 10 mM methanolic solution of DMZ.

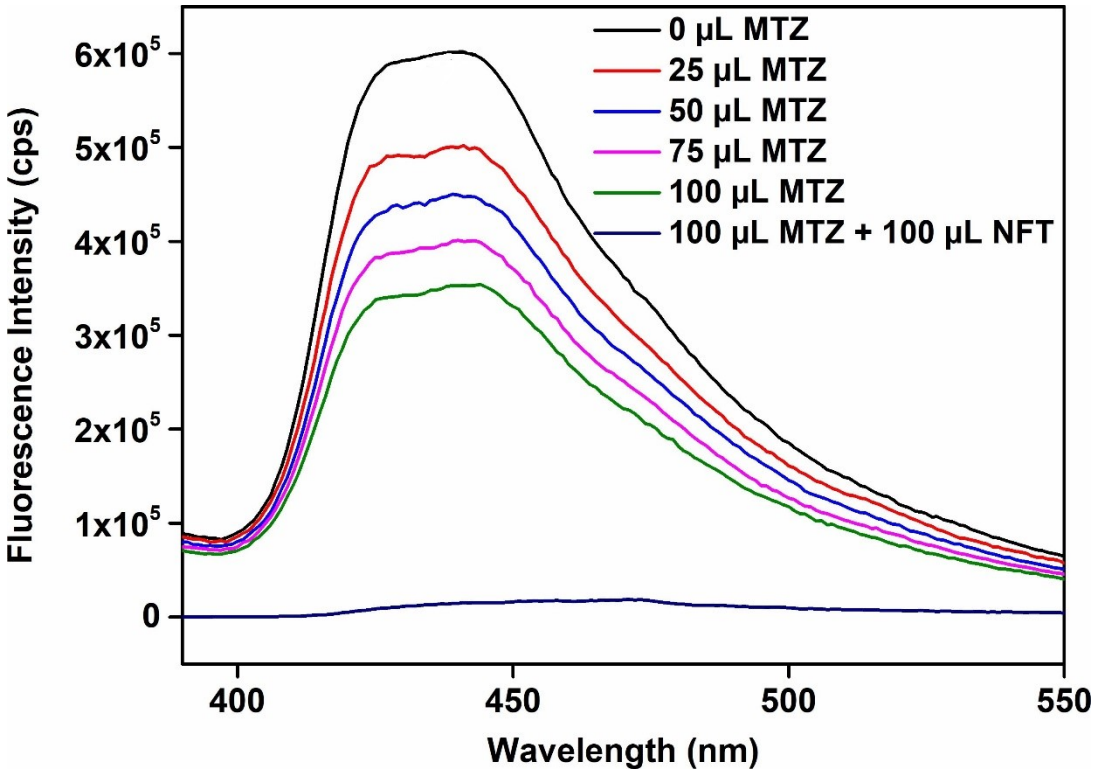

Fig. S59. Quenching in fluorescence emission intensity of the methanolic solution of **IITG-5a** after addition of 100 µL of 10 mM methanolic NFT in presence of 100 µL of 10 mM methanolic solution of MTZ.

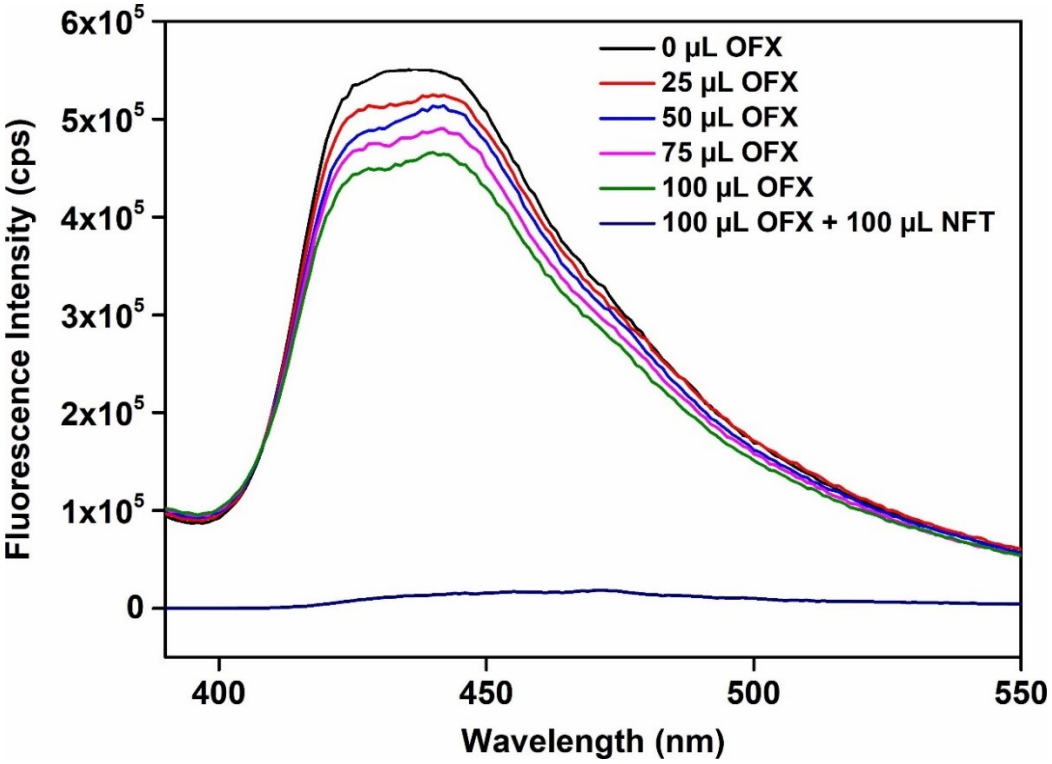

Fig. S60. Quenching in fluorescence emission intensity of the methanolic solution of **IITG-5a** after addition of 100 µL of 10 mM methanolic NFT in presence of 100 µL of 10 mM methanolic solution of OFX.

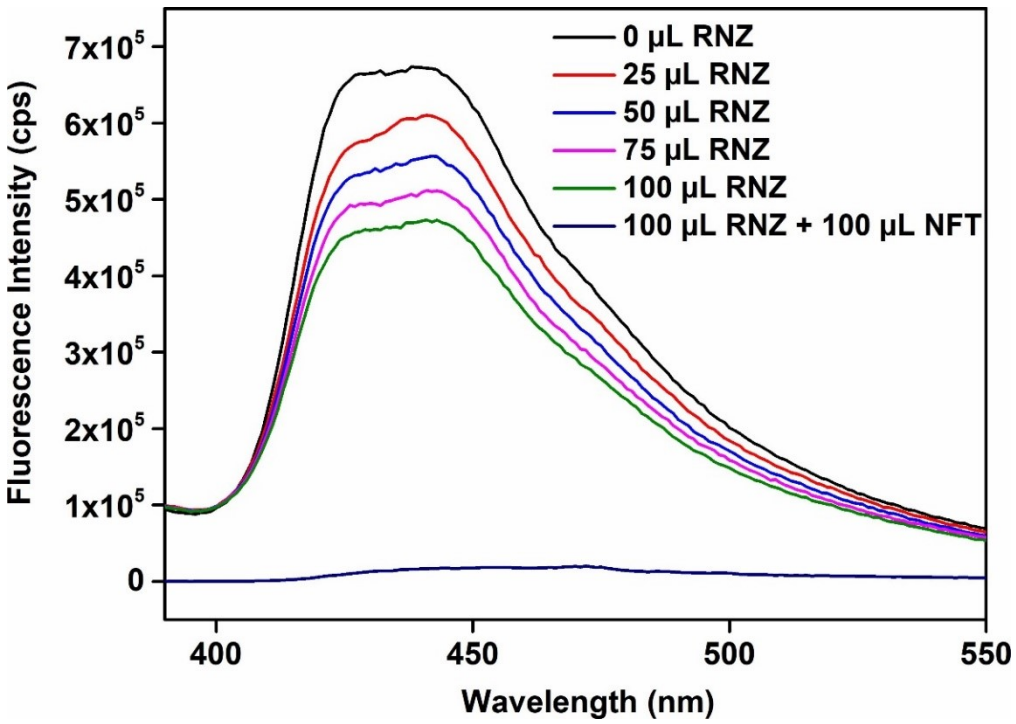

Fig. S61. Quenching in fluorescence emission intensity of the methanolic solution of **IITG-5a** after addition of 100 µL of 10 mM methanolic NFT in presence of 100 µL of 10 mM methanolic solution of RNZ.

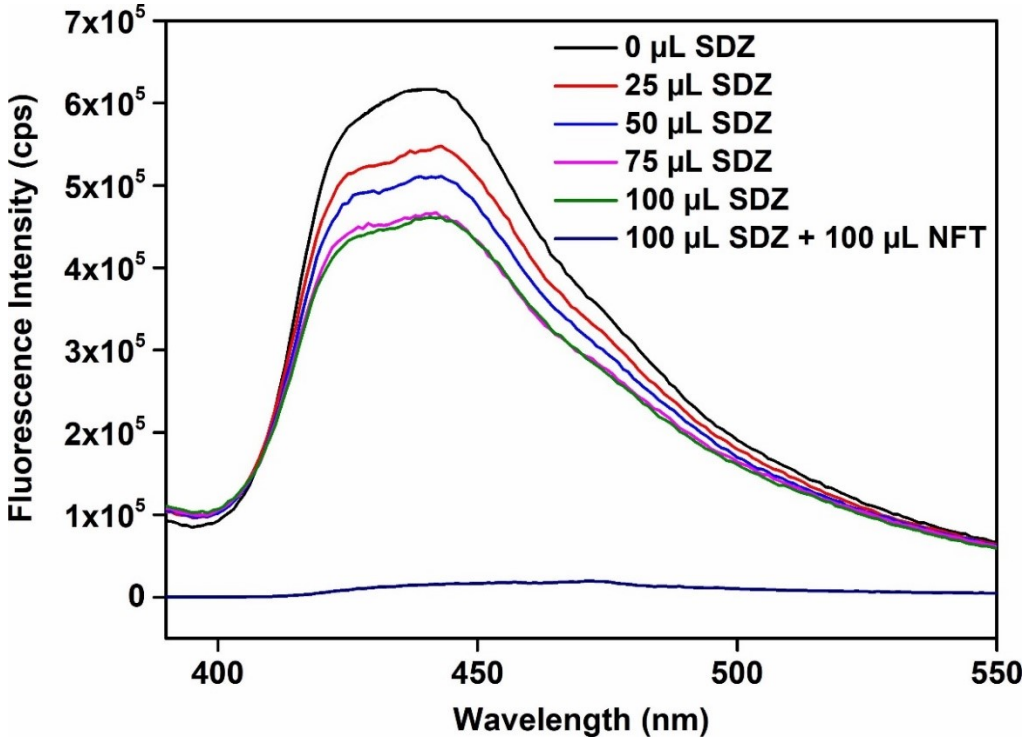

Fig. S62. Quenching in fluorescence emission intensity of the methanolic solution of **IITG-5a** after addition of 100 µL of 10 mM methanolic NFT in presence of 100 µL of 10 mM methanolic solution of SDZ.

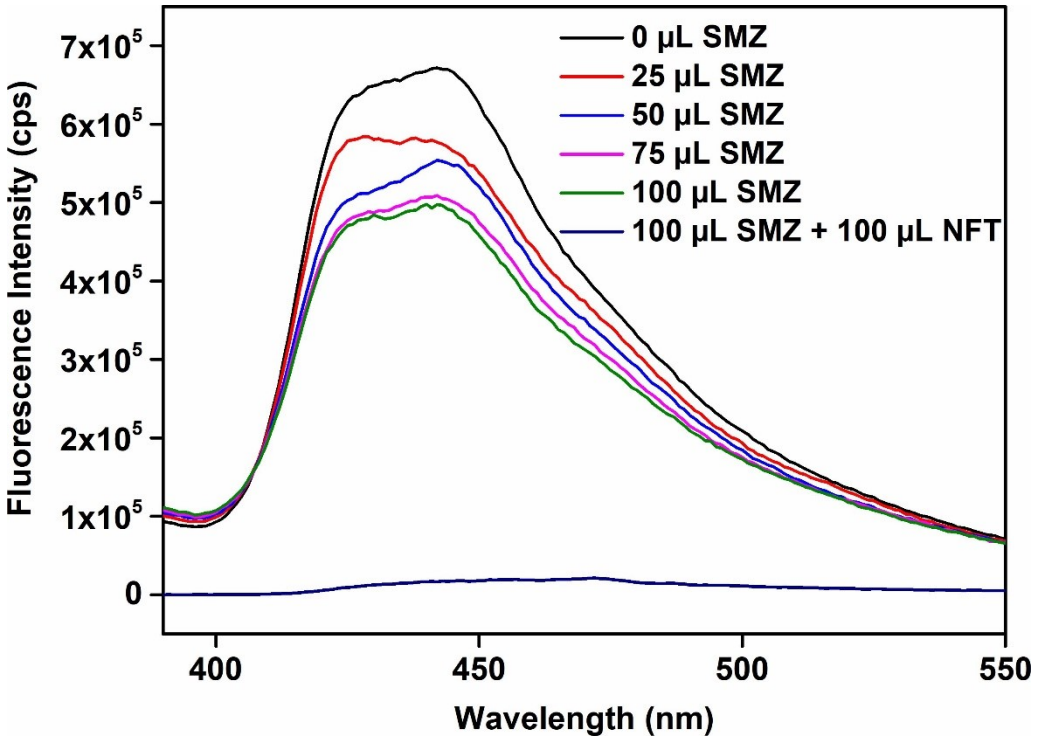

Fig S63. Quenching in fluorescence emission intensity of the methanolic solution of **IITG-5a** after addition of 100 µL of 10 mM methanolic NFT in presence of 100 µL of 10 mM methanolic solution of SMZ.

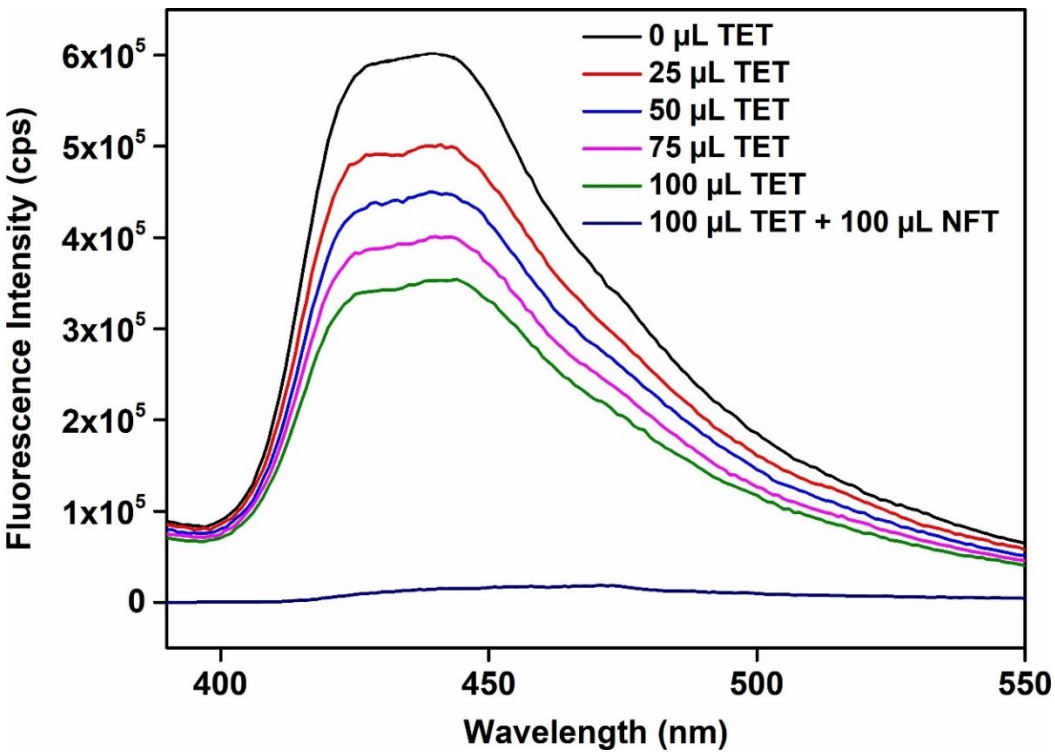

Fig. S64. Quenching in fluorescence emission intensity of the methanolic solution of **IITG-5a** after addition of 100 µL of 10 mM methanolic NFT in presence of 100 µL of 10 mM methanolic solution of TET.

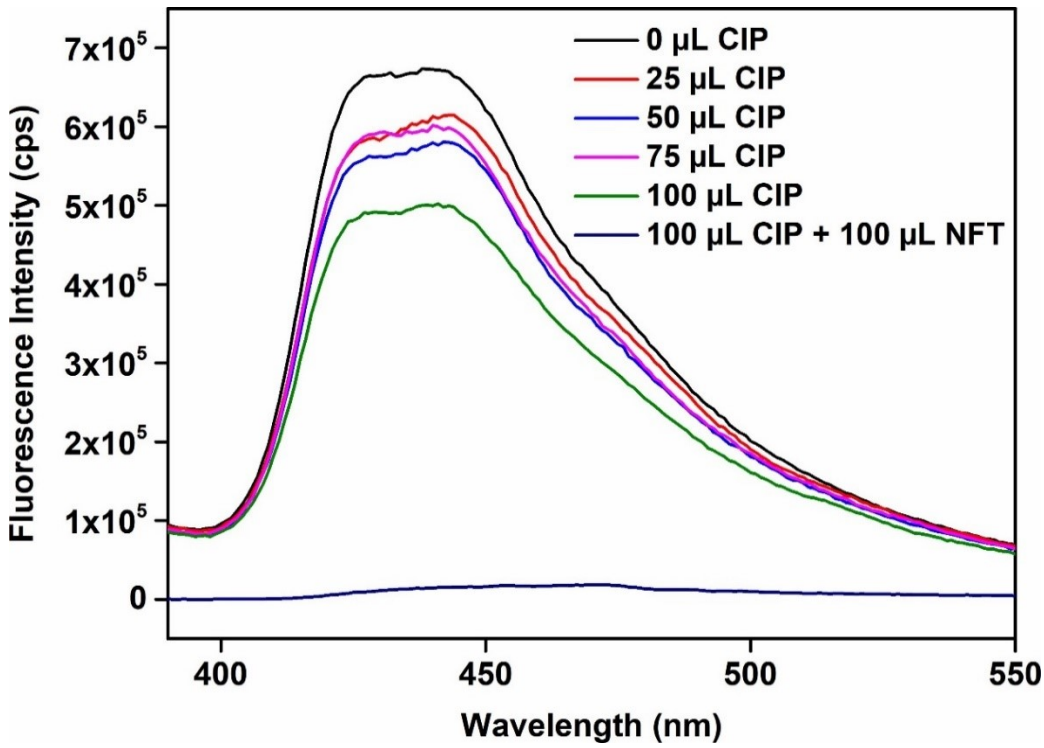

Fig. S65. Quenching in fluorescence emission intensity of the methanolic solution of **IITG-5a** after addition of 100 µL of 10 mM methanolic NFT in presence of 100 µL of 10 mM methanolic solution of CIP.

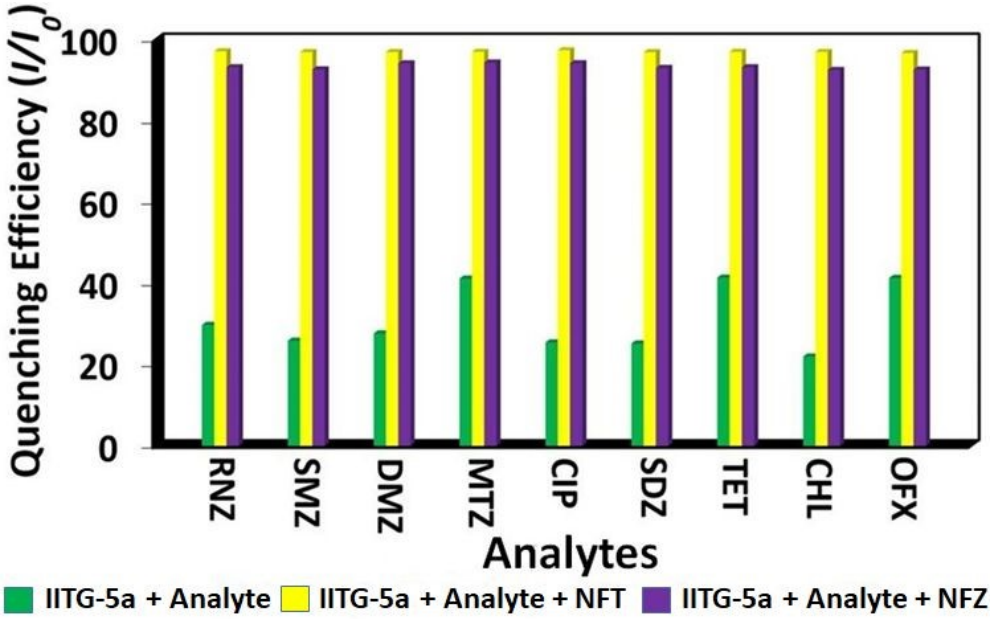

Fig. S66. Switch-off in fluorescence emission intensity of **IITG-5a** after addition (100 µL) of 10 mM of NFZ and NFT solutions in presence of 100 µL of 10 mM solutions (in MeOH) of other competitor antibiotics (λ_{ex} = 370 nm, λ_{em} = 442 nm).

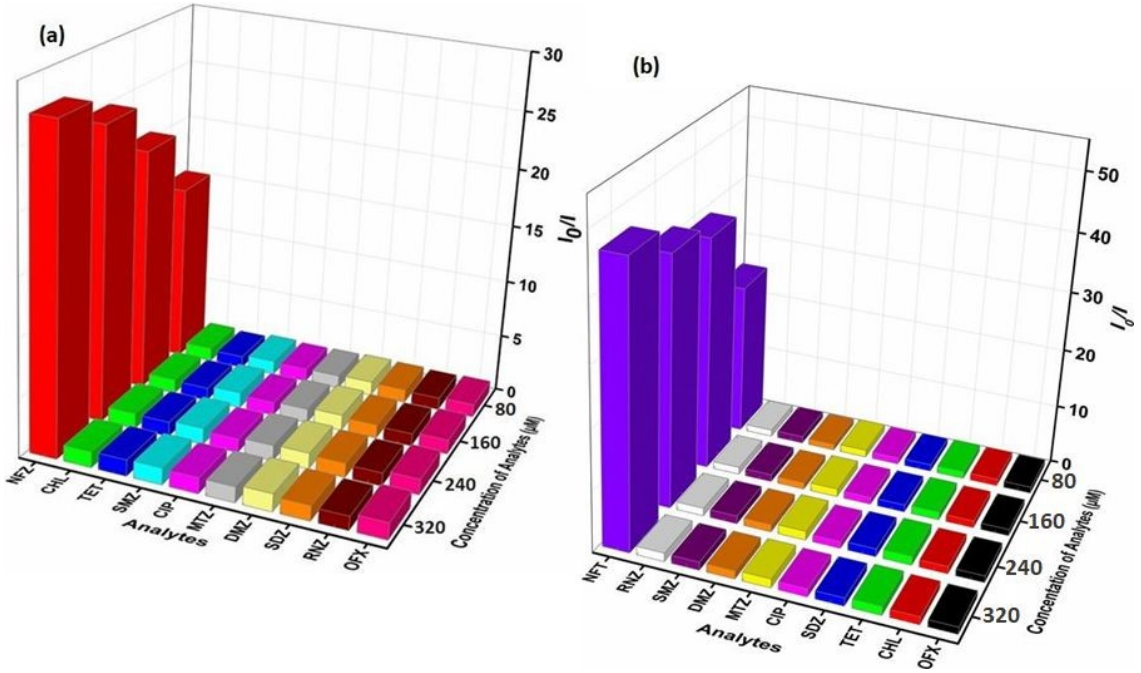

Fig. S67. S-V plots for the decrease in luminescence intensities of **IITG-5a** with gradual addition of various antibiotics in case of (a) NFZ and (b) NFT sensing.

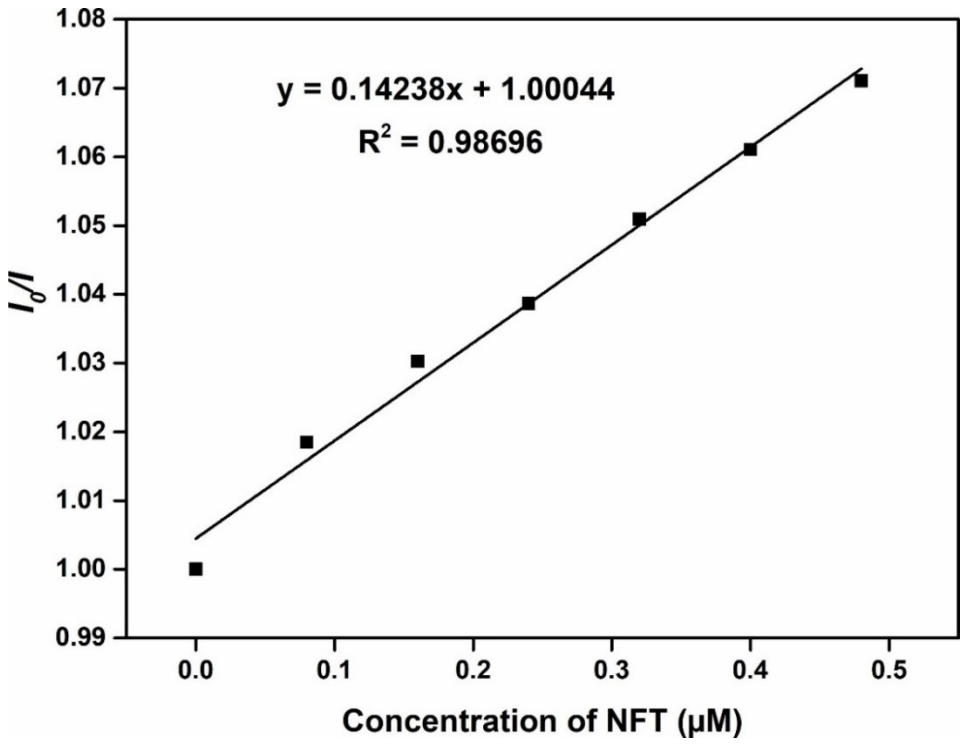

Fig. S68. Stern-Volmer plot for the fluorescence emission quenching of **IITG-5a** in presence of NFZ solution.

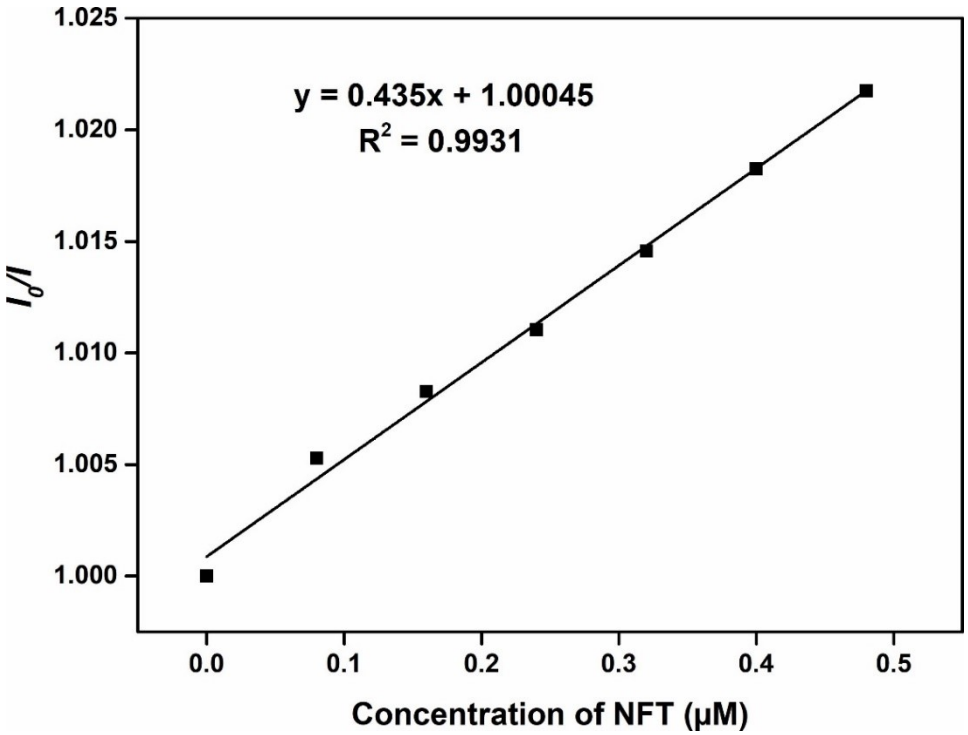

Fig. S69. Stern-Volmer plot for the fluorescence emission quenching of **IITG-5a** in presence of NFT solution.

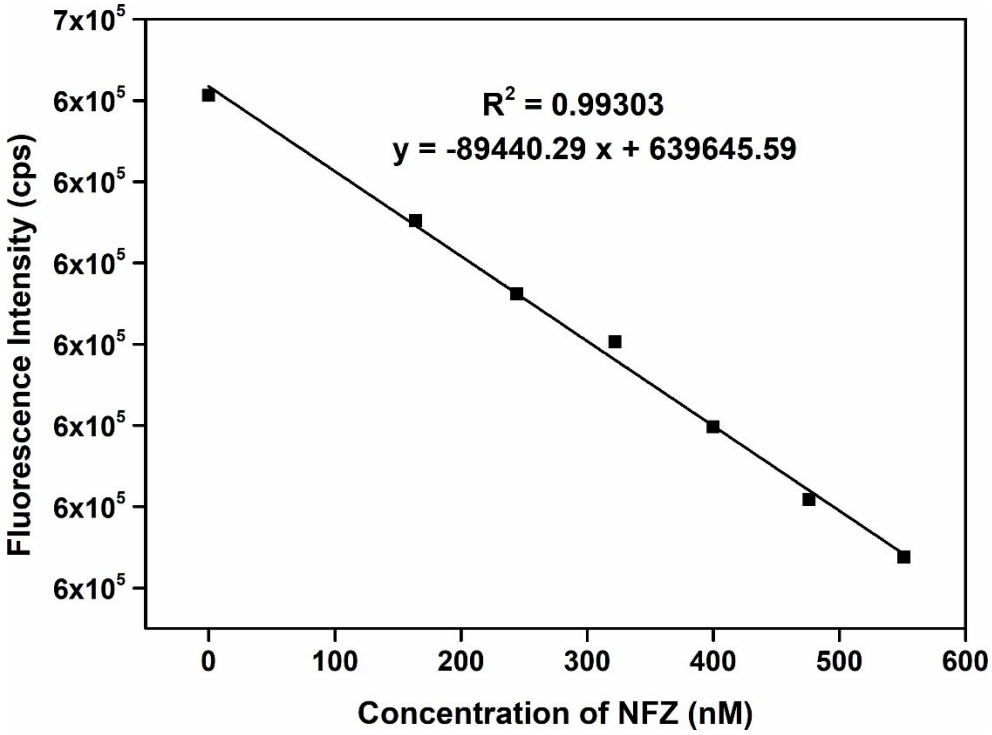

Fig. S70. Change in the fluorescence intensity of **IITG-5a** in MeOH as a function of concentration of NFZ.

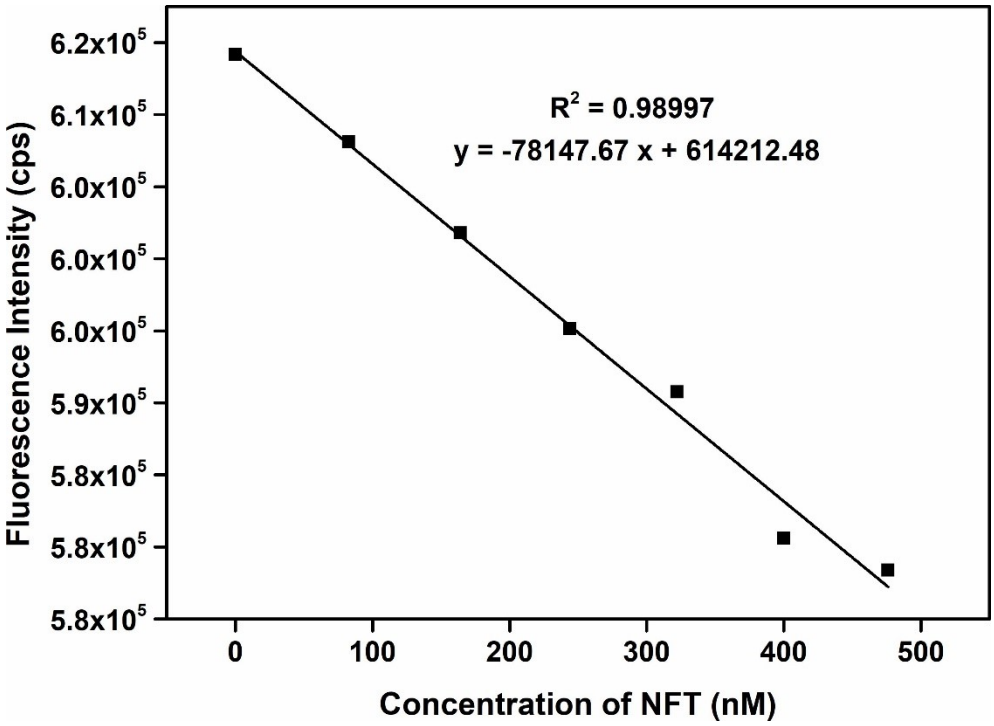

Fig. S71. Change in the fluorescence intensity of **IITG-5a** in MeOH as a function of concentration of NFT.

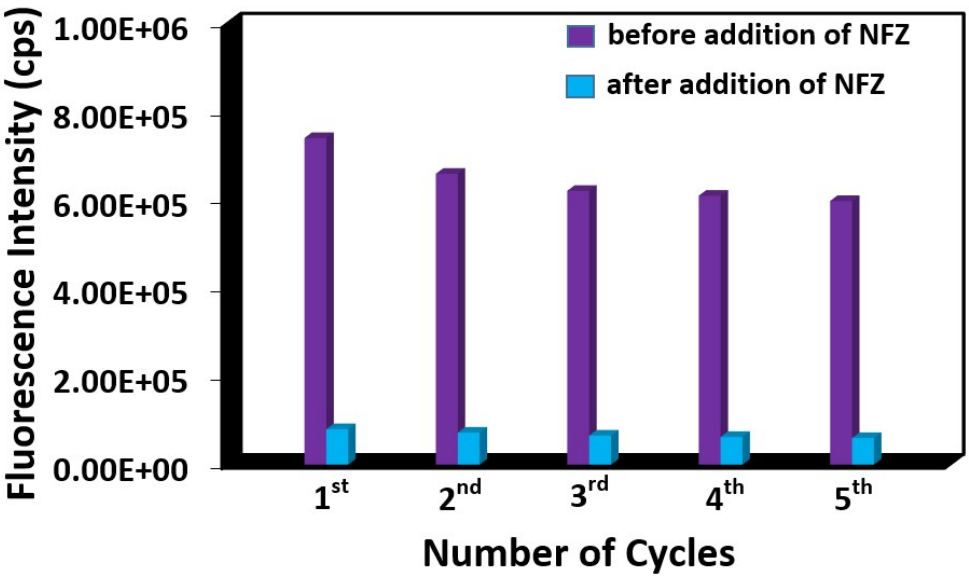

Fig. S72. Recyclability plot of **IITG-5a** towards the sensing of NFZ in MeOH.

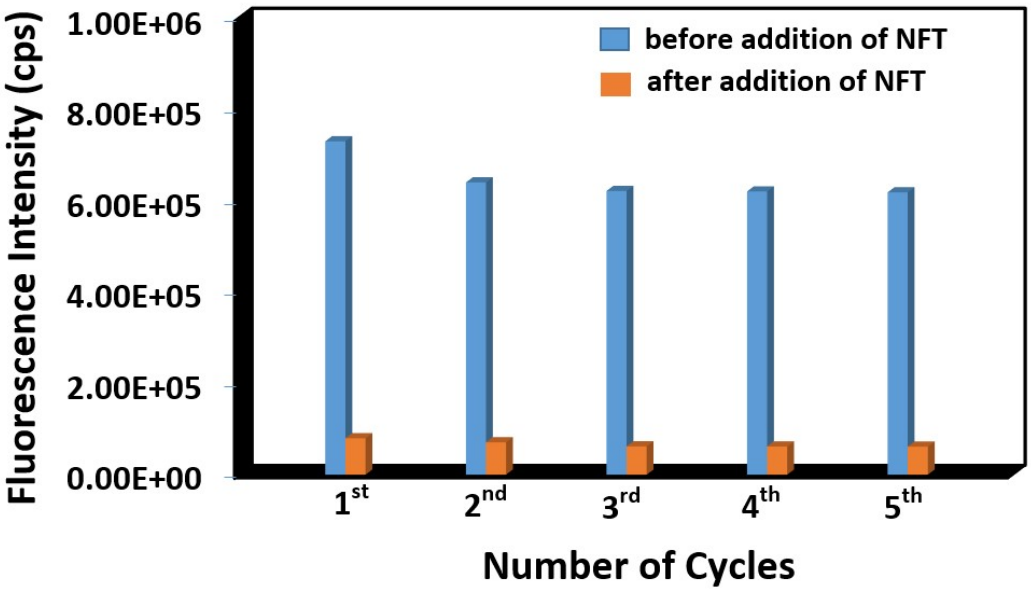

Fig. S73. Recyclability plot of **IITG-5a** towards the sensing of NFT in MeOH.

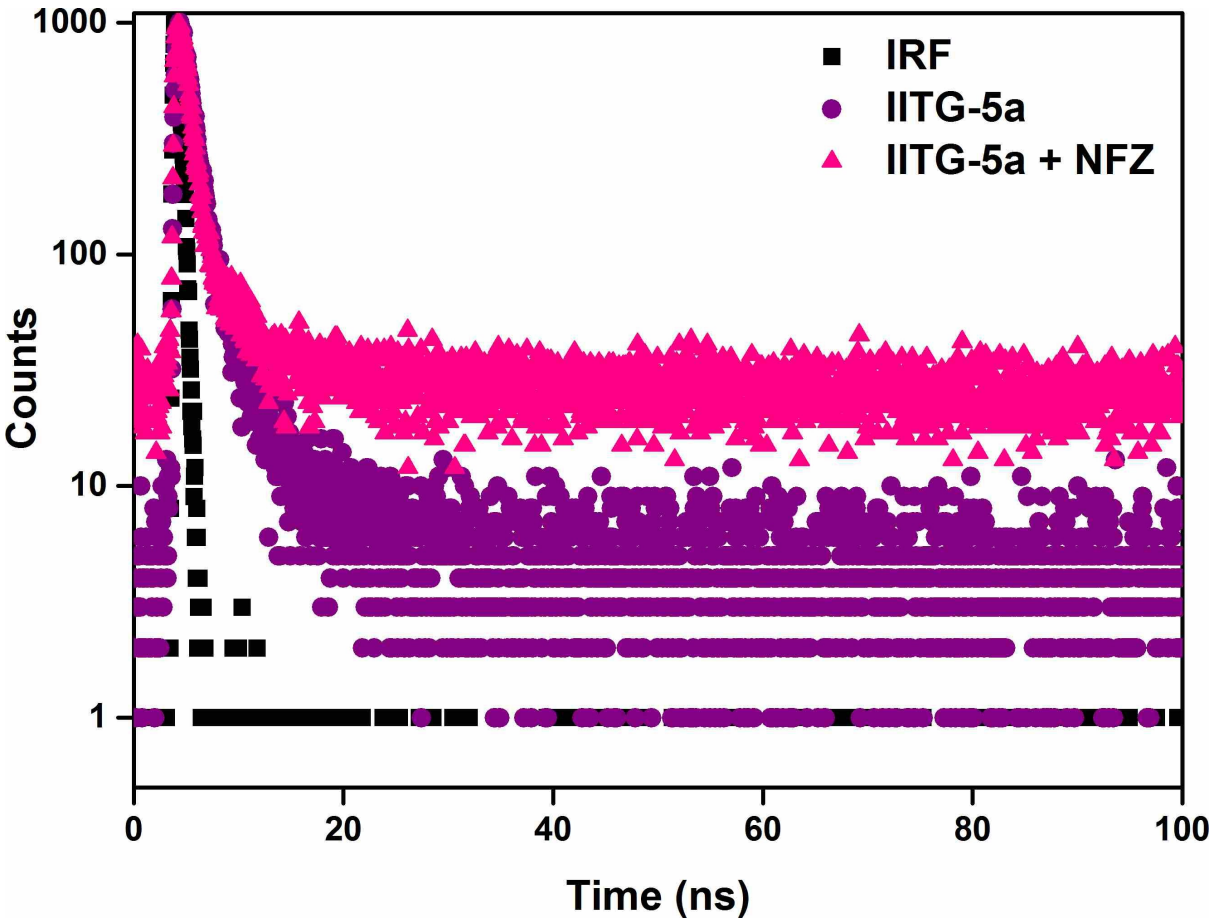

Fig. S74. Lifetime decay profile of **IITG-5a** in absence and presence of NFZ solution (λ_{ex} = 320 nm, monitored at 308 nm). Here, IRF = instrument response function.

Table S3. Fluorescence lifetimes of **IITG-5a** before and after the addition of NFZ solution (λ_{ex} = 308 nm, pulsed diode laser).

Volume of NFZ solution added (μL)	a_1	a_2	τ_1 (ns)	τ_2 (ns)	$<\tau>$* (ns)
0	0.73	0.27	0.94	3.67	1.68
100	0.76	0.24	0.70	3.12	1.28

* $<\tau> = a_1\tau_1 + a_2\tau_2$

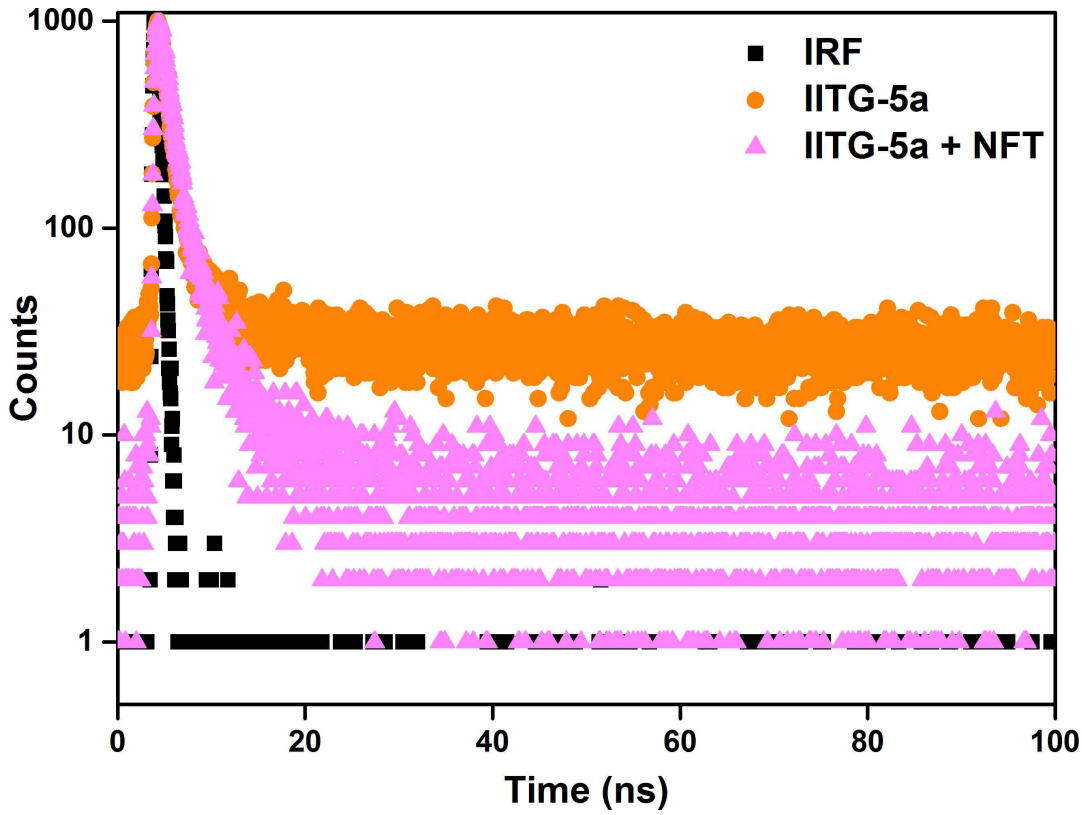

Fig. S75. Lifetime decay profile of **IITG-5a** in absence and presence of NFT solution (λ_{ex} = 320 nm, monitored at 308 nm). Here, IRF = instrument response function.

Table S4. Fluorescence lifetimes of **IITG-5a** before and after the addition of NFT solution (λ_{ex} = 308 nm, pulsed diode laser).

Volume of NFT solution added (μL)	a_1	a_2	τ_1 (ns)	τ_2 (ns)	$<\tau>$* (ns)
0	0.73	0.27	0.94	3.67	1.68
100	0.72	0.28	0.58	3.47	1.38

* $<\tau> = a_1\tau_1 + a_2\tau_2$

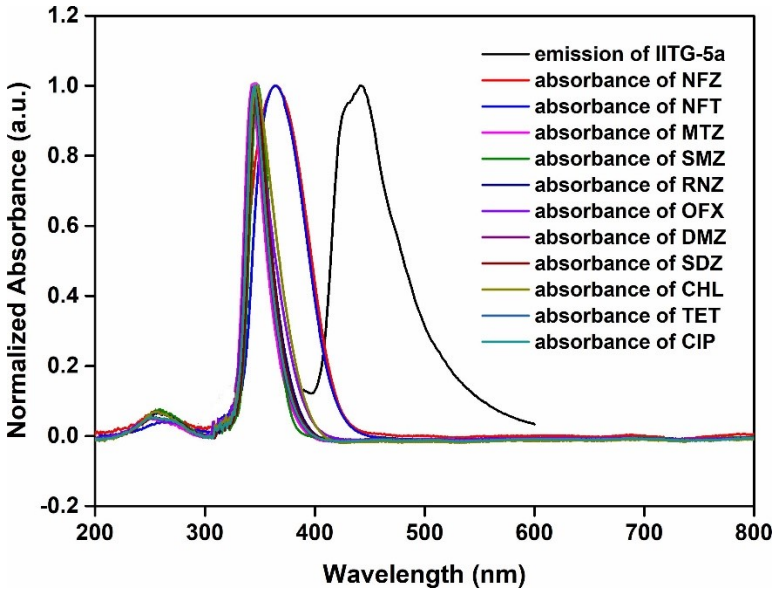

Fig. S76. Spectral overlap between emission spectrum of **IITG-5a** and absorption spectra of antibiotics.

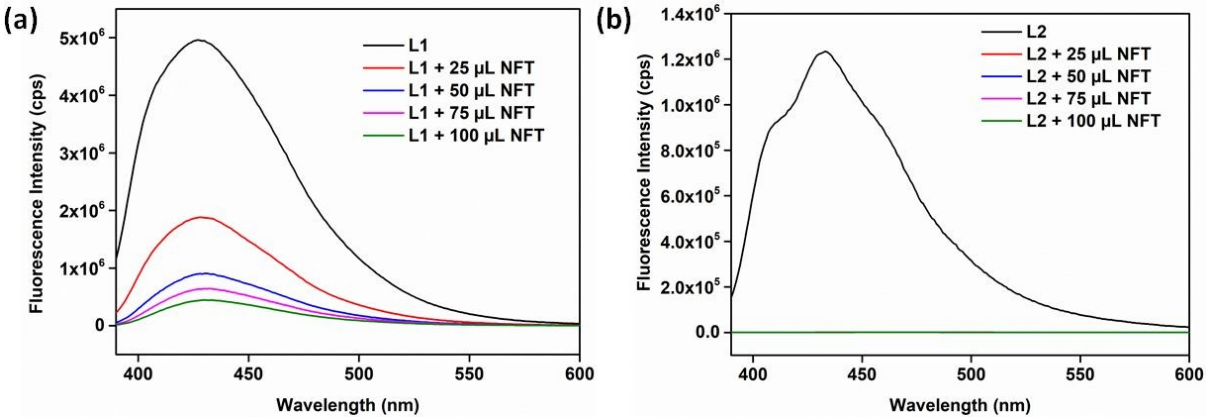

Fig. S77. Change in fluorescence emission intensity of the methanolic solution of **L1** (a) and **L2** (b) linkers after addition of 100 µL of 10 mM methanolic NFT solution.

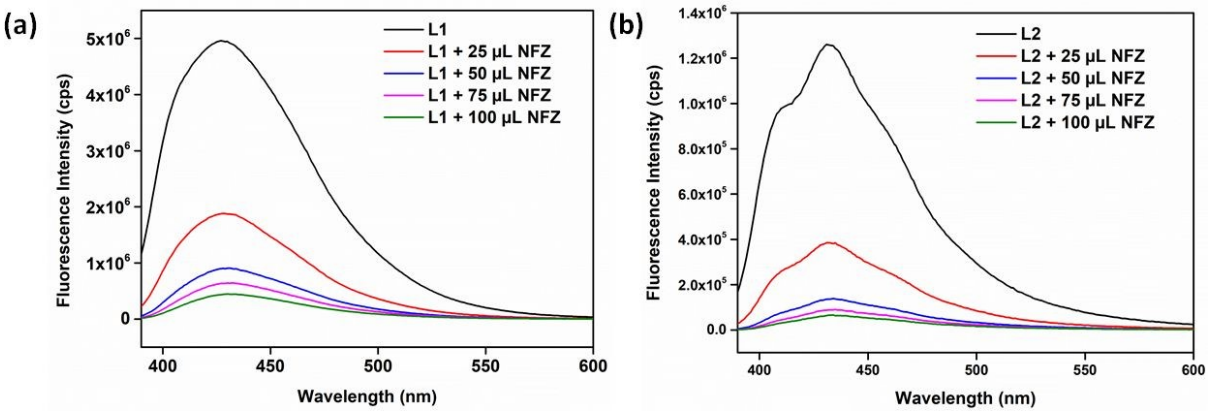

Fig. S78. Change in fluorescence emission intensity of the methanolic solution of **L1** (a) and **L2** (b) linkers after addition of 100 µL of 10 mM methanolic NFZ solution.

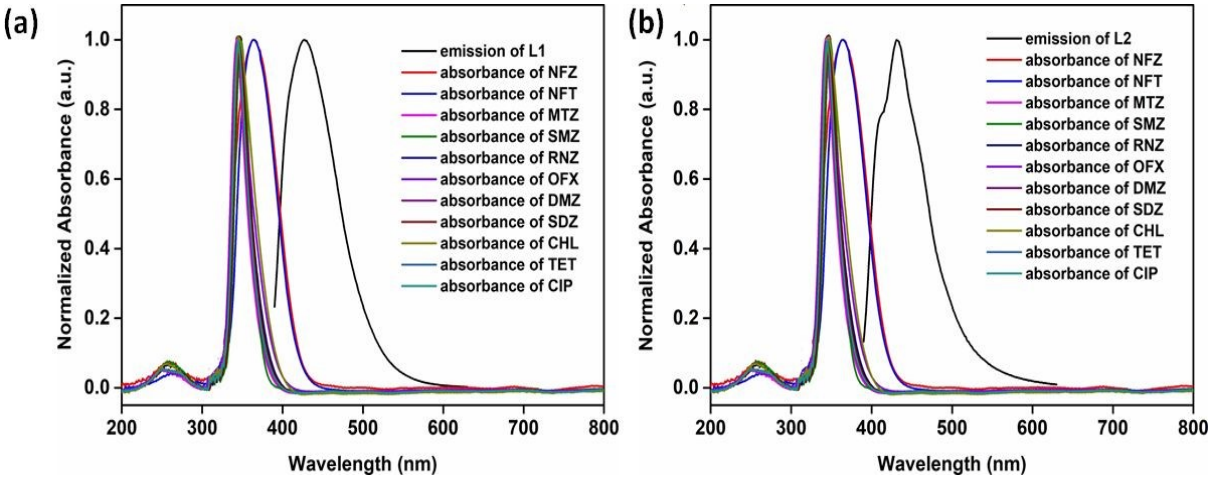

Fig. S79. Spectral overlap between emission spectrum of **L1** (a) and **L2** (b) linkers with the absorption spectra of antibiotics.

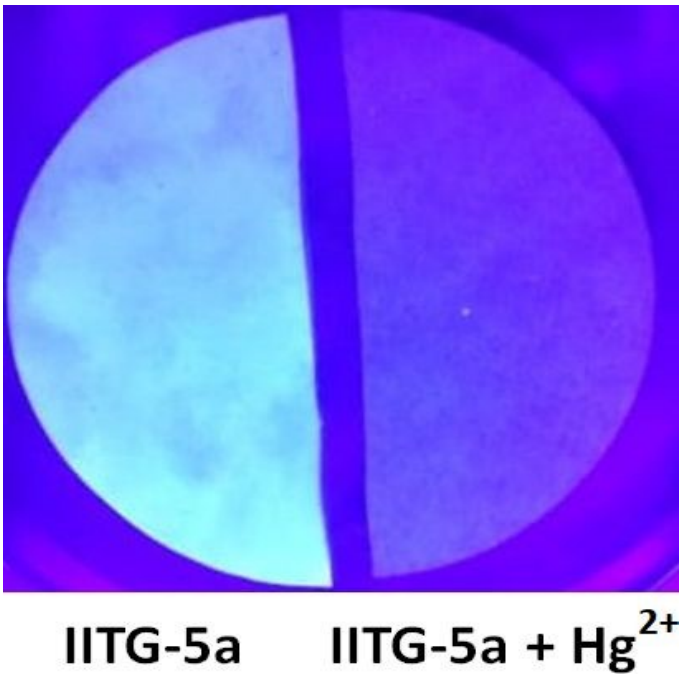

Fig. S80. Images of **IITG-5a-**coated paper strips under UV lamp after and before the treatment of 10 mM aqueous Hg^{2+} solution.

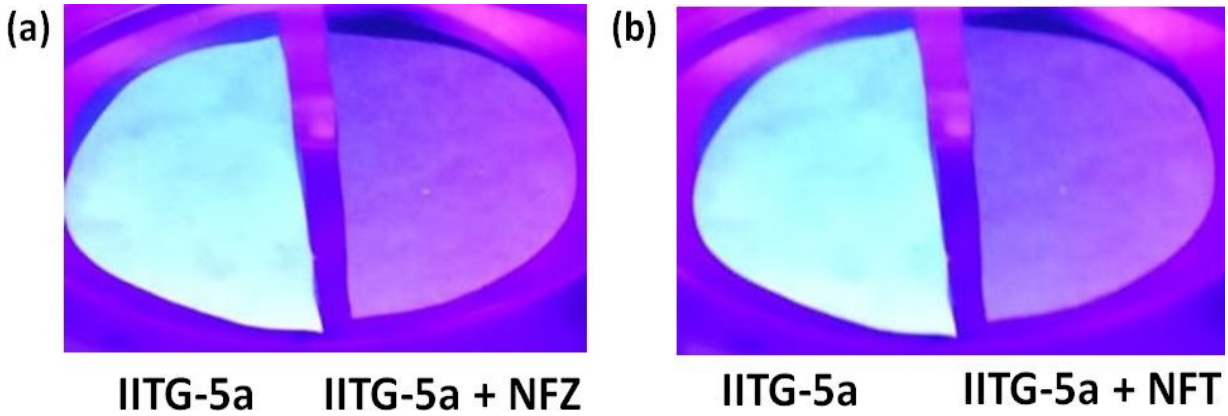

Fig. S81. Images of **IITG-5a-**coated paper strips under UV lamp after and before the treatment of 10 mM methanolic(a) NFZ & (b) NFT solution.

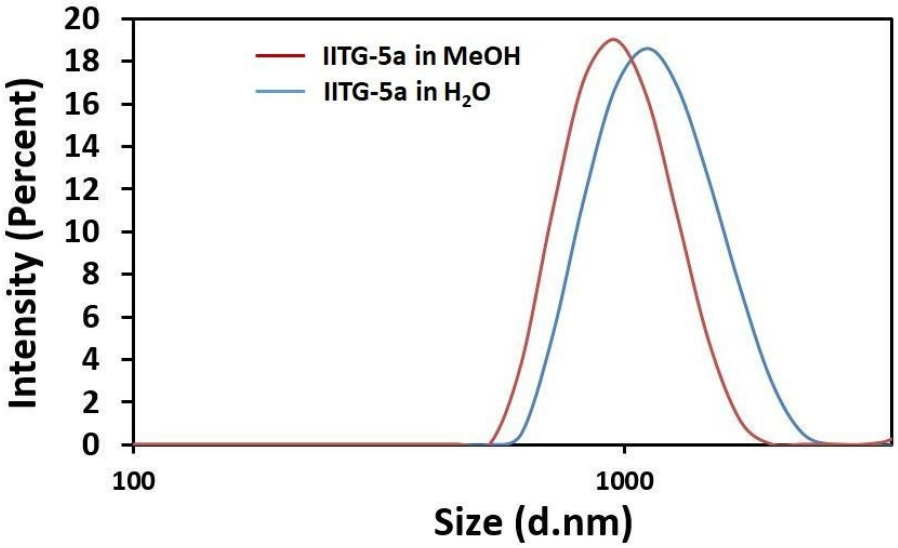

Fig. S82. Particle size distribution of the aqueous (blue) and MeOH (red) dispersion of IITG-5a measured by DLS method.

Table S5. Comparison of the response time, detection limit and sensing media used for the reported chemosensors of Hg^{2+} in the literature.

Sl. No.	Sensor Material	Type of Material	Sensing Medium	Detection Limit (nM)	Response Time (min)	Detection method	Ref
1	Thiosemicarbazone	organic-molecule	0.01 M acetic acid/sodium acetate buffer	770	-	Fluorescence	2
2	GT capped AgNPs	nanoparticles	water	0.037	0-60	Fluorescence	3

3	Azo Crown ether	organic molecule	methanol	13900	-	Fluorescence	4
4	Silver nanoparticles	nanoparticles	water	850	30	Colorimetric	5
5	Rhodamine 6 G based	Rh-complex	THF: Water (8:2, v/v, pH = 7)	30.37	-	Fluorescence	6
6	Tetraphenyl ethylene based AIE probe	organic molecule	water	63	-	Fluorescence	7
7	Squaraine based fluorescent probe	organic molecule	Ethanol: Water (20:80, v/v)	21.9	3	Fluorescence	8
8	Rhodamine appended terphenyl	organic molecule	THF	500	30	Fluorescence	9
9	Ruthenium complex	Metal complex	Ethanol	100	-	Spectrophotometry	10
10	Double naphthalene Schiff base	organic compound	DMSO	55.9	80	Fluorescence	11
11	Gold nanoparticles	nanoparticles	water	50	0.16	Potentiometric	12
12	Gold nanoparticles	nanoparticles	water	50	40	Colorimetric	13
13	Poly (vinyl chloride)	polymer	Tris buffer	20	10	Potentiometric	14
14	Polyaniline-naflon nanostructure	nanoparticles	PBS buffer	50	1.47-2.1	Amperometry	15

15	Thiol functionalized reduced GO	nanoparticles	water	20	180	Electrochemical	16
16	2-Hydroxy benzothiazole modified rhodol	organic compound	THF: HEPES (4:6, v/v)	270	-	Fluorescence	17
17	Nitrogen-doped carbon quantum dots	quantum dots	water	230	15	Fluorescence	18
18	$[Ni(3\text{-}bpd)_2(NCS)_2]_n$	MOF	water	-	120	Fluorescence	19
19	[PCN-221]	MOF	water	10	1	Fluorescence	20
20	[Cu(Dcbb)(Bpe)].Cl	MOF	HEPES buffer	3.2 and 3.3	30	Fluorescence	21
21	UiO-66@ Butyne	MOF	water	10.9	3	Fluorescence	22
22	$Ln(TATAB)\cdot(DMF)_4(H_2O)(MeOH)_{0.5}$	MOF	water	4.4	-	Fluorescence	23
23	Eu^{3+}/CDs@MOF-253	MOF	water	47.88	3	Fluorescence	24
24	$[Cu(Cdcbp)(H_2O)2\cdot 2H_2O]_n$	MOF	water	(2.3 ± 0.8)	2	Fluorescence	25
25	Al-MOF (TAM)	MOF	water	2.94	0.5	Fluorescence	26
26	$[Cu(Cbdcp)(Dps)(H_2O)_3]\cdot 6H_2O_n$	MOF	HEPES buffer	2.6	10	Fluorescence	27

27	Cd−EDDA	MOF	water	2	0.25	Fluorescence	28
28	tetrahydrodibenzo phenanthridine derivatives	organic compound	DMSO : THF = 1 : 1	0.91 and 0.041	-	Fluorescence	29
29	$[Zn(L)(BBI).(H_2O)_2]$ $[Cd(L)(TPOM)0_{.75}]\cdot xS$	MOF	water	-	-	Fluorescence	30
30	**IITG-5a**	MOF	water	5	1	Fluorescence	this wor k

Table S6. Comparison of the response time, detection limit and sensing media used for the reported chemosensors of NFT and NFZ in the literature.

Sl. No	Sensor Material	Type of Material	Name of antibiotic	Sensing Medium	Detection Limit (nM)	Response Time (min)	Detection method	Ref
1	HNU-52	MOF	NFT NFZ	DMF	920 720	1	Fluorescence	31
2	$\{[Zn(TTPBA\text{-}4)_{0.5}(TPA)]\cdot H_2O\cdot 0.5DMF\}_n$	MOF	NFT NFZ	DMAc	-	-	Fluorescence	32
3	Cr-MIL-101/A	MOF	NFT	-	3	10	Electrochemical	33
4	CNDs	nanoparticles	NFT	-	1400	-	Fluorescence	34
5	Gold nimrods	nanorods	NFT	-	6510	60	voltammetry	35
6	MIPs	polymers	NFT	acetonitrile + 0.2% dimethyl sulfoxide	5000	-	voltammetry	36
7	$(Me_2NH_2)1.5[In1.5(FBDC)(BDC)]2.5NMF.CH_3CN$	MOF	NFT	water	1900	60	Fluorescence	37
8	$[Cd_3(DBPT)_2(H_2O)_4]\cdot 5H_2O$		NFT	methanol	5000	-	Fluorescence	38
9	Ag-SDS electrode	nanoparticles	NFZ	ternary choline chloride−urea−glycerol	370	-	voltammetry	39

10	rGO/Fe_3O_4NR	nanorod	NFT	water	1.14	-	electrochemical sensor	40
11	TiO_2-rGO NC	nanoparticles	NFT	water	2.28	20	voltammetry	41
12	TbIJTCPB)IJDMF		NFZ NFT	water	55000 120000	120	Fluorescence	42
13	MIP film	polymer	NFT	real serum samples	0.3	30	electrochemical sensor	43
14	LMNS	nanospheres	NFT	water	72	20	voltammetry	44
15	$\{[Cd_3(TDCPB)\cdot 2DMAc]\cdot DMAc\cdot 4H_2O\}_n$	MOF	NFT NFZ	DMAc	60000	1.25	Fluorescence	45
16	**4**⊃DEASM	MOF	NFZ	water	208	-	Fluorescence	46
17	**IITG-5a**	MOF	NFT NFZ	MeOH	96.3 156.7	1	Fluorescence	this work

Table S7. Lattice parameter and crystallographic data obtained from the Rietveld refinement of **IITG-5**.

compound	**IITG-5**
space group	*Fm*-3*m*
$a = b = c$ [Å]	26.5967(11)
R_{wp} [%]	4.95
R_{Bragg} [%]	2.62
GoF	1.02

CIF file for IITG-5 obtained from Rietveld refinement:

```
data_IITG-5
_chemical_name_mineral ??
_cell_length_a 26.5967(11)
_cell_length_b 26.5967(11)
_cell_length_c 26.5967(11)
_cell_angle_alpha 90
_cell_angle_beta 90
_cell_angle_gamma 90
_cell_volume 18814(2)
_symmetry_space_group_name_H-M FM-3M
loop_
        _symmetry_equiv_pos_as_xyz
        'x, y, z '
        '-x, -y, z '
```

'-x, -z, -y '
'-x, -z, y '
'-x, z, -y '
'-x, z, y '
'-x, y, -z '
'-x, y, z '
'-y, -x, -z '
'-y, -x, z '
'-y, -z, -x '
'-y, -z, x '
'-y, z, -x '
'-y, z, x '
'-y, x, -z '
'-y, x, z '
'-z, -x, -y '
'-z, -x, y '
'-z, -y, -x '
'-z, -y, x '
'-z, y, -x '
'-z, y, x '
'-z, x, -y '
'-z, x, y '
'z, -x, -y '
'z, -x, y '
'z, -y, -x '
'z, -y, x '
'z, y, -x '
'z, y, x '
'z, x, -y '
'z, x, y '
'y, -x, -z '
'y, -x, z '
'y, -z, -x '
'y, -z, x '
'y, z, -x '
'y, z, x '
'y, x, -z '
'y, x, z '
'x, -y, -z '
'x, -y, z '
'x, -z, -y '
'x, -z, y '
'x, z, -y '
'x, z, y '
'x, y, -z '
'-x, -y, -z '

'x+1/2, y+1/2, z '
'-x+1/2, -y+1/2, z '
'-x+1/2, -z+1/2, -y '
'-x+1/2, -z+1/2, y '
'-x+1/2, z+1/2, -y '
'-x+1/2, z+1/2, y '
'-x+1/2, y+1/2, -z '
'-x+1/2, y+1/2, z '
'-y+1/2, -x+1/2, -z '
'-y+1/2, -x+1/2, z '
'-y+1/2, -z+1/2, -x '
'-y+1/2, -z+1/2, x '
'-y+1/2, z+1/2, -x '
'-y+1/2, z+1/2, x '
'-y+1/2, x+1/2, -z '
'-y+1/2, x+1/2, z '
'-z+1/2, -x+1/2, -y '
'-z+1/2, -x+1/2, y '
'-z+1/2, -y+1/2, -x '
'-z+1/2, -y+1/2, x '
'-z+1/2, y+1/2, -x '
'-z+1/2, y+1/2, x '
'-z+1/2, x+1/2, -y '
'-z+1/2, x+1/2, y '
'z+1/2, -x+1/2, -y '
'z+1/2, -x+1/2, y '
'z+1/2, -y+1/2, -x '
'z+1/2, -y+1/2, x '
'z+1/2, y+1/2, -x '
'z+1/2, y+1/2, x '
'z+1/2, x+1/2, -y '
'z+1/2, x+1/2, y '
'y+1/2, -x+1/2, -z '
'y+1/2, -x+1/2, z '
'y+1/2, -z+1/2, -x '
'y+1/2, -z+1/2, x '
'y+1/2, z+1/2, -x '
'y+1/2, z+1/2, x '
'y+1/2, x+1/2, -z '
'y+1/2, x+1/2, z '
'x+1/2, -y+1/2, -z '
'x+1/2, -y+1/2, z '
'x+1/2, -z+1/2, -y '
'x+1/2, -z+1/2, y '
'x+1/2, z+1/2, -y '
'x+1/2, z+1/2, y '

'x+1/2, y+1/2, -z '
'-x+1/2, -y+1/2, -z '
'x+1/2, y, z+1/2 '
'-x+1/2, -y, z+1/2 '
'-x+1/2, -z, -y+1/2 '
'-x+1/2, -z, y+1/2 '
'-x+1/2, z, -y+1/2 '
'-x+1/2, z, y+1/2 '
'-x+1/2, y, -z+1/2 '
'-x+1/2, y, z+1/2 '
'-y+1/2, -x, -z+1/2 '
'-y+1/2, -x, z+1/2 '
'-y+1/2, -z, -x+1/2 '
'-y+1/2, -z, x+1/2 '
'-y+1/2, z, -x+1/2 '
'-y+1/2, z, x+1/2 '
'-y+1/2, x, -z+1/2 '
'-y+1/2, x, z+1/2 '
'-z+1/2, -x, -y+1/2 '
'-z+1/2, -x, y+1/2 '
'-z+1/2, -y, -x+1/2 '
'-z+1/2, -y, x+1/2 '
'-z+1/2, y, -x+1/2 '
'-z+1/2, y, x+1/2 '
'-z+1/2, x, -y+1/2 '
'-z+1/2, x, y+1/2 '
'z+1/2, -x, -y+1/2 '
'z+1/2, -x, y+1/2 '
'z+1/2, -y, -x+1/2 '
'z+1/2, -y, x+1/2 '
'z+1/2, y, -x+1/2 '
'z+1/2, y, x+1/2 '
'z+1/2, x, -y+1/2 '
'z+1/2, x, y+1/2 '
'y+1/2, -x, -z+1/2 '
'y+1/2, -x, z+1/2 '
'y+1/2, -z, -x+1/2 '
'y+1/2, -z, x+1/2 '
'y+1/2, z, -x+1/2 '
'y+1/2, z, x+1/2 '
'y+1/2, x, -z+1/2 '
'y+1/2, x, z+1/2 '
'x+1/2, -y, -z+1/2 '
'x+1/2, -y, z+1/2 '
'x+1/2, -z, -y+1/2 '
'x+1/2, -z, y+1/2 '

'x+1/2, z, -y+1/2 '
'x+1/2, z, y+1/2 '
'x+1/2, y, -z+1/2 '
'-x+1/2, -y, -z+1/2 '
'x, y+1/2, z+1/2 '
'-x, -y+1/2, z+1/2 '
'-x, -z+1/2, -y+1/2 '
'-x, -z+1/2, y+1/2 '
'-x, z+1/2, -y+1/2 '
'-x, z+1/2, y+1/2 '
'-x, y+1/2, -z+1/2 '
'-x, y+1/2, z+1/2 '
'-y, -x+1/2, -z+1/2 '
'-y, -x+1/2, z+1/2 '
'-y, -z+1/2, -x+1/2 '
'-y, -z+1/2, x+1/2 '
'-y, z+1/2, -x+1/2 '
'-y, z+1/2, x+1/2 '
'-y, x+1/2, -z+1/2 '
'-y, x+1/2, z+1/2 '
'-z, -x+1/2, -y+1/2 '
'-z, -x+1/2, y+1/2 '
'-z, -y+1/2, -x+1/2 '
'-z, -y+1/2, x+1/2 '
'-z, y+1/2, -x+1/2 '
'-z, y+1/2, x+1/2 '
'-z, x+1/2, -y+1/2 '
'-z, x+1/2, y+1/2 '
'z, -x+1/2, -y+1/2 '
'z, -x+1/2, y+1/2 '
'z, -y+1/2, -x+1/2 '
'z, -y+1/2, x+1/2 '
'z, y+1/2, -x+1/2 '
'z, y+1/2, x+1/2 '
'z, x+1/2, -y+1/2 '
'z, x+1/2, y+1/2 '
'y, -x+1/2, -z+1/2 '
'y, -x+1/2, z+1/2 '
'y, -z+1/2, -x+1/2 '
'y, -z+1/2, x+1/2 '
'y, z+1/2, -x+1/2 '
'y, z+1/2, x+1/2 '
'y, x+1/2, -z+1/2 '
'y, x+1/2, z+1/2 '
'x, -y+1/2, -z+1/2 '
'x, -y+1/2, z+1/2 '

```
        'x, -z+1/2, -y+1/2 '
        'x, -z+1/2, y+1/2 '
        'x, z+1/2, -y+1/2 '
        'x, z+1/2, y+1/2 '
        'x, y+1/2, -z+1/2 '
        '-x, -y+1/2, -z+1/2 '
loop_
_atom_site_label
_atom_site_type_symbol
_atom_site_symmetry_multiplicity
_atom_site_fract_x
_atom_site_fract_y
_atom_site_fract_z
_atom_site_occupancy
_atom_site_B_iso_or_equiv
Zr1 Zr  24 0.0936(3) 0 0 1 0.2(2)
C1 C  48 0.2865(13) 0.5 0.2865(13) 1 0.2(2)
C2 C  96 0.3000(11) 0.5 0.2365(11) 1 0.2(2)
C3 C  96 0.211(5) 0 0.154(3) 0.5 0.2(2)
S1 S  96 0.2203(15) 0 0.1361(10) 0.5 0.2(2)
C4 C  48 0.1598(14) 0 0.1598(14) 1 0.2(2)
C5 C  48 0.1211(16) 0 0.1211(16) 1 0.2(2)
O1 O  96 0.1334(8) 0 0.0747(7) 1 0.2(2)
O2 O  32 0.0482(8) 0.0482(8) 0.0482(8) 1 0.2(2)
```

References:

1. Q. Tao, T. Liu, L. Duan, Y. Cai, W. Xiong, P. Wang, H. Tan, G. Lei, Y. Pei, W. Zhu, R. Yang and Y. Sun, Wide bandgap copolymers with vertical benzodithiophene dicarboxylate for high-performance polymer solar cells with an efficiency up to 7.49%, *J. Mater. Chem. A*, 2016, **4**, 18792-18803.
2. Y. Yu, L.-R. Lin, K.-B. Yang, X. Zhong, R.-B. Huang and L.-S. Zheng, p-Dimethylaminobenzaldehyde thiosemicarbazone: A simple novel selective and sensitive fluorescent sensor for mercury(II) in aqueous solution, *Talanta*, 2006, **69**, 103-106.
3. P. G. Mahajan, N. C. Dige, B. D. Vanjare, A. R. Phull, S. J. Kim and K. H. Lee, Gallotannin mediated silver colloidal nanoparticles as multifunctional nano platform: rapid colorimetric and turn-on fluorescent sensor for Hg^{2+}, catalytic and in vitro anticancer activities, *J. Lumin.*, 2019, **206**, 624–633.
4. Y. C. Hsieh, J. L. Chir, H. H. Wu, P. S. Chang and A. T. Wu, A sugar-aza-crown ether-based fluorescent sensor for Hg^{2+} and Cu^{2+}, *Carbohydr. Res.*, 2009, **344**, 2236–2239.
5. M. L. Firdaus, I. Fitriani, S. Wyantuti, Y. W. Hartati, R. Khaydarov, J. A. Mcalister, H. Obata and T. Gamo, Colorimetric detection of mercury(II) ion in aqueous solution using silver nanoparticles, *Anal. Sci.*, 2017, **33**, 831–837.
6. B. D. Vanjare, P. G. Mahajan, H.-I. Ryoozz, N. C. Dige, N. G. Choi, Y. Han, S. J. Kim, C.-H. Kim and K. H. Lee, Novel rhodamine based chemosensor for detection of

Hg^{2+}: Nanomolar detection, real water sample analysis, and intracellular cell imaging *Sens. Actuators B Chem.*, 2021, **330**, 129308-129322.

7. V. Bhalla, R. Tejpal and M. Kumar, Rhodamine appended terphenyl: a reversible 'off-on' fluorescent chemosensor for mercury ions, *Sensors Actuators, B Chem.*, 2010, **151**, 180–185.
8. B. Yuan, D. X. Wang, L. N. Zhu, Y. L. Lan, M. Cheng, L. M. Zhang, J. Q. Chu, X. Z. Li and D. M. Kong, Dinuclear HgII tetracarbene complex-triggered aggregationinduced emission for rapid and selective sensing of Hg^{2+} and organomercury species, *Chem. Sci.*, 2019, **10**, 4220–4226.
9. S. Y. Lin, H. J. Zhu, W. J. Xu, G. M. Wang and N. Y. Fu, A squaraine based fluorescent probe for mercury ion via coordination induced deaggregation signaling, *Chin. Chem. Lett.*, 2014, **25**, 1291–1295.
10. J. S. Do, K. H. Lin and R. Ohara, Preparation of urease/nano-structured polyanilineNafion®/Au/Al2O3 electrode for inhibitive detection of mercury ion, *J. Taiwan Inst. Chem. Eng.*, 2011, **42**, 662–668.
11. T. B. Wei, G. Y. Gao, W. J. Qu, B. B. Shi, Q. Lin, H. Yao and Y. M. Zhang, Selective fluorescent sensor for mercury(II) ion based on an easy to prepare double naphthalene Schiff base, *Sensors Actuators, B Chem.*, 2014, **199**, 142–147.
12. Y. Yang, Z. Wang, M. Yang, M. Guo, Z. Wu and G. Shen, Inhibitive determination of mercury ion using a renewable urea biosensor based on self-assembled gold nanoparticles, *Sensors Actuators, B Chem.*, 2006, **114**, 1–8.
13. G. H. Chen, W. Y. Chen, Y. C. Yen, C. W. Wang, H. T. Chang and C. F. Chen, Detection of mercury (II) ions using colorimetric gold nanoparticles on paper-based analytical devices, *Anal. Chem.*, 2014, **86**, 6843–6849.
14. T. K. V. Krawczyk, M. Moszczynska and M. Trojanowicz, Inhibitive determination of mercury and other metal ions by potentiometric urea biosensor, *Biosens. Bioelectron.*, 2000, **15**, 681–691.
15. J. S. Do, K. H. Lin and R. Ohara, Preparation of urease/nano-structured polyaniline Nafion®/Au/Al2O3 electrode for inhibitive detection of mercury ion, *J. Taiwan. Inst. Chem. Eng.*, 2011, **42**, 662–668.
16. N. R. Devi, M. Sasidharan and A. K. Sundramoorthy, Gold nanoparticles-thiolFunctionalized reduced graphene oxide coated electrochemical sensor system for selective detection of mercury ion, *J. Electrochem. Soc.*, 2018, **165**, B3046–B3053.
17. S. Chen, W. Wang, M. Yan, Q. Tu, S. W. Chen, T. Li, M. S. Yuan and J. Wang, 2-Hydroxy benzothiazole modified rhodol: aggregation-induced emission and dualchannel fluorescence sensing of Hg^{2+} and Ag+ ions, *Sensors Actuators, B Chem.*, 2018, **255**, 2086–2094.
18. R. Zhang and W. Chen, Nitrogen-doped carbon quantum dots: facile synthesis and application as a 'turn-off' fluorescent probe for detection of Hg^{2+} ions, *Biosens. Bioelectron.*, 2013, **55**, 83–90.
19. S. Halder, J. Mondal, J. O. -Castro, A. Frontera and P. Roy, A Ni-based MOF for selective detection and removal of Hg^{2+} in aqueous medium: a facile strategy, *Dalton Trans.*, 2017, **46**, 1943-1950.
20. E. Moradi, R. Rahimi and V. Safarifard, Porphyrinic zirconium-based MOF with exposed pyrrole Lewis base site as an efficient fluorescence sensing for Hg^{2+} ions, DMF small molecule, and adsorption of Hg^{2+} ions from water solution, *J. Solid State Chem.*, 2020, **286**, 121277-121286.
21. P.-P. Hu, N. Liu, K.-Y. Wu, L.-Y. Zhai, B.-P. Xie, B. Sun, W.-J. Duan, W.-H. Zhang and J.-X. Chen, Successive and Specific Detection of Hg^{2+} and I– by a DNA@MOF Biosensor: Experimental and Simulation Studies, *Inorg. Chem.*, 2018, **57**, 8382–8389.

22. P. Samant, A. V. Desai, S. Sharma, P. Chandra and S. K. Ghosh, Selective Recognition of Hg^{2+} ion in Water by a Functionalized Metal–Organic Framework (MOF) Based Chemodosimeter, *Inorg. Chem.*, 2018, **57**, 2360−2364.
23. T. Xia, T. Song, G. Zhang, Y. Cui, Y. Yang, Z. Wang and G. Qian, A Terbium Metal–Organic Framework for Highly Selective and Sensitive Luminescence Sensing of Hg^{2+} Ions in Aqueous Solution, *Chem. Eur. J.*, 2016, **22**, 18429-18434.
24. X.-Y. Xu and B. Yan, Fabrication and application of a ratiometric and colorimetric fluorescent probe for Hg^{2+} based on dual-emissive metal–organic framework hybrids with carbon dots and Eu^{3+}, *J. Mater. Chem. C*, 2016, **4**, 1543-1549.
25. N.-H. Huang, R.-T. Li, C. Fan, K.-Y. Wu, Z. Zhang and J.-X. Chen, Rapid sequential detection of Hg2+ and biothiols by a probe DNA—MOF hybrid sensory system, *J. Inorg. Biochem.*, 2019, **197**, 110690-110697.
26. A. Radwan, I. M. E. -Sewify, A. Shahat, H. M. E. Azzazy, M. M. H. Khalil and M. F. E. -Shahat, Multiuse Al-MOF Chemosensors for Visual Detection and Removal of Mercury Ions in Water and Skin-Whitening Cosmetics, *ACS Sustainable Chem. Eng.*, 2020, **8**, 15097–15107.
27. N.-H. Huang, Y. Liu, R.-T. Li, J. Chen, P.-P. Hu, D. J. Young, J.-X. Chen and W.-H. Zhang, Sequential Ag^{+}/biothiol and synchronous Ag^{+}/Hg^{2+} biosensing with zwitterionic Cu^{2+}-based metal-organic frameworks, *Analyst*, 2020, **145**, 2779-2788.
28. P. Wu, Y. Liu, Y. Liu, J. Wang, Y. Li, W. Liu and J. Wang, Cadmium-Based Metal−Organic Framework as a Highly Selective and Sensitive Ratiometric Luminescent Sensor for Mercury(II), *Inorg. Chem.*, 2015, **54**, 11046−11048.
29. M. Ponram, U. Balijapalli, B. Sambath, S. K. Iyer, V. B, R. Cingarama and K. N. Sundaramurthy, Development of paper-based chemosensor for the detection of mercury ions using mono- and tetra-sulfur bearing phenanthridines, *New J. Chem.*, 2018, **42**, 8530--8536.
30. Y. Zhao, X. Xu, L. Qiu, X. Kang, L. Wen and B. Zhang, Metal−Organic Frameworks Constructed from a New ThiopheneFunctionalized Dicarboxylate: Luminescence Sensing and Pesticide Removal, *ACS Appl. Mater. Interfaces*, 2017, **9**, 15164−15175.
31. Y. Yang, G. Ren, W. Yang, X. Qin, D. Gu, Z. Liang, D.-Y. Guo and Q. Pan, A new MOF-based fluorescent sensor for the detection of nitrofuran antibiotics, *Polyhedron*, 2021, **194**, 114923-114928.
32. H.-B. Zhu, Y. Shen, Z.-Z. Fu, Y.-Y. Yu, Y.-F. Jiang and Y. Zhao, A multifunctional Zn(II)-based four-fold interpenetrated metal-organic framework for highly sensitive sensing 2,4,6-trinitrophenol (TNP), nitrofurazone (NFZ) and nitrofurantoin (NFT), *Inorg. Chem. Commun.*, 2019, **103**, 21–24.
33. J. Cheng, Y. Li, J. Zhong, Z. Lu, G. Wang, M. Sun, Y. Jiang, P. Zou, X. Wang, Q. Zhao, Y. Wang and H. Rao, Molecularly imprinted electrochemical sensor based on biomass carbon decorated with MOF-derived Cr2O3 and silver nanoparticles for selective and sensitive detection of nitrofurazone, *Chem. Eng. Sci.*, 2020, **318**, 125664-126671.
34. B. R. A.-Hashimi, K. M. Omer, H. S. Rahman and H. H. Othman, Inner filter effect as a sensitive sensing platform for detection of nitrofurantoin using luminescent drug-based carbon nanodots, *Spectrochimica Acta Part A: Molecular and Biomol. Spectra.*, 2021, **244**, 118835-118834.
35. A. Rahi, N. Sattarahmady, R. D. Vais and H. Heli, Sonoelectrodeposition of gold nanorods at a gold surface – Application for electrocatalytic reduction and determination of nitrofurazone, *Sens. Actuators, B*, 2015, **210**, 96–102.

36. U. Athikomrattanakul, N. G. -Eichelmann and F. W. Scheller, Thermometric Sensing of Nitrofurantoin by Noncovalently Imprinted Polymers Containing Two Complementary Functional Monomers, *Anal. Chem.*, 2011, **83**, 7704–7711.
37. Q. Chu, B. Zhang, H. Zhou, B. Liu, L. Hou and Y.-Y. Wang, Effective C_2H_2 Separation and Nitrofurazone Detection in a Stable Indium−Organic Framework, *Inorg. Chem.*, 2020, **59**, 2853–2860.
38. B.-X. Dong, Y.-M. Pan, W.-L. Liu and Y.-L. Teng, An Ultrastable Luminescent Metal−Organic Framework for Selective Sensing of Nitroaromatic Compounds and Nitroimidazole-Based Drug Molecules, *Cryst. Growth Des.*, 2018, **18**, 431−440.
39. Y.-S. Lu, W.-Y. Pan, T.-C. Hung and Y.-T. Hsieh, Electrodeposition of Silver in a Ternary Deep Eutectic Solvent and the Electrochemical Sensing Ability of the Ag-Modified Electrode for Nitrofurazone, *Langmuir*, 2020, **36**, 11358−11365.
40. B. He and J. Li, A sensitive electrochemical sensor based on reduced graphene oxide/Fe3O4 nanorod composites for detection of nitrofurantoin and its metabolite, *Anal. Methods*, 2019, **11**, 1427–1435.
41. T.-W. Chen, E. Tamilalagan, D. A. A. Farraj, S.-M. Chen, A. Muthumariappan, S. Maheshwaran and M. S. Elshikh, Improving sensitivity of antimicrobial drug nitrofurazone detection in food and biological samples based on nanostructured anatase-titania sheathed reduced graphene oxide, *Nanotechnology*, 2020, **31**, 445502-445511.
42. J. Zhang, L. Gao, Y. Wang, L. Zhai, X. Niu and T. Hu, A bifunctional 3D Tb-based metal–organic framework for sensing and removal of antibiotics in aqueous medium, *CrystEngComm*, 2019, **21**, 7286–7292.
43. M. Roushani and Z. Rahmati, Development of electrochemical sensor based on molecularly imprinted copolymer for detection of nitrofurantoin, *J. Iran. Chem. Soc.*, 2019, **16**, 999–1006.
44. B. Karuppaiah, R. Ramachandran, S.-M. Chen, S. W. -Ling and J. Y. Wan, Hierarchical construction and characterization of lanthanum molybdate nanospheres as an unassailable electrode material for electrocatalytic sensing of the antibiotic drug nitrofurantoin, *New J. Chem.*, 2020, **44**, 46--54.
45. Q.-Q. Zhu, Q.-S. Zhou, H.-W. Zhang, W.-W. Zhang, D.-Q. Lu, M.-T. Guo, Y. Yuan, F. Sun and H. He, Design and Construction of a Metal−Organic Framework as an Efficient Luminescent Sensor for Detecting Antibiotics, *59*, 2020, 1323-1331.
46. K. Xing, R. Fan, X. Du, X. Zheng, X. Zhou, S. Gai, P. Wang and Y. Yang, Dye-insertion dynamic breathing MOF as dual-emission platform for antibiotics detection and logic molecular operation, *Sens. Actuators, B*, 2019, **288**, 307–315.